ANALYSIS AND DESIGN OF BROADBAND ACOUSTIC BEAMFORMERS

CHRISTOPHER J. WHITT

ANALYSIS AND DESIGN OF BROADBAND ACOUSTIC BEAMFORMERS

by

© Christopher J. Whitt

A thesis submitted to the
School of Graduate Studies
in partial fulfillment of the
requirements for the degree of
Master of Engineering

Faculty of Engineering and Applied Science
Memorial University

April 2010

St. John's Newfoundland

Abstract

This thesis is concerned with the methods for designing broadband acoustic beamformers. A beamformer is a signal processing system consisting of an array of transducers combined with appropriate signal processing to produce desired directional characteristics. Beamformers have applications in many areas including radar, sonar, astrophysics, medical imaging, multimedia, and electroacoustics.

Narrowband beamformers are designed to operate at a single frequency or narrow range of frequencies. The techniques for design of narrowband beamformers have been well studied. With advances in signal processing it is now practical to consider a wider range of applications for beamformers, including beamformers which operate over wider frequency ranges, called broadband beamformers.

There has been an increasing amount of research over the last few decades in broadband beamformers, yet there is a lack of comprehensive summaries and tutorials of the state of the art in broadband beamformer design.

This thesis proceeds by reviewing analysis of beamformer performance, and the creation of a MATLAB tool to allow the visualization of broadband beamformer response and the rapid comparison of different beamformers. Then classical narrowband design techniques are reviewed as well as several recent broadband methods.

It is demonstrated how the visualization tool facilitates deeper insight into the fundamental principles that underlie beamformer design.

With a firm understanding of the underlying principles of beamformers, it is possible to perform useful comparisons and contrasts between sophisticated modern design methods and see their relationship to the widely known narrowband techniques.

Much of the beamforming literature makes simplifying assumptions about the physical array geometry to be used. With an understanding of the underlying principles, a basis is given for choosing array geometries and understanding the performance that can be achieved for a given geometry.

The contributions of this thesis include a visualization tool for beamformer analysis, a guide for selecting and evaluating array geometries, and direct comparison of several broadband design techniques. These contributions provide a foundation for the successful design of broadband acoustic beamformers.

Acknowledgments

Thanks to my supervisor, Dr. Cecilia Moloney, who provided me complete freedom to try ideas and be essentially self-directed, and gave support when it was needed.

Financial support from the National Sciences and Engineering Research Council of Canada (NSERC) and from the Government of Newfoundland and Labrador was greatly appreciated.

I could not have completed this project without the support of my family. Thanks to my parents, who have always supported me. Special thanks to Krista for her constant encouragement while I got this thesis through its final stages.

Contents

List of Tables

List of Figures

List of Symbols and Acronyms

λ	Wavelength	6
FIR	Finite impulse response	10
FFT	Fast Fourier transform	10
IFFT	Inverse FFT	10
k	Circular wavenumber	16
f	Frequency	16
c	Speed of propagation	16
DTFT	Discrete time Fourier transform	20
$\hat{k}$	Unit vector in the direction of wave propagation	23
$\vec{k}$	Wave vector	23
ULA	Uniform linear array	54
SRC	Stochastic region contraction	60
MAS	Modal Analysis Synthesis	61
MSD	Modal Subspace Decomposition	61

Chapter 1

Introduction

A beamformer is the combination of an array of transducers with signal processing to produce a directional transducer system. Beamformers are used to achieve greater performance than would be possible at the level of an individual transducer.

Transducers are characterized by many parameters, such as gain or sensitivity, bandwidth, efficiency, frequency response, and radiation pattern. The radiation pattern of a transducer is the directional dependence of the amplitude of the radiation transmitted or received by the transducer. Directivity is a property of the radiation pattern. Directivity is defined as "the ratio of the radiation intensity in a given direction from the [source] to the radiation intensity averaged over all directions[1]."

For a single transducer, the radiation pattern can be controlled by the design of the transducer itself, or by the use of reflectors, horns and waveguides. When the gain, directivity or implementation details make a single transducer inadequate, sometimes a beamformer using an array of transducers can meet the design requirements. Beamformers can be based on arrays of directional elements to improve upon the characteristics of the underlying transducer. They can even be made with simple isotropic elements for reasons of cost or simplicity.

Applications have traditionally included sonar, radar and radio transmission. Arrays also hold potential for acoustic applications such as teleconferencing systems and sound reinforcement. Arrays are important in several areas of professional interest to me, including loudspeaker arrays for sound reinforcement in musical concert settings, and hydrophone arrays used for passive acoustic detection, localization and monitoring of marine mammals.

1.1 Motivation and Approach

Early uses of beamformers were narrowband systems based on one-dimensional arrays, called line arrays, such as in radar systems. As the directional properties of line arrays became known, they were applied to broadband systems, such as loudspeakers for sound and music reproduction.

Near the end of the twentieth century line array based loudspeaker systems were becoming very popular, yet they were (and still are) very expensive and the performance of these systems was still far from ideal. I became interested in the theory of line arrays in order to understand if some better solutions might be possible. I focused particularly on discrete arrays, as these are most practical in acoustical applications.

To my knowledge a comprehesive tutorial on the performance limits and design of broadband arrays does not exist. As I moved toward primary research sources I found many publications on specific design techniques focused on specific applications, but relatively little that provided a framework for the whole field.

Each design technique seemed to claim great, even optimal results, but I found it difficult to find a basis for comparing the results of applying the various methods.

To address this, and to learn more about the fundamental principles of beamformer design, I found it useful to build a software tool to visualize the performance of generic beamformers, which allowed direct and rapid comparisons between multiple design techniques. This tool uses a numerical simulation approach that easily accomodates arbitrary beamformer configurations and computes the beamformer power output directly without the necessity to make small angle approximations. This is important because analytical expressions for the beampattern and other characteristics of arrays are usually limited to specific array geometries, and also sometimes rely on far-field assumptions – that is small-angle approximations are assumed in deriving the beampattern.

The use of this visualization tool led to greater insight into the body of literature and an understanding of some underlying physical principles which guide the design of broadband beamformers.

This thesis addresses the lack of tutorial information on the design of broadband beamformers, in particular the fundamental relationship between array geometry and the potential performance achievable for a given design problem. The contributions of the thesis are a summary of the basics of broadband beamformer design; the development of a software tool to compare performance of various beamformers; examination of the relationship between array geometry and potential beamformer performance, and the comparison the results of several published broadband beamformer design methods.

1.2 Literature Review

The array signal processing literature is wide and varied. Narrowband array principles were first developed for radar systems in the first half of the twentieth century. In the mid- to late-twentieth century both electromagnetic and acoustic array research included both wideband and narrowband arrays in applications such as naval sonar arrays, radio astronomy, radar, teleconferencing, ultrasound, medical imaging, geophysical exploration, hearing aids and musical sound reinforcement, among others.

1.2.1 Survey and Tutorial Papers

Krummer [2] and Hansen [3] both provide tutorial papers covering narrowband linear arrays, as well as practical aspects such as array imperfections and the effects on beampattern. Krummer also touches on planar and conformal arrays.

The 1988 Van Veen and Buckley [4] review of research in array theory and processing is thorough and widely cited. It includes a good tutorial of array basics, and covers both traditional filter-and-sum (data independent) beamforming as well as adaptive beamformers. This paper provides a comparison of the main classes of adaptive beamformers and their tradeoffs, and gives some consideration to research on the design of frequency-invariant broadband beamformers.

A subsequent review by Krim and Viberg [5] covers some more recent methods, focusing on subspace-based methods of parameter estimation as opposed to traditional beamforming. While some methods examined in this thesis do use subspace concepts, I focus primarily on beamforming aspects.

1.2.2 Books

There are many texts that address basic array theory. Books focusing on radio frequency applications [6, 7, 8, 9, 10, 11, 12, 13] often restrict their coverage to narrowband linear or planar arrays and to basic aperture distributions such as Dolph-Chebychev and Taylor, while those addressing acoustic and sonar applications [14, 15] or general array theory [16, 17, 18, 19] may briefly cover broadband and adaptive beamforming.

One of the better introductions to linear narrowband arrays is the 1998 text *Phased Array Antennas*, by Hansen [9]. A more extensive tutorial on beamforming in two and three dimensions, covering data-independent and adaptive beamformers and impementation issues related to ultrasound and sonar systems can be found in Chapter 6 of *Advanced Signal Processing Handbook* [20] (see Section 1.2.4).

1.2.3 Classical Narrowband Synthesis Papers

The classical synthesis techniques for an optimal tradeoff between mainlobe width and sidelobe level for narrowband linear arrays are Dolph-Chebyshev [21] for discrete arrays and Taylor [22] for continuous apertures. Taylor also provides an analogous method for circular [23] arrays. These methods are frequently summarized in the texts listed in Section 1.2.2. Villeneuve [24] presents an exact discrete array equivalent to the Taylor method for continuous apertures. There are many other papers on approximations and numerical computation of Dolph-Chebychev and Taylor coefficients; however, with the current widespread availability of low-cost computer power, these approximations have become less important and are not cited here.

Lockhart and Miller [25] and Futterman and Lockhart [26] present methods for

applying Taylor weightings to planar arrays when they are steered off broadside.

Another classical result is that the Fourier transform of the gains for elements of an equally-spaced linear array is related to the far-field beampattern of the array. This approach is often used for narrowband beamformer synthesis [22, 27]. The Fourier transform relationship is touched on briefly in Section 2.1.1. A detailed proof of the transform relationship between the aperture distribution and farfield beampattern for finite, continuous apertures is given by Hansen [6].

All of the synthesis methods mentioned so far rely on uniform $\lambda/2$ array element spacing to allow analytical design approaches, where λ is wavelength. Most approaches that allow non-uniform or arbitrary element spacings rely on iterative or numerical approaches. There are many published papers in this area and several more recent papers present overviews of previous results [28, 29, 30, 31].

An early example of using numerical synthesis techniques with non-uniform elements spacing is given by Wang [32], whose technique for narrowband arrays minimizes the power in the sidelobes and produces weightings that vary with beam steering direction. The beamformer performance is comparable to narrowband arrays with Taylor weightings. The author uses an example of a logarithmically spaced linear array that might be useful for broadband beamforming, but the justification for the specific choice of array geometry is not given.

Several authors present methods of controlling sidelobe level or mainlobe width by placement of elements. Harrington [33] perturbs an equally spaced array, Lo [34] randomly places elements and Ishimaru [35] places the elements over a much wider average spacing.

Unz [36] presents a method to analyze the pattern of a linear array with arbitrary spacings using a Bessel-function expansion of the complex exponential.

Schjaer-Jacobsen and Madsen [37] use non-linear minimax optimization techniques to perturb the spacings of a uniformly-weighted array to achieve mainlobe width and sidelobe levels similar to Dolph-Chebyshev weighted arrays. Unfortunately, the minimax optimization process gives little intuitive insight into array geometry design.

1.2.4 Adaptive Beamformers

Beamformers can be divided into two broad classes: data-independent, static beamformers, and adaptive beamformers. Data-independent beamformers do not vary their internal signal processing or beampatterns with time. Adaptive beamformers can modify their internal processing and resulting beampatterns over time, usually based on actual measured signal statistics.

As has already been mentioned, Van Veen and Buckley [4] gave a comprehesive review of adaptive techniques in 1988. A more recent text with some coverage of adaptive beamformers is Chapter 6 of *Advanced Signal Processing Handbook* [20]. This thesis will focus on data-independent beamformers.

1.2.5 Superdirectivity

So-called "normal" beamformers use uniform phase, or at most constant-phase delays between array elements to effect beam steering. Some non-linear phase designs use destructive interference to improve the directivity of the beamformer and decrease the mainlobe width. This phenomenon is known as *superdirectivity*, or sometimes *supergain*. In the antenna literature the standard definition of superdirectivity is "the condition that occurs when the antenna illumination efficiency significantly exceeds

100%" and it is noted that "superdirectivity is only obtained at a cost of a large increase in the ratio of average stored energy to energy radiated per cycle [1]."

The use of superdirectivity was the subject of much research in the 1950s [3], and an extensive list of references is given by Hansen [38]. The maximum possible directivity increases are for endfire arrays [39]. Circular and broadside linear superdirective arrays are less effective.

Superdirective arrays are sensitive to element gain mismatches and positioning errors, which increase with the amount of directivity gain realized. Some more recent researchers have investigated limited application of superdirectivity to achieve modest directivity gains while limiting the negative consequences [40]. Aside from the ability of the Modal Subspace Decomposition (MSD) method to selectively add superdirectivity to a broadband design, superdirectivity will not be examined in further detail in this thesis.

1.2.6 Broadband Frequency-Invariant Array Design

Papers on broadband arrays design are often more properly classified as papers on broadband frequency-invariant array design, which is a subset of general broadband array design. A frequency-invariant array is one which has a constant beampattern over its design frequency range. Early papers often aimed for an even simpler goal: to hold only the mainlobe width constant over frequency.

The broadband design technique commonly known as harmonic nesting [41, 42, 43, 44, 45, 46] combines multiple narrowband arrays with equally-spaced elements. Each subarray is designed for a frequency which is a multiple of a primary frequency so that the element spacings are also multiples. Array elements are placed so that some elements can be reused in more than one subarray, reducing the total number

of elements needed. The output of each subarray is combined to produce a total beamformer output that has an acceptable variation over the entire design bandwidth.

Another early technique uses multiple pencil beams added together, each steered slightly off-axis to compensate for the natural narrowing of the mainlobe with increasing frequency [47, 48, 49, 50].

Other authors propose curved or twisted arrays to produce constant beamwidth [51, 52], which rely on directionality in individual elements to maintain mainlobe width at higher frequencies.

1.2.7 Generalized Broadband Array Design

A key element in broadband array design is ensuring that the chosen array geometry adequately samples the array aperture over the entire frequency range of interest. Perhaps because experts in the field consider this to be obvious, there is very little discussion in the literature of the minimal requirements for array geometries. Doles and Benedict [53] give perhaps the first description of the minimum spacing for elements in a discrete linear broadband array, although Ward et al. [54] provide a clearer description and Van der Wal et al. [55] demonstrated the implementation of microphone and loudspeaker arrays according to the theory. Understanding minimum requirements for element placement is a very useful tool for analyzing arrays, and will be discussed further in Chapter 4.

In a method related to the narrowband synthesis techniques already referenced, Haykin and Kessler [56] showed that a two-dimensional Fourier transform relationship exists between element gains and beampattern of a broadband beamformer. This result can be used to synthesize element gains but only when the array consists

of a large number of elements, equally-spaced at half the smallest wavelength.

Broadband beamformer designs are often implemented as digital systems. A time-domain implementation uses finite impulse response (FIR) filters or tapped delay lines for each array element. A frequency-domain implementation uses fast Fourier transforms (FFTs) to transform each transducer output into the frequency domain, perform a filter and sum operation, and then use an inverse FFT (IFFT) to produce the final beamformer output. The frequency domain approach offers efficiencies in systems where multiple beams are formed simultaneously from the same transducer data. This suggests another approach to designing a broadband array is to use FFT techniques to create many narrowband frequency bins and then apply narrowband synthesis techniques in each band [57, 58]. This is called frequency decomposition beamformer design.

Many authors have proposed numerical methods to design arbitrary broadband beamformers, treating the choice of array element positions and gains as a multidimensional optimization problem.

Bucci et al. [59] suggested a general framework for antenna design using general numerical optimization techniques. A review of optimization techniques for array synthesis is provided, however it is noted that for general global optimization problems there is no guarantee of finding an optimal solution. Bucci's general framework introduces a system of notation for expressing general antenna synthesis problems, but the application of the method resorts to simplifying specific design problems to standard optimization problems for the antenna structure (ie array geometry or reflector shape) and antenna excitation (array gain or reflector illumination).

Lebret and Boyd [60] proposed methods for a subset of synthesis problems that can be solved with convex optimization algorithms, including designs for some types

of adaptive arrays. While convex problems can be solved reliably and efficiently, the methods still provide little insight into the physical nature of broadband array design.

Blank and Hutt [61] shows how to adapt numerical optimization techniques to account for real-world effects such as mutual coupling between antenna elements.

Early numerical optimization methods made simplifications to reduce the computational complexity of the optimization problem. Berger and Silverman [62] used Stochastic Region Contracting to compute element positions and gains for microphone arrays for speech acquisition. Later authors have applied more general methods like simulated annealing to a variety of specific problems [63, 64, 65, 66].

Ward et al. [54] developed a method of broadband array design based on a theoretical continuous sensor. The method provides an analytical technique for design of broadband beamformers using a spatial Fourier transform. Subsequently Abhayapala [67, 68] used spherical harmonic solutions of the wave equation to apply the well-known far-field solutions to near field and steerable arrays. Parra [69] summarized this work with a demonstration of broadband frequency-invariant design for arbitrary array geometries.

Finally, Williams et al. [70] gives a method of producing the optimum beamformer for an arbitrary geometry by projecting a desired beampattern onto a subspace of acheivable patterns for the given geometry. This is a powerful technique, and highlights the importance of a strong understanding of the relationship between achievable beampatterns and array geometry.

1.3 Scope and Outline of Thesis

In this chapter I have given some background and motivation for the thesis, and reviewed a portion of the extensive literature on beamformer analysis and synthesis.

In the remainder of the thesis I will address the analysis and design of broadband acoustic beamformers. While the principles of beamformer design are common across application domains, the design examples presented are either explicitly or implicitly based on acoustic design problems. Additionally, the focus of the thesis is on static (or data-independent) beamformers. Adaptive (data-dependent) beamformer design is beyond the scope of this thesis.

The analysis and design of broadband beamformers based on one-dimensional linear arrays of discrete elements provides enough to study, so two- and three-dimensional arrays and continuous apertures are briefly mentioned but not exhaustively explored.

Chapter 2 will present the basic concepts of analysis, with illustrations and examples. This includes the various ways of understanding beamformer performance, including the beampattern, as well as directivity.

A numerical simulation method for arbitrary beamformers and the BeamVisualizer tool are discussed in Chapter 3. BeamVisualizer is a MATLAB tool which I developed to understand and compare various beamformer designs. BeamVisualizer allows a designer to visualize the broadband characteristics of a beamformer design, compare the characteristics of several different beamformers, and quickly see the results of adjusting the design parameters for a particular synthesis technique. BeamVisualizer was used to produce nearly all the figures used throughout the thesis.

Chapter 4 introduces beamformer design with background on the essential classical narrowband techniques of uniform linear arrays, as well as the Taylor and Dolph-Chebychev aperture weightings. The basic and widely used broadband design technique of harmonic nesting is introduced. Another major contribution of this thesis is the analysis of the relationship between the geometry and performance of the harmonic nesting technique, and then the introduction of optimal broadband array spacing. At the end of Chapter 4 implementation details for several other broadband techniques are presented.

Chapter 5 presents the results of applying the design techniques from Chapter 4 to several broadband problems. Many of the examples are taken from the published examples of the various broadband design techniques presented in Chapter 4. The various plots and graphs produced by BeamVisualizer are used to compare the performance of beamformers designed by the various techniques. This chapter includes discussion of these comparisons and the significance for other broadband designs.

Chapter 6 presents conclusions for this thesis and summarizes some design guidelines for broadband acoustic beamformers using linear arrays of discrete elements. The thesis concludes with recommendations for further work.

Chapter 2

Background

A beamformer can be seen as a spatial filter, where the response to the signal direction of propagation is analogous to the frequency response of a classical filter. Similar to filter design, beamformer design has two complimentary parts: analysis and synthesis. The analysis task is to characterize important aspects of beamformer performance, such as the dependance of response with direction. The directional response of an beamformer is often called the beampattern, and usually the primary characteristic of interest. The beampattern is related to the directivity, which is a measure of the array gain for correlated signals. Another important aspect of a beamformer performance is the white noise gain, which is a measure of the beamformer response to uncorrelated noise.

If the bandwidth of operation of a beamformer is small relative to the center frequency, the beamformer is considered narrowband. By definition the directional response of a narrowband beamformer at the center frequency is representative of the performance over the entire bandwidth. When the bandwidth of the beamformer is large relative to the centre frequency it is considered broadband. Visualizing the beampattern of a broadband beamformer requires one additional dimension beyond

the required number of spatial dimensions.

In the classical literature both analysis and synthesis are usually based on analytical expressions. Creating an analytical expression for the beampattern of a beamformer is only possible in certain restricted cases, for example linear arrays with equally spaced elements. Calculating a beampattern numerically for an arbitrary array is relatively straightforward. In this thesis I will not deal with analytical array analysis.

Conversely, there are recent powerful techniques for beamformer synthesis, even for arbitrary array geometries. Earlier numerical approaches to beamformer synthesis usually reduce to difficult global non-convex optimization problems unless the synthesis problem is suitably restricted. These numerical synthesis techniques generally give little insight into the structure of the synthesis problem.

Because of reciprocity, the relationship between the array beam pattern and the array weighting function is the same for transmitting or receiving arrays. Without loss of generality, I will use the terminology for receiving arrays in this thesis.

2.1 Beampattern

2.1.1 Narrowband Linear Array

To start understanding how an array works and the benefits it can provide, I will explain one of the simplest cases: a linear array intended to operate primarily at a single frequency, and provide directional control in two dimensions. The end result is similar if the array is a continuous aperture (as in optics or some kinds of radio antennas) or a set of discrete transducers (which is more common in acoustic applications such as hydrophone or microphone or loudspeaker arrays).

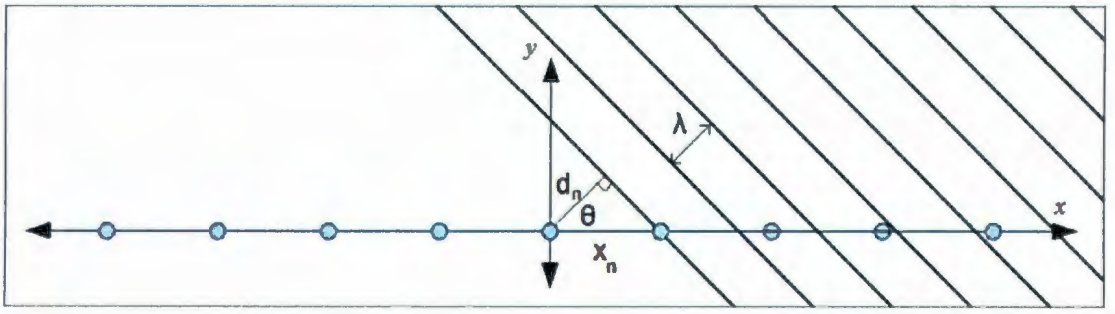

Figure 2.1: A plane wave arriving at a uniformly-spaced array.

Consider a set of N omnidirectional transducers in a straight line receiving a plane wave signal as shown in Figure 2.1. Define the x-axis as coincident with the array elements, with the origin at the midpoint of the line. The arriving plane wave signal is coming from a direction θ relative to the x-axis. If $\theta = \pi/2$ the wave is arriving perpendicular to the array and all elements will output in-phase replicas of the arriving signal. In general, the output of each element will have a relative phase shift depending on θ. The source signal is $s(t) = \cos(\omega t)$ with frequency ω and wavelength $\lambda = \frac{c}{f}$, where c is the speed of propagation and $f = \omega/2\pi$. I arbitrarily choose a time when the phase of the signal is 0 at the origin. The difference in distance d_n that the source signal travels to arrive at transducer n from transducer $n-1$ will be $d_n = x_n \cos\theta$ and the relative phase shift of $s(t)$ at transducer n is $\phi_n = \frac{2\pi}{\lambda} d_n = k d_n = k x_n \cos\theta$ where $k = 2\pi/\lambda$ is the circular wavenumber, and x_n is the distance from the origin to transducer n.

If the source is sufficiently distant then the signal arriving at each array element will have approximately the same amplitude. The output of each transducer is simply a scaled and phase shifted copy of the source signal and the total output of the array

formed by summing the output of all transducers is

$$r(\omega, t, \theta) = \sum_{n=0}^{N-1} e^{j(\omega t + \phi_n)}. \tag{2.1}$$

The magnitude and phase of the array output are readily calculated, and the instantaneous value of $r(\omega, t, \theta)$ is simply the real part of Equation 2.1.

It is conventional in the literature to omit the time and frequency dependence for notational clarity. This is the beampattern of the array, also known as the array factor in antenna literature.

$$r(\theta) = \sum_{n=0}^{N-1} e^{j\phi_n} \tag{2.2}$$

The beampattern of an array with 21 isotropic elements, equally spaced at $\lambda/2$, with uniform gains is shown in Figure 2.2. The same plot in polar coordinates is shown in Figure 2.3. The largest response of the beamformer is to plane wave signals arriving in phase at all elements, that is from the direction 90 degrees from the axis of the array. This direction is called broadside, and the response lobe centered here is called the mainlobe. The other smaller lobes are called minor lobes or sidelobes, and decay with an approximate sinc x envelope. The direction along the array axis is known as endfire.

If the array element spacing is less than $\lambda/2$ then spatial aliasing is possible under certain conditions. When this happens the beampattern will exhibit sidelobes at the same level as the mainlobe. These aliasing lobes are sometimes referred to as grating lobes.

In the special case of equally spaced array elements the phase shift between each

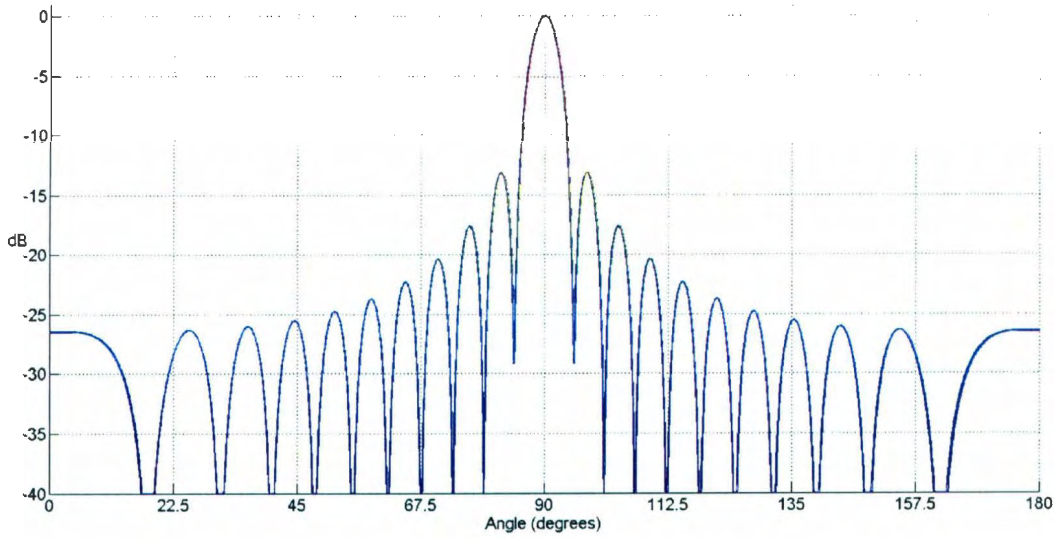

Figure 2.2: The beampattern of a 21-element linear array with $\lambda/2$-spacing and uniform gains, plotted as amplitude vs. θ.

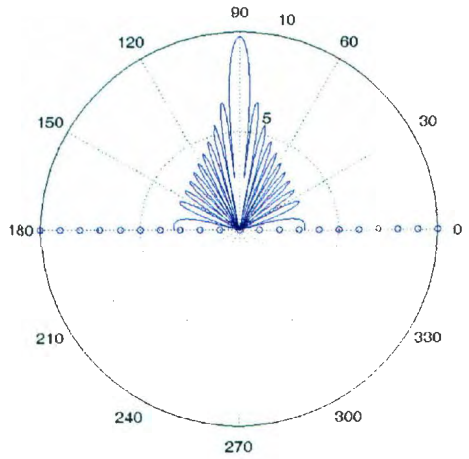

Figure 2.3: The beampattern of a 21-element linear array with uniform gains.

successive element is constant. Taking the first element as the reference point, the phase shift in the far-field becomes $\phi_n = knd\cos\theta$. Let Φ be the phase shift from one element to the next, such that $\Phi = \phi_1 = kd\cos\theta$. We adjust the summation indices appropriately and the beampattern simplifies to

$$r(\theta) = \sum_{n=0}^{N-1} e^{jn\Phi} \tag{2.3}$$

$$\begin{aligned} r(\theta) &= \frac{1 - e^{jN\Phi}}{1 - e^{j\Phi}} \\ &= \frac{e^{jN\Phi/2}}{e^{j\Phi/2}} \left(\frac{e^{jN\Phi/2} - e^{-jN\Phi/2}}{e^{j\Phi/2} - e^{-j\Phi/2}} \right) \\ &= \frac{\sin(N\Phi/2)}{\sin(\Phi/2)} \angle\Psi \end{aligned} \tag{2.4}$$

The response of a continuous sensor can be considered the limiting case of an infinite number of array elements where the summation becomes integration. In this case the array can be thought of as an aperture as in optics or antennas. Assuming that the continuous sensor extends for a distance $L/2$ from the origin in both directions, the beam pattern is given by

$$r(\theta) = \int_{-\frac{L}{2}}^{\frac{L}{2}} e^{jkx\cos\theta} dx \tag{2.5}$$

where $kx\cos\theta$ is the phase contribution to the far-field beampattern at observation angle θ from the portion of the aperture at distance x along the sensor.

In the simple case of uniform sensitivity along the array aperture, the beampattern is

$$
\begin{aligned}
r(\theta) &= \int_{-\frac{L}{2}}^{\frac{L}{2}} e^{jkx\cos\theta} dx && (2.6)\\
&= \frac{e^{jk\frac{L}{2}\cos\theta} - e^{-jk\frac{L}{2}\cos\theta}}{jk\cos\theta} && (2.7)\\
&= L\frac{\sin(jk\frac{L}{2}\cos\theta)}{k\frac{L}{2}\cos\theta} && (2.8)\\
&= L\mathrm{sinc}(k\frac{L}{2}\cos\theta) && (2.9)
\end{aligned}
$$

In both the continuous and discrete case the beampattern has the form of a sinc function. The uniform gain across the aperture in both cases is equivalent to a rectangle function. Thus, we can see that the beampattern is the continuous Fourier transform or discrete time Fourier transform (DTFT) of the aperture function transform in the continuous and discrete array cases, respectively, at least for a uniform aperture.

The remainder of the thesis will focus on discrete arrays.

2.1.2 Three Dimensional Arrays

For arbitrary three-dimensional arrays and signals arriving from arbitrary directions it is convenient to use a spherical coordinate system, with the location of a source represented by range, zenith and azimuth angle, r, θ, ϕ respectively. An array element represented in spherical coordinates is shown in Figure 2.4 and the conversions to cartesian coordinates are

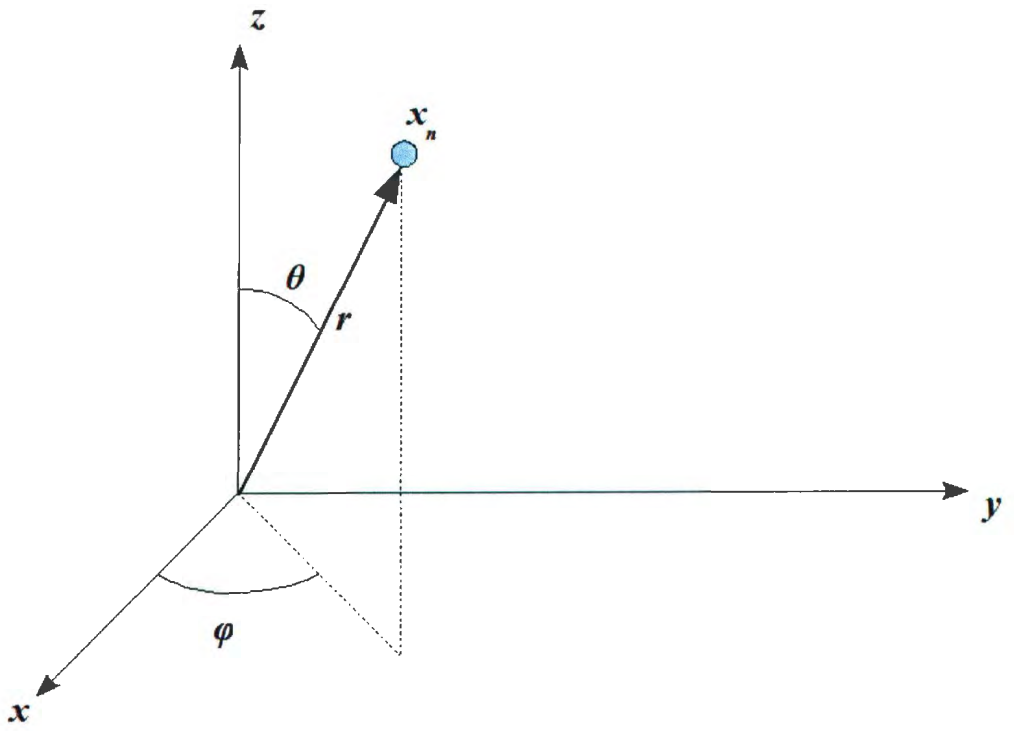

Figure 2.4: The location of an array element in spherical coordinates.

$$\begin{aligned} x &= r\sin\theta\cos\phi \\ y &= r\sin\theta\sin\phi \\ z &= r\cos\theta. \end{aligned} \tag{2.10}$$

If two array elements are exactly on the z-axis, the distance each wavefront travels between one element and the next is $d\cos\theta$, where d is the distance between the elements, and θ is zenith angle of the propagating wave as shown in Figure 2.5. Similarly, the distance between the origin and a wavefront passing through a given array element is $z\cos\theta$, where z is the element's position on the z-axis. The phase of

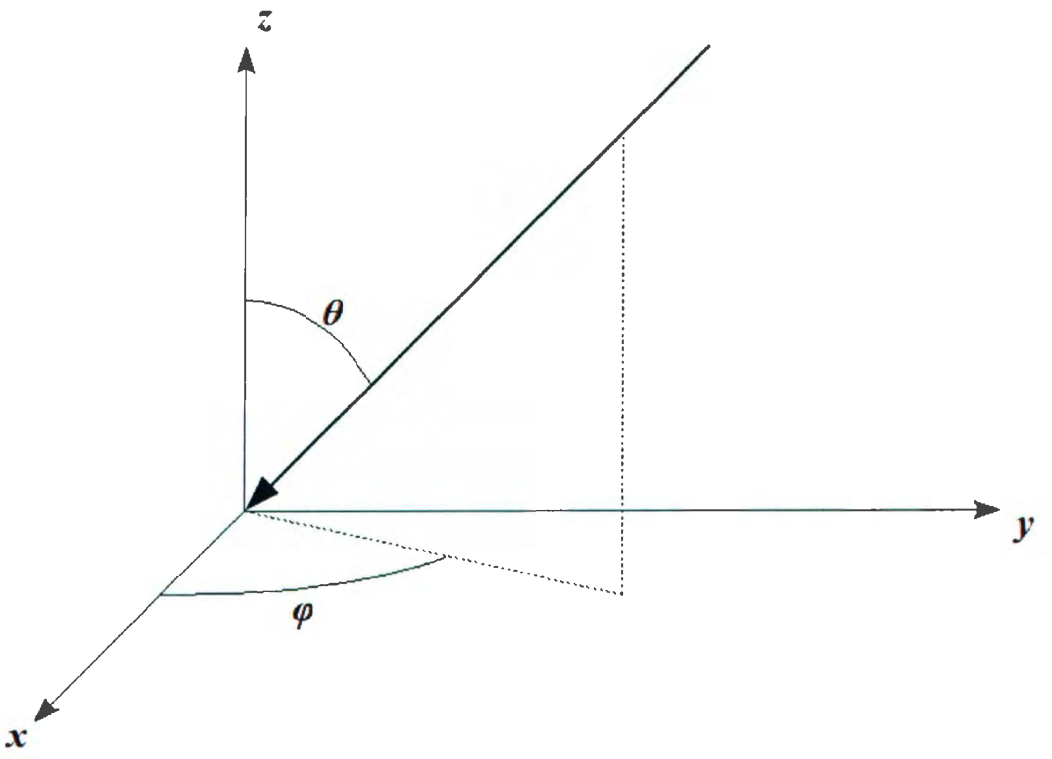

Figure 2.5: A vector in the direction of propagating wave.

the signal at the array element relative the origin is then $\frac{2\pi}{\lambda} z \cos\theta$ or $kz\cos\theta$, where $k = \frac{2\pi}{\lambda}$ is the circular wavenumber. This is equivalent to the linear array case already discussed.

The distance between the origin and a wavefront passing through a given array element can also be thought of as the projection of the position vector for that array element onto a unit vector in the direction of wave propagation. This is simply the dot product. If $\hat{k}$ is a unit vector in the direction of wave propagation, and $\vec{x}_n$ is the position of the nth array element, then the distance between the origin and a wavefront passing through that array element is $\hat{k} \cdot \vec{x}_n = |x_n| \cos\theta$ where θ is the

angle between the position vector and propagation vector. The phase of the signal at that array element relative to the origin is now $\vec{k} \cdot \vec{x}$, where $\vec{k} = k\hat{k}$ is the wave vector.

The total output of an array of N discrete elements located at positions $\vec{x}_n$ to a plane wave of frequency f arriving from direction $\hat{k}$ is

$$r(\vec{k}) = \sum_{n=1}^{N} e^{j\vec{k}\cdot\vec{x_n}} \tag{2.11}$$

where $\vec{k}$ is the wavevector [45].

2.2 Directivity

When analyzing and synthesizing arrays, the beampattern is often the main characteristic reported in the literature. To compare similar designs, it is helpful to have additional tools.

In the antenna literature, gain (in a given direction) for an antenna is defined as "the ratio of radiation intensity, in a given direction, to the radiation intensity that would be obtained if the power accepted by the antenna were radiated isotropically" and it is noted that "if an antenna is without dissipative loss, then in any given direction, its gain is equal to its directivity. [1]"

In the beamforming literature the array gain is defined as the improvement in signal-to-noise ratio (SNR) due to beamforming [71]. Gains relative to different types of noise give insight into different aspects of the array design performance.

Array gain against spherically isotropic noise - noise originating in the far field of

the array which is correlated at all elements of the array - is often called the directivity, and is a measure of the spatial or directional selectivity of the beampattern. This definition is compatible with the definition of antenna gain and directivity given above.

Array gain against uncorrelated noise (sometimes called spatially white noise) is called the "white noise gain". White noise gain is commonly used to measure the tolerance or sensitivity of the array to gain errors, sensor self-noise, and element position errors. This can be thought of as simply the output power of the array for the desired signal, relative to the output power for a single omnidirectional element at unity gain.

Two arrays with the same directivity may have very different white noise gain. Directivity is a measure of the output power of the desired signal relative to signals from other directions. White noise gain is the output power of the desired signal relative to an external reference. An array which attenuates signals from all directions, but attentuates signals outside the desired direction much more than the desired direction may have acceptable directivity but poor white noise gain.

In the following discussion the frequency variable is omitted for simplicity, assuming a constant value for k. In reality, the peak response and beampattern of most beamformers both change with frequency, so directivity and white noise gain are often frequency dependent.

The directivity of an array is a measure of the spatial selectivity of the array geometry and element gains. An array with a high directivity will have relatively high output power for signals from a specific point, area or direction in space, and relatively low output power for noise signals from other points or directions.

Thinking of directivity as a signal to noise ratio, directivity can be defined as the

signal power divided by the noise power. More specifically, directivity is the ratio of power per unit solid angle in a specific direction to the power per unit solid angle for an isotropic transducer. The general case is [6]

$$G = \frac{4\pi \left| r(\rho_o, \varphi_o) \right|^2}{\int_A \left| r(\rho, \phi) \right|^2 dA} \tag{2.12}$$

where A is the surface area of the entire unit sphere, dA is the unit solid angle, and ρ_o, ϕ_o are the azimuth and elevation of the maximum response of the beampattern.

For the two-dimensional case, if the response of the array to a signal from direction θ is given by $r(\theta)$ then the directivity [67] is

$$G = \frac{2\pi r(\theta_0) r^*(\theta_0)}{\int_{-\pi}^{\pi} r(\theta) r^*(\theta) d\theta} \tag{2.13}$$

where θ_0 is the angle of the maximum response of the beampattern, and $*$ represents complex conjugation.

The analysis method described in this chapter can be used to calculate the array output from the desired signal direction, as well as an arbitrary number of additional directions. If the array beampattern is calculated by a regular sampling of all possible angles from $-\pi$ to π radians, then the integrand in the denominator of Equation 2.13 can be approximated with the trapezoidal rule with a scaling factor based on the number of sampling points. The numerator can be calculated directly.

Alternatively, array gain can be defined as [71]

$$G = \frac{|w^* d|^2}{w^* Q w} \tag{2.14}$$

where w is a column vector of the weights, or gains of each sensor element, d is a

vector of phase delays to align the sensor outputs with the desired signal direction, and Q is the normalized cross power spectral density matrix of the noise. $Q = E(xx^*)$ if x is a column vector of the instantaneous noise output at each sensor.

2.3 White Noise Gain

In the analysis method described in this chapter, the signal level received at each sensor is calculated based on spherical spreading loss before the beamforming calculations are performed. The output of a single omnidirectional element would then simply be the signal level after the spreading loss calculation. The array element gains should either be normalized to be less than or equal to unity, or the gain of the single omnidirectional element should be equal to the maximum gain used in the array. The white noise gain is simply calculated by dividing the output power of the array in the desired signal direction by the output power of the single omnidirectional element.

Alternatively, the white noise gain can be calculated using 2.14, by realizing that with uncorrelated noise at each element, the noise cross power spectral density matrix becomes the identity matrix I, and the white noise gain is defined as

$$G = \frac{|w^* d|^2}{w^* w} \leq M \tag{2.15}$$

where M is the number of sensors [72].

2.4 Beamformer Signal Processing

2.4.1 Array Element Gain

The relative gains of each element in the array is the primary factor controlling the width of the main beam as well as the amplitude and location of the sidelobes. While there are limitations in practice, if the gain of the nth array element is considered to be an arbitrary complex number g_n then Equation 2.2 becomes

$$r(\theta) = \sum_{n=1}^{N} g_n e^{j\phi_n} \tag{2.16}$$

and Equation 2.11 becomes

$$r(\vec{k}) = \sum_{n=1}^{N} g_n e^{j\vec{k}\cdot\vec{x_n}}. \tag{2.17}$$

In the case of the continuous sensor, the gain becomes a function of distance along the sensor, $\rho(x)$, Equation 2.5 becomes

$$r(\theta) = \int_{-L/2}^{L/2} \rho(x) e^{j\phi(x,\theta)} dx \tag{2.18}$$

2.4.2 Array Steering

Most array implementations use signal processing to control the direction of the main lobe. This process is often called steering. In a narrowband array the steering can be achieved by time delaying the signal at each sensor, or by adding a phase shift at each sensor. When considering broadband arrays, a fixed phase shift to steer the main beam results in a variable effect on the beam direction at different frequencies in the operating bandwidth. If a fixed time delay is used for each element the effect

on the beam is constant at all frequencies. This can be implemented as a variable phase shift at each element that is a linear function of frequency, but this thesis will always describe a steered beam using time delays. The phase effect of a time delay at a specific frequency is found by multiplying by c and the wavenumber k.

If each element of an array has an arbitrary time delay added, then Equation 2.16 becomes

$$r(\theta) = \sum_{n-1}^{N} g_n e^{j(\phi_n + k t_n c)}. \tag{2.19}$$

Equation 2.17 becomes

$$r(\vec{k}) = \sum_{n=1}^{N} g_n e^{j(\vec{k}\cdot\vec{x_n} k t_n c)}, \tag{2.20}$$

and Equation 2.18 becomes

$$r(\theta) = \int_{-L/2}^{L/2} \rho(x) e^{jk(x\cos\theta + \tau(x)c)} dx, \tag{2.21}$$

where c is the propagation speed, and t_n or $\tau(x)$ are the time delays for the nth array element and at position x along the continuous aperture, respectively.

In practical implementations of digital systems, the steering delays are constrained to integer multiples of the system sample rate, unless time interpolation is used [58]. This is a significant consideration [73] particularly if the system is to be used for direction estimation and source locating, but these topics will not be addressed further in order to focus on the basic theoretical aspects of broadband beamformer design.

2.5 Array Geometry

Since a beamformer consists of both a physical array of transducers and some signal processing applied to the signals from the transducers, both analysis and synthesis should consist of two distinct but closely related parts: one for the array geometry and the other for the applied signal processing.

In much of the literature both analysis and synthesis focus primarily on the signal processing at the expense of the array geometry. This can be attributed to several factors: early applications were often narrowband designs with simpler geometry requirements, practical implementation issues often drastically restrict the geometry choices, and certain regular geometries are required for some analytical analysis and synthesis approaches.

Once the physical array geometry is fixed in the synthesis process, it is possible and in fact usual to analyze the entire beamformer as one system with no distinct consideration of the array geometry specifically. Analyzing an array geometry in isolation does not necessarily give insight into the synthesis process for that array. However, for effective synthesis a beamformer designer needs to have a good understanding of the fundamental possibilities and limitations of a given array geometry before or in concert with the design of the associated signal processing.

2.5.1 Symmetry in Beampatterns

The simplest array geometry is a linear array, where all transducers are arranged on a single axis. For linear arrays the spatial response is axially symmetric (as long as the transducers are omnidirectional), since there is no difference in the array geometry regardless of which reference plane containing the array axis is chosen. This is a very

typical array geometry and in the literature a two-dimensional beampattern plot is generally understood to represent the magnitude response of the beamformer at a single frequency in any plane containing the array axis, with the x-axis typically representing the angle relative to the array axis. Alternately, a polar plot can show the same information. In either case the beampattern at one frequency can be effectively represented in two dimensions. To display the beampattern at a few discrete frequencies different line types or colors can be used on a two-dimensional plot. To display a larger number of frequencies a pseudo-three-dimensional plot can be used.

For a planar (two-dimensional) array there is a mirror symmetry in the beampattern on either side of the plane containing the array. For some regular patterns of array elements there may also be rotational symmetry about the axis normal to the plane of the array, if the beam is also directed normal to the array. At a single frequency the beampattern can be suitably represented in a pseudo-three-dimensional plot. For the rotationally-symmetric case it is technically possible to show the broadband response of the array by representing frequency on one axis and a slice through the beampattern in a plane containing the axis of symmetry on the other, but this may not be visually intuitive to most readers.

Figure 2.6 shows the three-dimensional beampattern of a uniformly-spaced linear array beamformer at a single frequency, with the beam steered to 45 degrees off the array axis. Figure 2.7 shows the beampattern of a square, uniformly spaced planar array beamformer, with the beam steered to 45 degrees away from the axis normal to the plane containing the array. Each plot shows the unit-less normalized response of the array in decibels.

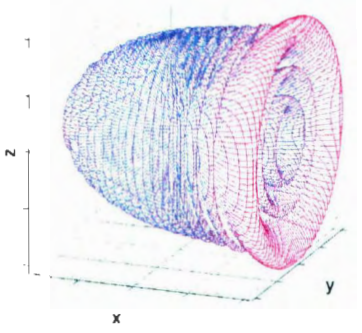

Figure 2.6: The normalized three-dimensional response of a linear array on the x-axis, steered to 45 degrees away from the array axis, at one frequency.

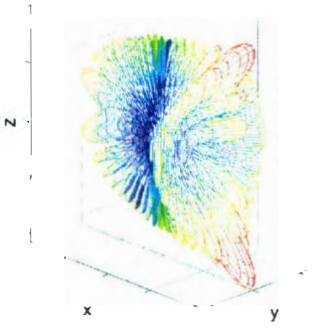

Figure 2.7: The normalized three-dimensional response of a planar array on the xy-plane, steered to 45 degrees away from the axis normal to the xy-plane, at one frequency.

For a general three dimensional array there is no guarantee of any kind of symmetry in the beampattern. Any plot of beamformer response necessarily fixes one or more of the variables of azimuth, elevation and frequency, even in pseudo-three dimensional plots. Clearly visualizing the three-dimensional response of planar or volumetric arrays is difficult, and is beyond the scope of this thesis.

2.5.2 Analogy Between Spatial and Temporal Frequency

Consider the case of a linear array of elements. If the beamformer is thought of as a spatial filter, then a signal arriving from the broadside direction can be considered analogous to a DC signal in a temporal signal processing context. The in-phase wavefronts appear simultaneously with equal amplitude at all sample points, which are the array elements. Plane waves arriving from progressively larger angles correspond to increasing frequencies in a time-series signal, as the phase difference between adjacent samples increases in direct proportion to angle, just as it is in direct proportion to frequency in the time-series case.

This provides insight into element spacing requirements. Typically, linear arrays are designed with elements uniformly spaced at $\lambda/2$, which is consistent with the requirements of the sampling theorem. A wider spacing would admit the possibility of spatial aliasing under certain conditions, while a narrower spacing would reduce the overall aperture size, and possible spatial resolution for a given number of elements.

It is not reasonable to expect to recover signals up to precisely the Nyquist frequency in any real system. In the spatial filtering analogy a signal arriving along the array axis is equivalent to a signal at the Nyquist frequency in a temporal system. In temporal signal processing there is no clear physical meaning for a negative frequency, however in the spatial filtering case a negative frequency is a plane wave

signal arriving from the opposite direction along the array axis. Beampatterns of arrays with $\lambda/2$ spacing steered to endfire clearly show the spatial aliasing lobe at the negative Nyquist frequency. This is why endfire arrays are sometimes designed with higher spatial sampling frequencies, such as elements spaced at $\lambda/4$, to avoid aliasing [44].

However, if no steering is intended or required, then sampling at lower than the Nyquist rate can be acceptable. A beamformer with no time-delay steering is analogous to a low pass filter. When interpreted as analog frequency, the frequency response of a discrete filter is periodic with repetitions at multiples of the sample rate. Only when the spatial sampling rate drops to λ will the periodic repetition of the filter response become physically visible along the array axis. The physical explanation is a signal exactly at the desired frequency will appear in phase at each element whether it arrived from a direction normal to the array axis or along the array axis. This suggests why some authors have found that the optimum element spacing for a broadside array is actually between $\lambda/2$ and λ, since for the same number of elements, a wider spacing gives a larger overall aperture, narrower mainlobe width and higher directivity.

2.6 Summary

This chapter has introduced the terminology of beamformers and explained the basic principles of beamformer operation. The main beamformer characteristics are beampattern, directivity and white noise gain. The main synthesis parameters are array geometry, array element gain, and time delay applied to each element for beam steering.

Chapter 3

Beamformer Analysis

This chapter describes the general principles and specific tools used in the remainder of the thesis for the analysis of beamformers based on discrete linear arrays. The numerical simulation method is briefly introduced, followed by the MATLAB program BeamVisualizer. The BeamVisualizer tool was a key enabler for me to consolidate the concepts presented in individual papers and established research.

The first section of the chapter will describe the basic numerical simulation method, which I created myself as I was designing BeamVisualizer, but which is quite elementary and based on well-established principles from the literature. The second section describes the user interface and general features of BeamVisualizer, which is one of the key contributions of this thesis.

3.1 Numerical Simulation Method

The response of a beamformer to an arbitrary source in three dimensions is given by Equation 2.20. The beamformer is treated as a receiving system and each element is assumed to be an ideal isotropic point-receiver. As explained in Chapter 2, there is a

reciprocity relationship between receiving and transmitting systems, so in the case of a transmitting beamformer, each element would be assumed to be an ideal isotropic point-source. There is no consideration of mutual coupling between elements, nor any assumptions of infinite baffles.

While Equation 2.20 is tidy, it depends on a far field assumption – that is, the signals received at each array element all come from the same direction, namely $\hat{k}$. This implies an infinitely distant source. When computing the beampattern numerically, a simple alternative approach is to compute the beamformer response to a signal from a hypothetical source location by calculating the distance from each element to the source, finding the relative phase of the signal at each element and performing the complex summation. This approach is given in Equation 3.1.

To make the simulation complete it is necessary to add to each distance an additional amount to account for any time delay applied at each array element. The relative gain of the signal at each element is also scaled by the inverse square law, then multiplied by the element gain.

This process can be repeated as necessary for many source locations and frequencies to approximate the beampattern to any desired degree of precision and form a picture of the entire beamformer response.

$$r(x_r, y_r, z_r) = \sum_{n=1}^{N} g_n e^{jkd_{rn}} \tag{3.1}$$

where

$$d_{rn} = \left[(x_r - x_n)^2 + (y_r - y_n)^2 + (z_r - z_n)^2\right]^{1/2} + t_n c \tag{3.2}$$

where k is the circular wavenumber corresponding to the desired frequency, c is the propagation speed, N is the number of array transducers, g_n is the complex gain of

each element, x_r, y_r, z_r, x_n, y_n, z_n, are the x, y, and z coordinates of the current observation point and the nth array element, respectively. The time delay applied to the nth array element is t_n.

The limitations of visualizing a beampattern usually determine the choice of hypothetical source locations. As already discussed, when studying broadband beamformers, one display axis is required for frequency, which only allows two dimensional slices of the beampattern to be displayed at any one time. This is adequate for beamformers based on linear arrays with rotational symmetry about the array axis, which is the main type of beamformer I will consider in this thesis. The observation points are usually oriented in a circle about the array, to allow easy plotting of the beamformer response.

Each observation point can represent a sound source or a receiver. If, for example, the beamformer is based on a loudspeaker array, the function evaluated at the observation point represents the sound intensity from the array heard at that observation point. For a microphone array, the function evaluated at the observation point represents the electrical output of the array due to a source located at the observation point.

The formulation in Equation 3.1 is very general. In contrast with analytical formulations for the beampattern of specific aperture functions, such as Equation 2.4, this numerical approach has the advantage of avoiding plane wave assumptions and small-angle approximations. The distance from each source to each array element is separately computed, instead of assuming parallel wavefronts and calculating an offset based on the angle of incidence and the separation of array elements. This is important because it cannot be assumed that the observation point will be in the far field for very low frequencies with long wavelengths. In musical acoustic applications,

wavelengths of low frequencies are significant even when compared to the dimensions of large concert halls. In underwater applications the much higher sound velocity means that wavelengths are proportionally longer, so the near field of the array is much larger at a given frequency.

3.2 BeamVisualizer Software

To help understand and compare various synthesis methods, I wrote a MATLAB graphical utility that I call BeamVisualizer. This program is primarily an analysis package that computes the response of an arbitrary beamformer at discrete frequencies and spatial positions, and displays the resulting information in various two-dimensional graphs. It also has the capability of calling various synthesis scripts and functions to dynamically generate different beamformer designs for easy comparison of beam patterns and other parameters. BeamVisualizer is intended to allow rapid interactive comparisons of different beamformers. Most beamformers are simulated and displayed in a second or two and plots like those in this chapter can be produced about as quickly as the user can adjust the parameters through the user interface.

The general analysis method of Section 3.1 is used. There are no inherent limitations to two dimensions or any particular medium, transducer type, or frequency range. Implementation details such as individual transducer beampatterns, coupling, or other effects are not considered. Because my main interests are in acoustics, the default frequencies are audible frequencies and propagation speeds are appropriate for sound in air or water, but this is not essential to the software design. However, I will use often terminology specific to acoustics.

As already mentioned, displaying beampatterns in three spatial dimensions and

over a wide frequency range is difficult. Since this thesis primarily focuses on linear arrays, the visual portion of the software is based on displaying two dimensional slices of a beampattern. This is because linear arrays have rotational symmetry about their axis, as explained in Section 2.5.1.

To aid with understanding different synthesis methods and comparing resulting designs, BeamVisualizer also displays several other attributes of the beamformer such as frequency-dependent gain of each element, directivity, white noise gain, frequency response of the beamformer for a chosen look angle and a polar plot of the beampattern at a chosen frequency.

An additional dropdown menu is added to the standard menus provided by MATLAB. Called Options, it allows any of the plots to take over the entire display, and the options panels to be hidden. In this chapter the entire GUI is shown with screen captures, but in subsequent chapters I will most often include just the relevant plots. Most of the figures in this thesis are produced directly from BeamVisualizer using standard MATLAB graphics export commands along with the individual plot highlighting and user interface suppression options in the Options menu.

The code for beam visualizer is available from the author on request.

3.2.1 Main Beampattern Display

Figure 3.1 shows the main display of the BeamVisualizer software. The main plot is the simulated beampattern, and there are six secondary plots: array element filter display, beamformer polar response, effective aperture size, frequency response, directivity and white noise gain. There are two user-interface options panels: the display options panel and array design options panel.

The beampattern plot is a pseudo-three-dimensional mesh that occupies most

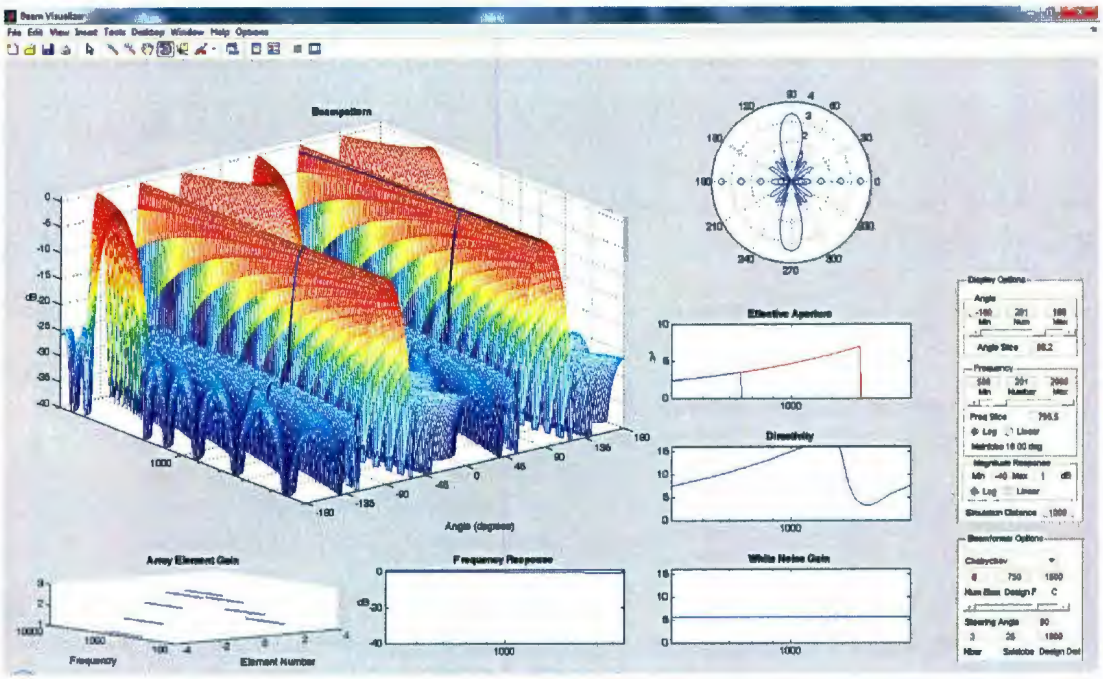

Figure 3.1: Main Beampattern Display.

of the GUI. This displays the two-dimensional response of a broadband array, with direction along the primary axis (on the right in Figure 3.1) and frequency on the secondary axis (on the left in Figure 3.1). Array response is displayed vertically. MATLAB allows this mesh to be easily rotated with the mouse.

The polar plot shows the two-dimensional beampattern of the array at one selected frequency. The frequency shown on the polar plot is indicated by a dark blue horizontal line in the main beampattern display, and by a slider in the display options panel. As an additional aid to visualization, the relative positions of the array elements are superimposed on the polar response plot.

The effective aperture plot shows the relative portion of the array which is useful at a given frequency. The y-axis is in units of λ. The criteria for determining usefulness depends on the intent of the specific beamformer design, so the blue and red

lines represent the portion of the array spaced at or less than $\lambda/2$ and λ, respectively.

The frequency response plot shows the frequency response of the array in one specified look direction. The direction for the frequency plot is shown by another blue line in the main beampattern display, and by a second slider in the display options panel.

The array element filter display is a line graph of the frequency-dependent weights of each element in the array. This is useful to visualize the relationship between array geometry, element gains, and beampattern response. Figure 3.2 shows a 25-element array designed to maintain a constant beampattern over a wide frequency range. The filters applied to the output of each array element to realize this beampattern are shown directly below the main beampattern display.

The Options menu of the MATLAB GUI allows the user to select any of the seven plots to be displayed alone. Figure 3.3 shows the array element filter plot of Figure 3.1 enlarged and rotated slightly.

The last two plots show the array directivity and white noise gain versus frequency, as described in Section 2.2 and Section 2.3. Figure 3.4 shows a non-uniformly spaced linear array with unusual directivity and white noise gain plots due to the unusual geometry. The range of both plots is fixed, rather than allowing MATLAB to automatically adjust the axis limits, to facilitate easier comparison between different beamformer designs. However this sometimes also obscures detail in the plots.

3.2.2 Display Options

The display options panel contains controls to define and manipulate the views of beamformer performance offered by BeamVisualizer. The array design options panel contains controls to select different beamformer types, array geometries and other

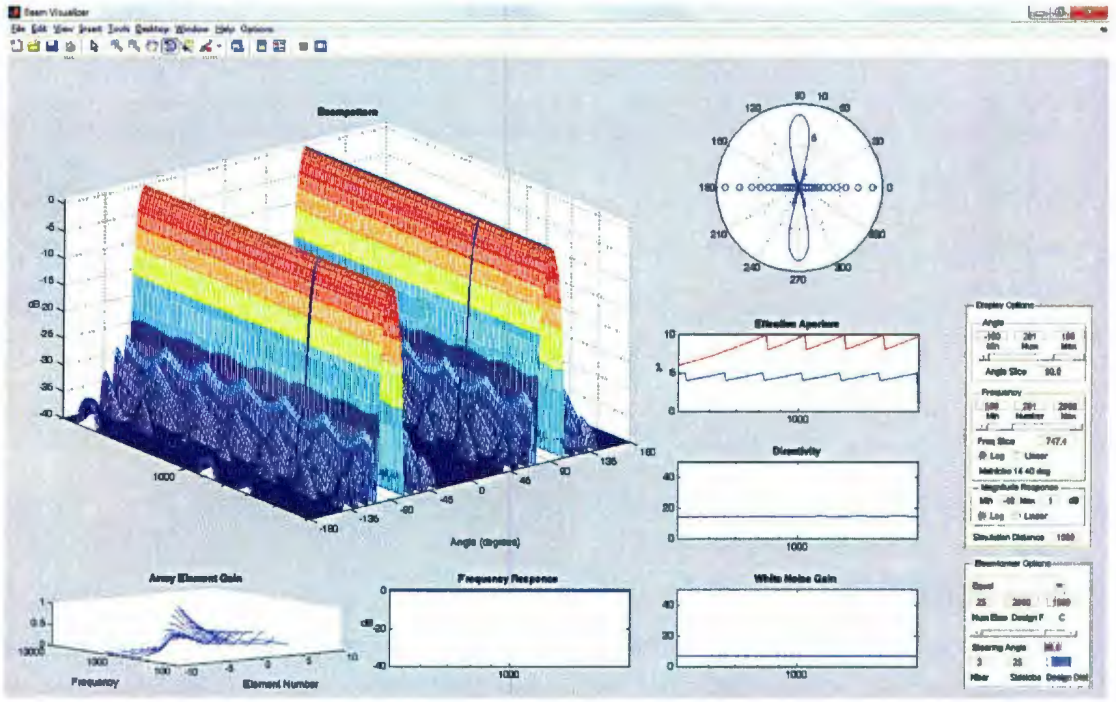

Figure 3.2: Beampattern of a broadband, constant beamwidth array design.

synthesis parameters for modelling and display.

The first few controls are the angular display controls. These control the portion of an imaginary circle around the center of the array that is used for simulation, and this is reflected in the main beampattern display and polar plot. The first three edit boxes are minimum angle, number of angles to calculate, and maximum angle. The slider controls which angle is used for the frequency response plot. This angle is also highlighted in blue on the main beampattern display. This angle is shown and can be modified in the Angle Slice edit box. The set of possible angles to display is determined by evenly distributing the number of desired angles between the chosen minimum and maximum value. When an angle is typed into the Angle Slice box, the nearest available angle that has already been computed is used, instead of computing a new angular slice.

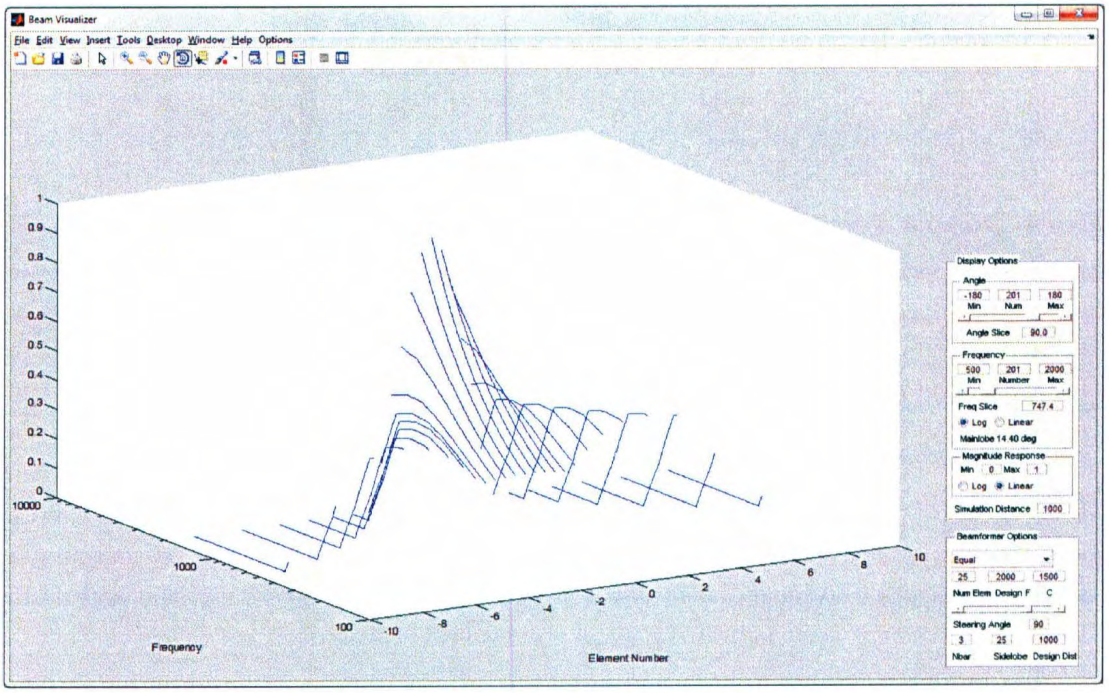

Figure 3.3: Element weights for broadband, constant beamwidth array shown in Figure 3.2.

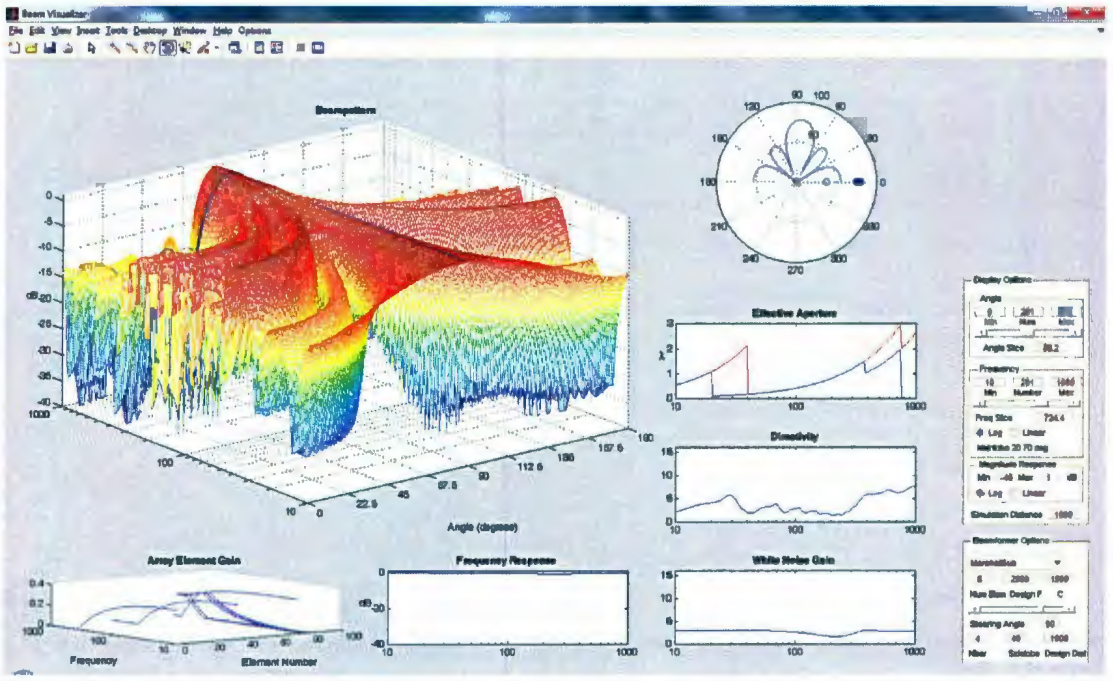

Figure 3.4: A non-uniformly spaced array with uniform gains.

The next controls are the frequency display controls. These control the minimum and maximum simulated frequency and the number of frequencies to simulate in between the minimum and maximum. These controls affect the axes of the main beampattern display, and all other plots besides the polar plot. The slider selects what frequency within the range is highlighted in blue, and also displayed on the polar plot. The edit box can also set the highlighted frequency. The Log and Linear radiobuttons select either linear or logarithmic plotting on the frequency axis where applicable. A rough estimate of the mainlobe width is done by finding the point of maximum beamformer response at the highlighted frequency, then determining the included angle around that angle for which the beamformer response is within 3 dB of the maximum. The precision of this measurement is determined by the minimum and maximum angle and the number of simulated angles in that range, and so it

should be used with care, particularly when the mainlobe width is small and the number of angles being simulated is low to medium.

Figure 3.5 shows a plot of only angles 0 to 180 degrees (see Section 4.2.3 for information on Taylor weighting). The limited analysis range is shown in both the main beampattern display and the polar plot.

The final group of controls is the Magnitude Response section. This is fairly straightforward and defines the z-axis limits for the beampattern plot and y-axis limits for the frequency response plot, as well as whether the data are displayed on linear or logarithmically. The simulation range option determines the distance from the array used in the calculation of the beamformer response.

The logarithmic display is the default for both frequency and response axes. Using a linear axis to display a beampattern can be misleading, especially on the response axis, but it is useful for comparison of results when previously published results are displayed on linear scales. Figure 3.6 shows the same beamformer as Figure 3.2 displayed on linear frequency and beamformer response scales.

3.2.3 Beamformer Design Options

The beamformer design panel contains options to choose the beamformer to be simulated and displayed. BeamVisualizer internally uses a standard data structure to represent a beamformer, which simplifies the process of integrating code which implements a new beamformer synthesis method.

A synthesis function is expected to return the standard data structure that conforms to the expectations of the numerical simulation method presented. This structure contains several fields. For each element there is an entry for the three spatial

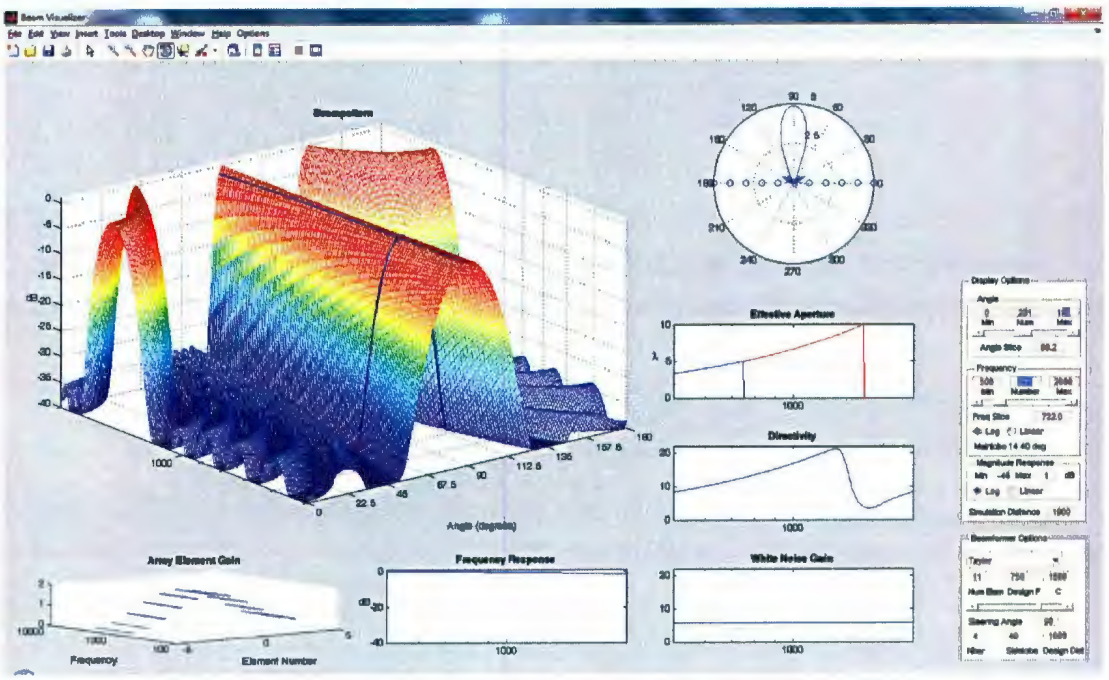

Figure 3.5: An 11-element linear array beamformer with a Taylor weighting and -25 dB sidelobes.

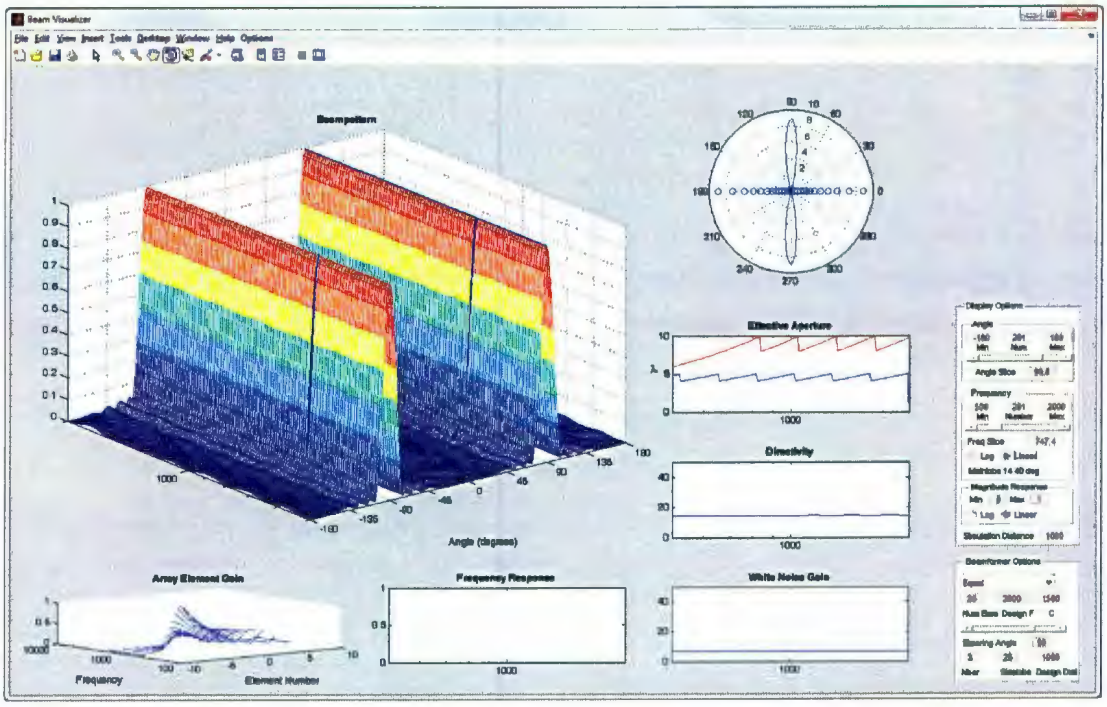

Figure 3.6: The same beamformer as Figure 3.2 shown with linear frequency and beamformer response axes.

coordinates and time delay, and repeated entries are allowed. This allows completely general beamformers, including those that perform multiple samples at different times from the same point in space. There is a gain matrix, and there is a row in the gain matrix which represents the frequency-dependent gain for each space-time sample location. Finally, there is a vector of frequencies that identify the columns in the gain matrix.

Each synthesis function accepts whichever of the following design parameters are appropriate, e.g. the number of desired elements, design frequency, the propagation speed in the medium c, sidelobe specification, steering direction, etc., and returns the standard beamformer data structure. For the case of synthesis techniques that require inconveniently long computational times, there is a facility for loading a MAT-file, which is a binary data file containing the beamformer data structure, which can be computed separately.

The first drop down box selects the general type of beamformer to be simulated. The remaining options do not apply to every beamformer type. The leftmost editbox is for the number of array elements, followed by design frequency and propagation speed. Typically, the design frequency determines the array spacing for simpler beamformer types. Figure 3.5 shows an 11-element linear array designed for 750 Hz in water ($c = 1500\,\mathrm{m/s}$), which implies an element spacing of 2 m. The beamformer is designed with a Taylor weighting (see Section 4.2.3) with a target sidelobe level of -25 dB. The beamformer look direction is set to 104.4 degrees, reflected in both the beampattern response plot and the polar plot. The frequency response plot shows the frequency response of the beamformer to a signal from the direction 99 degrees, which rolls off with increasing frequency since the mainlobe gets narrower with frequency.

A limitation of BeamVisualizer is that the internal code and the user interface

must be modified in order to implement synthesis methods that require other parameters besides those already existing in the interface.

The final editboxes are design parameters specific to only a few beamformer types. Several types of synthesis methods accept a sidelobe specification, notably the Taylor and Dolph-Chebyshev weightings. Nbar is an input to the calculation of Taylor weightings and the design distance is an input to the Modal Analysis Synthesis (MAS) method.

3.2.4 Relative Aperture Size

As discussed in Section 2.5.2, the criteria for choosing an element spacing depends somewhat on the intended application of the array. However, most authors choose to use $\lambda/2$ to satisfy the requirements of the sampling theorem.

I was unable to find any quantitative method for evaluating or comparing array geometries in the literature. As a tool for evaluating some of the broadband array designs in subsequent chapters I decided to produce a plot of effective array aperture (in wavelengths) over all the desired frequencies. The criteria I used to determine the effective array aperture at any given frequency was the extent of the array which was sampled at a density greater or equal to $\lambda/2$.

For linear arrays designed for broadband beamformers, the typical configuration consists of a symetrical arrangement of elements with the most closely spaced elements in the middle, and more widely spaced elements occurring as elements are placed further from the center of the array.

I only evaluate arrays on this criteria when the array has elements with uniformly increasing element separations. I have not attempted to implement an algorithm to evaluate arrays that may have multiple, separate regions of high density sampling

separated by sections of low density sampling. This would have been unnecessarily complex since most arrays of interest meet the criteria above. Additionally, it is unclear how to best quantify the aperture size for an array with more than one section of high element density. The further these sections are apart, the more each may appear like an independent beamformer.

I have also only designed this to evaluate linear arrays and have not attempted to extend this to two- or three-dimensional arrays. The algorithmic complexity of determining areas or volumes that are sampled at or above a particular spatial frequency given an arbitrary distribution of array elements is beyond the scope of this thesis.

3.3 Summary

This chapter described methods and tools for the numerical computation of an arbitrary beamformer. The MATLAB tool which implements this beampattern simulation technique is described. BeamVisualizer provides a convenient display which shows many useful characteristics of a beamformer simultaneously. The software allows the designer to interactively modify the various displays, as well as switch nearly instantaneously between different beamformers designed with the same design parameters. This instantaneous comparison provides quicker feedback and more rewarding insight than that obtained by painstaking comparison of published results in books and papers, which invariably use different plot types, scales and view points.

Chapter 4

Beamformer Synthesis

There are many methods to synthesize a beamformer. Ideally the choice of method will take into account the required bandwidth, available number of sensors, desired beam pattern, available computational power and possibly other factors.

The earliest design methods referenced in Section 1.2.3 concentrated on narrow frequency ranges. This situation is common in many array applications including radio, radar, ultrasound, radio astronomy and active sonar. Broadband beamformers are used in areas such as passive sonar, teleconferencing, and consumer audio. This is a newer area of research, and has a relatively higher proportion of acoustics applications.

This chapter begins with basic information on electronic steering of arrays, and then summarizes the classical narrowband beamformers: uniform, Dolph-Chebychev and Taylor apertures. BeamVisualizer is used to generate plots to illustrate the characteristics of these beamformers over broadband frequency ranges. The first broadband design method introduced is harmonic nesting, and the impact of array geometry on broadband performance will be illustrated, again using the visual output from BeamVisualizer. Finally, several modern broadband design methods are

summarized and illustrated.

4.1 Beamformer Steering

To steer the main beam of a beamformer, the output of each array element must be time delayed separately so that a signal arriving from the desired direction will sum coherently at the final output of the beamformer processing system. To calculate the required time delay, we take an arbitrary reference point. For convenience we choose the origin as a reference point.

If the choice of reference point results in a negative delay, it is trivial to apply a constant delay to all array elements large enough to make all delays positive.

The required steering delay for an individual element is calculated by considering the distance travelled by a wavefront between passing through the array element and passing through the reference point. This distance is divided by the propagation speed in the medium, c, to get the time of propagation for the wavefront from the array element to the reference, and thus, the required time delay for the element.

If the source can be considered to be infinitely distant, then the wavefront will be approximately a plane. If the reference is the origin, then the distance the wavefront will travel from the ith element to the reference is the distance of that array element from a plane normal to the direction of propagation and passing through the origin. This distance is the dot product of the element's position vector and a unit vector normal to the plane.

Under the assumption of plane waves and farfield sources, the required steering delays are the projection of each element position vector onto the unit vector in the direction of the wavefront. This projection is equivalent to the dot product of the

position vectors and the steering vector.

$$t_i = \frac{\vec{r}_i \cdot \hat{k}}{c} \tag{4.1}$$

where t_i is the required time delay and $\vec{r}_i$ is the position vector for the ith element, and $\hat{k}$ is the unit vector opposite to the direction of travel of the plane wave. In other words, $\hat{k}$ is a unit vector in the direction of the infinitely-distant source, which is equivalent to the desired look direction, or steering direction.

Note that if the array is one-dimensional along the x-axis and the analysis is restricted to the xy-plane then Equation 4.1 reduces to the following expression, which is geometrically intuitive:

$$t_i = \frac{1}{c}(x_i x_k + y_i y_k) \tag{4.2}$$

or equivalently

$$t_i = \frac{1}{c}(x_i cos\phi + y_i cos\phi) \tag{4.3}$$

or in polar coordinates

$$t_i = \frac{1}{c}(r_i cos(\theta_i - \phi) \tag{4.4}$$

where x_i and y_i are x and y components of the position vector of the ith array element, x_k and y_k are the x and y components of $\hat{k}$.

4.2 Narrowband Beamformers

Conceptually, a narrowband beamformer has a single design frequency. As a rule of thumb, an array that operates over a bandwidth that is a small fraction of the design

frequency is considered narrowband.

Recall from Section 2.1.1 that the analysis equation for a narrowband beamformer based on a uniformly weighted and equally spaced array has the same structure as the discrete time Fourier transform (DTFT) of a rectangular window function. This leads to the idea of a beamformer as a spatial filter. Each array element is a spatial sample point. In the same way that a different window function used on a time series can reduce spectral leakage, weighting the individual array elements differently (by adjusting the relative gain of each element) can reduce spatial leakage. Spatial leakage manifests as sidelobes in an array beampattern. Careful choice of gains for array elements can control the magnitude and angular position of sidelobes (and the mainlobe as well). Various early authors found several "optimal" array weightings (spatial windows if you like) based on different criteria. Particularly important windows include the rectangular window (used in the uniform linear array) as well as the Dolph-Chebychev and Taylor weighting functions. These will be discussed in the following sections.

Controlling the phase of the signal at each element can also affect the mainlobe width and sidelobe energy, particularly in the technique known as supergain. Supergain uses destructive interference between signals from array elements to reduce unwanted signals beyond what would otherwise be possible. Supergain has the disadvantage of dramatically reducing the white noise gain for a beamformer as well. Supergain is inherently possible in beamformers designed by the Modal Subspace Decomposition (MSD) method, but aside from those designs, supergain will not be analysed in further detail.

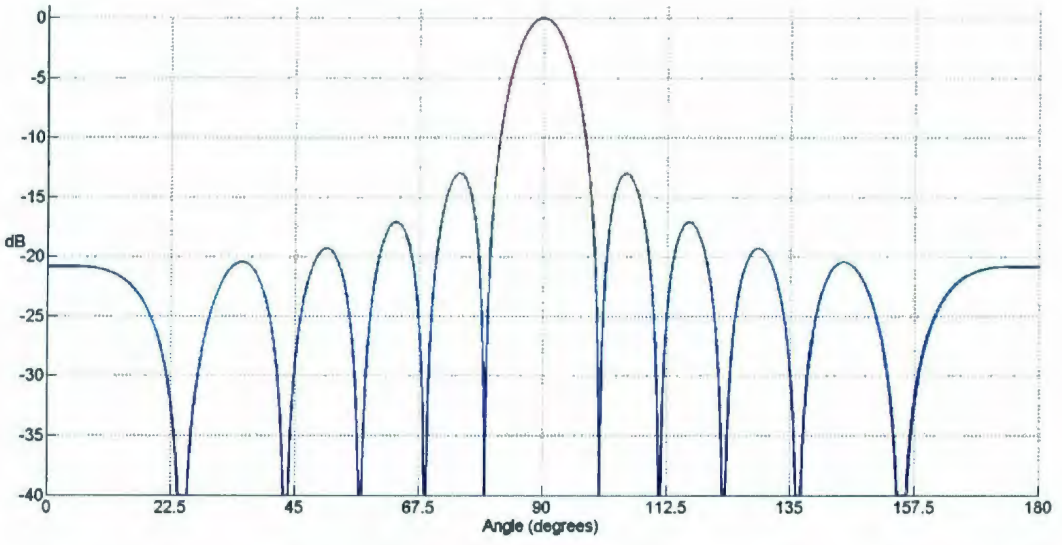

Figure 4.1: Beampattern of an 11-element uniform linear array.

4.2.1 Uniform Linear Array

The basic beamformer is a uniform linear array (ULA). A ULA has unity gain at each element and typically has equal $\lambda/2$ element spacing. The basic beampattern of the ULA has the first sidelobe at -13 dB relative to the main lobe.

The beampattern of a ULA beamformer based on a 11-element linear array at its design frequency is shown in Figure 4.1. Further discussion of design of the ULA and other narrowband beamformers is in Section 5.1.

4.2.2 Dolph-Chebyshev

The Dolph-Chebyshev Method uses Chebyshev polynomials to compute the weights for the beampattern with the narrowest possible mainlobe width (-3 dB points) for a given uniform sidelobe level. As the sidelobe specification becomes more aggressive,

the tradeoff is a wider main lobe.

The Dolph weighting has the minimum main-lobe width for a given sidelobe level [74]. In 1946 Dolph [21] found that a beampattern with equal sidelobes could be represented as a combination of Chebychev polynomials. This expression for the beampattern can be written as a finite expansion with a finite Fourier transform, and thus an analytical expression for the weights of an optimal beampattern can be found.

Lynch [74] presents a summary of the Dolph-Chebyshev design that is slightly different than the original papers, summarized as follows.

The Chebyshev polynomials are

$$T_n(x) = \begin{cases} \cos(n \cos^{-1} x), & |x| \leq 1; \\ \cosh(n \cosh^{-1} x), & |x| > 1. \end{cases} \tag{4.5}$$

and by inspection we can see that

$$\begin{aligned} T_0(x) &= 1, \\ T_1(x) &= x, \\ T_n(x) &= 2xT_{n-1}(x) - T_{n-2}(x), n \geq 2 \quad . \end{aligned} \tag{4.6}$$

$T_n(x)$ is an nth-order polynomial in x, is even or odd as n is even or odd, has n zeros in the interval $(-1, 1)$, has $n + 1$ extrema in the interval $[-1, 1]$, $T_n(x) > 1$ if $x > 1$, and $T_n(x)$ oscillates between -1 and $+1$ for x in $[-1, 1]$. If we define the desired array beampattern as

$$W(\theta) = \frac{T_{2M}[x_0 \cos(\theta/2)]}{T_{2M}(x_0)} \tag{4.7}$$

where $x_0 > 1$, then $W(\theta)$ is 1 at $\theta = 0$ and oscillates between $\pm r$ for angles approaching π, where $r = 1/T_{2M}(x_0)$. The transition point is θ_s such that $x_0 \cos(\theta_s/2) = 1$. $W(\theta)$ is symmetric about the origin and for a given sidelobe height r has a minimum mainlobe width. By using basic trigonometric identities, $W(\theta)$ can be rewritten as

$$W(\theta) = \sum_{n=-M}^{M} w_n e^{-jn\theta} \tag{4.8}$$

which has a finite Fourier transform. The coefficients w_n are the weights of the M array elements, computed by the inverse transform according to

$$w_n = \frac{1}{N}\left[1 + 2r \sum_{m=1}^{M} T_{2M}\left(x_0 \cos\frac{\theta_m}{2}\right) \cos(m\theta_n)\right] \tag{4.9}$$

where $|n| \leq M$, $N = 2M$, and $\theta_m = 2\pi m/N$.

Despite the fact that the Dolph-Chebyshev distribution is an optimal tradeoff between sidelobe amplitude and mainlobe width, it was not widely used because the gains of the end elements of the array are large relative to the other element gains (as may be inferred from the example in Figure 4.2), which makes a physical implementation more error-prone. Additionally, in many applications it is desirable for the amplitude of sidelobes to decay as θ increases, rather than remain constant [2, 24].

A five-element array with Chebyshev weightings for a -25 dB sidelobe specification is shown in Figure 4.2. This beamformer has a mainlobe width of 11.2 degrees, compared to 9.4 degrees for the uniform beamformer. Further comparison of uniform, Taylor and Dolph-Chebychev beamformers is in Section 5.1.

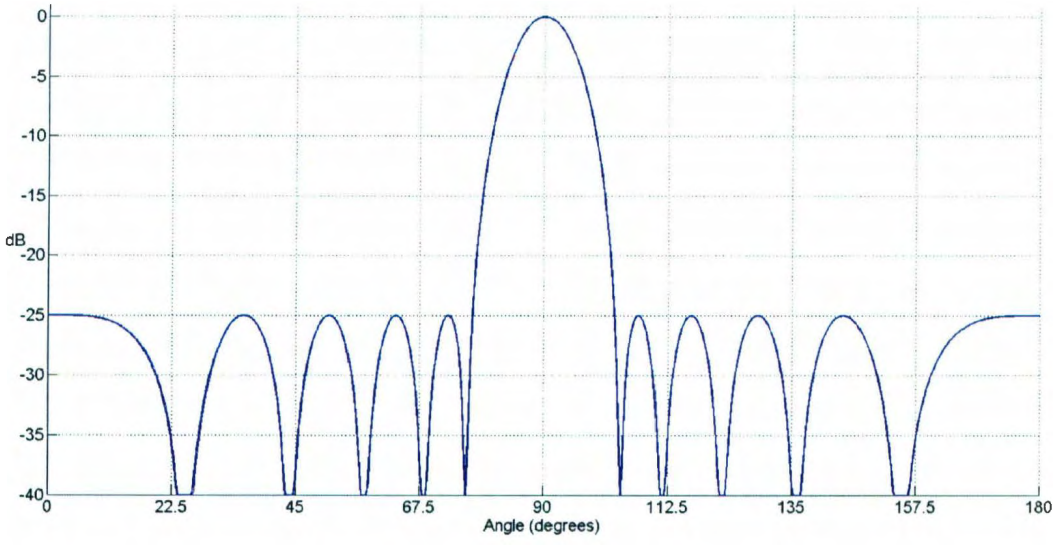

Figure 4.2: Beampattern of an 11-element Dolph-Chebyshev aperture beamformer.

4.2.3 Taylor

Taylor [22] showed that the aperture distribution forms a Fourier transform pair with the array beampattern. This leads directly to synthesis techniques, when the array geometry is uniformly spaced in each dimension. Although Taylor weighting functions have been derived for planar arrays, I will only consider the application to linear arrays.

The Taylor method reduces overall sidelobe energy by allowing sidelobes further from the mainlobe to decrease in amplitude. The tradeoff is that for unrealistic sidelobe specifications some sidelobes can exceed the specification and the mainlobe is wider than the equivalent Dolph-Chebyshev design.

There have been many papers on implementation details of synthesis using Taylor aperture distributions, such as adapting the Taylor distribution for continuous apertures to discrete arrays [24], or determining weights for non-uniformly spaced

arrays [26]. The equations implemented for this thesis are taken from Hansen [6].

The gains for elements of the Taylor distribution are computed as

$$g(p, A, \bar{n}) = 1 + 2\sum_{n=1}^{\bar{n}-1} F(n, A, \bar{n}) \cos np \tag{4.10}$$

where p is the position along the aperture, between $-\pi$ and π, A is the sidelobe specification, $\bar{n}$ is the number of sidelobes to keep at approximately the sidelobe specification before returning to the natural sinc envelope for the sidelobe amplitude, and

$$F(n, A, \bar{n}) = \frac{[(\bar{n}-1)!]^2}{(\bar{n}-1+n)!(\bar{n}-1-n)!} \prod_{m=1}^{n-1} \frac{1-n^2}{z_m^2} \tag{4.11}$$

with

$$z_n = \bar{n} \frac{\sqrt{A^2 + (n-\frac{1}{2})^2}}{\sqrt{A^2 + (\bar{n}-\frac{1}{2})^2}} \tag{4.12}$$

and finally

$$A = \frac{\cosh^{-1}(10^{\frac{S}{20}})}{\pi} \tag{4.13}$$

where S is the desired sidelobe ratio, in dB.

When the array elements are evenly spaced, the gains computed by Equation 4.10 can be used directly, however for non-uniform spacings the values need to be adjusted by a space-weighting factor to compensate for the unequal sampling of the total aperture. This is an essential step to make maximum use of an unequally spaced array in a broadband beamformer designed by frequency decompositions, to be discussed in Section 4.3.1.

An 11-element array with Taylor weightings is shown in Figure 4.3. This beamformer is designed with $\bar{n} = 3$ and sidelobe specification of -25 dB, with a resulting

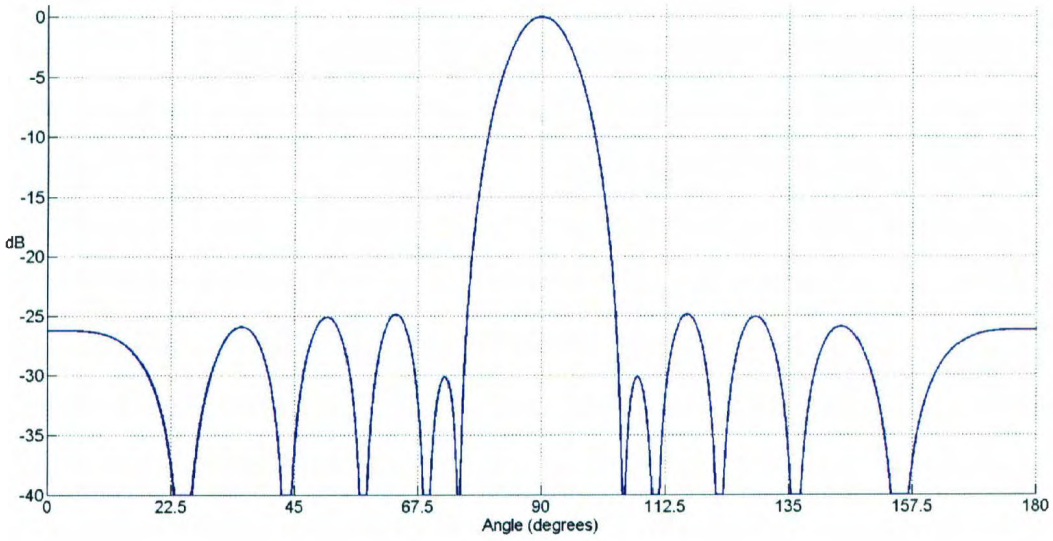

Figure 4.3: Beampattern of an 11-element Taylor aperture beamformer.

mainlobe width of 11.5 degress. Further comparisons of uniform, Dolph-Chebychev and Taylor beamformers are in Section 5.1.

4.3 Broadband Beamformers

The theoretical work of Dolph-Chebyschev and Taylor forms the foundation for most of the field of narrowband beamformer synthesis. While much research was done on implementations, fundamentally these early results form the key standards of what can be achieved with aperture weighting in narrowband arrays. Most applications either seek to minimize both sidelobe level and mainlobe width, or else maximum directivity and white noise gain, and on these criteria the previously discussed narrowband techniques are optimal.

More recently research has focused on methods to synthesize broadband beamformers. Early approaches such as those referenced in Section 1.2.6 involved frequency decomposition. Generally, this approach is to design several narrowband beamformers over a range of design frequencies, and then combine them in some way. From the perspective of contemporary digital signal processing, if the signal at each array element is digitized and then transformed into the frequency domain, each frequency bin can be treated as an individual narrowband beamformer, and classical techniques applied. This is a frequency-domain broadband beamformer. Equivalently, taking the gain in each frequency bin for one element as a filter response for the element, it is possible to use standard filter synthesis techniques to produce an FIR filter for each element to implement the beamformer. This is often referred to as a time-domain broadband beamformer. The time-domain beamformer can provide the simplest implementations for single beams, while frequency domain beamformers are well-suited to producing many different beamformers from the same underlying array.

A second approach to broadband beamformer design is to view the synthesis problem as a global optimization problem. This is tempting since it is relatively straightforward to numerically compute the beampattern of an arbitrary beamformer, which is likely a component of an optimization cost function. Because there are so many free variables, many researchers have considered stochastic techniques for broadband beamformer synthesis. Given a desired beampattern and some constraints on array geometry, element positions and gains can be selected by algorithms such as genetic algorithms, simulated annealing or stochastic region contraction (SRC). Several papers following this approach are described in Section 1.2.7.

A third approach is focused on decomposing some aspect of the beamformer into

a set of orthogonal basis functions that can be used for synthesis. These methods are particularly powerful and provide insight into the synthesis problem. This group of methods is generally referred to as modal techniques in this thesis, and two in particular will be examined.

The first modal technique, Modal Analysis Synthesis (MAS) [67] takes advantage of the fact that solutions to the Helmholtz wave equation can be decomposed into *modes* which are orthogonal functions of spatial coordinates. Since the received signal at a sensor satisfies the wave equation and the output of an arbitrary beamformer is a linear combination of the signals at each sensor, an arbitrary (real) beampattern is also a solution of the wave equation. As long as a beampattern represents the output of a realizable beamformer, a set of elementary aperture functions can be found, each corresponding to a mode of the solutions of the wave equations. The desired beamformer parameters can then be found by finding the correct linear combination of elementary aperture functions corresponding to the decomposition of the beampattern into its modes.

The second modal technique, Modal Subspace Decomposition (MSD) [70] finds a set of orthonormal basis vectors for the set of all attainable beamformers and a set of orthonormal basis functions for all achievable beampatterns for a given array geometry. A desired beampattern can then be projected onto the subspace of achievable beampatterns and the corresponding beamformer weighting coefficients computed, giving the optimum achievable beampattern for a given array geometry and desired beampattern. MSD also enables the designer to control the amount of supergain, if any, allowed in the resulting beamformer.

I will review these approaches: the frequency decomposition method for frequency-domain beamformers based on two different array geometries, both MAS

and MSD synthesis methods, as well as the SRC method for some limited cases.

4.3.1 Frequency Decomposition

Harmonically Nested Arrays

Several papers on harmonically nested broadband arrays are referenced in Section 1.2.6. The technique is to combine an array designed for one frequency with another designed for a multiple of the first frequency. Proper choice of the number of array elements and the scaling factor allow many of the array element positions to coincide, which reduces the total number of elements needed.

For example, for an array of n elements, where n is odd, scaling the array positions by a factor of one half to form a new array at twice the design frequency of the original array will yield a new array with $(n-1)/2$ element positions overlapping the original array.

Intuitively one might guess that for an array with an odd number of elements the most overlap between subarrays occurs for a scale factor of 2 or 1/2. This was verified by computing the scaled positions and number of overlapping elements for all reasonable scaling factors, for example all fractions with numerators up to 20. Correspondingly, for arrays with even numbers of elements the maximum overlap between subarrays happens for scale factors of 3 or 1/3. Most published designs are based on scale factors of 2, however Pirz [43] gives an example of a harmonically nested array with a scale factor of 3.

To get a true broadband design, early designers used analog filters to sum the output of two narrowband beamformers to achieve a smooth transition between the beampatterns at each frequency [41, 43]. With the availability of DSP power, this

is equivalent to transforming the output of each array element into the frequency domain and treating each frequency bin from all array elements as a separate narrowband beamformer. At this point the classical narrowband techniques from Section 4.2 can be applied to build a matrix of aperture coefficients for each element and frequency.

To avoid aliasing at all steering angles the safe approach is to only use array elements at or below the design frequency for the subarray to which they belong. This will be discussed in Section 5.2. The typical beampattern of a harmonically nested beamformer, for example that shown in Figure 5.4, is narrowest exactly at the highest design frequency and gradually widens with decreasing frequency until the next design frequency is reached, where the beampattern returns to the minimum mainlobe width.

The effect of element array element spacings has already been discussed in Section 2.5.2. As will be further explained in Section 5.5, it is possible to capitalize on the presense of additional elements at spacings larger than $\lambda/2$ to improve directivity under certain conditions, such as electronically steering the mainlobe away from broadside.

Optimally Spaced Arrays

The topic of unequally spaced arrays has appeared in the literature several times from different perspectives. The approach presented in this section appeared at least as early as 1995 [54, 55]. Van Der Wal et al. have been cited rarely, and while Ward et al. have been cited fairly often, the array geometry design method is a minor section in the original paper and has not been included in any books, reviews or tutorial papers to my knowledge. I developed the following array geometry guidelines independently

and only later discovered that it reproduces Ward et al. exactly. The extension of the method to generalized harmonic nesting I believe is novel, and unites both the optimally spaced arrays of this section and the harmonically nested arrays of the previous section.

It is well known that the resolving power of an aperture is proportional to its size. That is, a large aperture at a given frequency will have narrower beampattern lobes than a small aperture. To achieve equal performance at all frequencies the active portion of the aperture should remain constant when defined in terms of wavelength. The overall aperture size is determined by the lowest frequency, and the active portion should decrease as the wavelength decreases with increasing frequency.

In a harmonically nested array with subarrays spaced by even 2:1 or 3:1 frequency ratios the size of the active portion of the array in terms of wavelength has large discontinuous changes. Accordingly, the variation of the beampattern between design frequencies is considerable. Examples of this type of beampattern are found in Section 5.2. As previously mentioned, the output of each subarray can be combined using frequency-dependent filters to achieve a more frequency independent beampattern. Any array used above its design frequency could potentially suffer from spatial aliasing depending on steering angle, number of elements, and difference between the active frequency and the design frequency.

To keep the active portion of the array closer to a constant multiple of a wavelength and achieve a more constant beampattern without introducting grating lobes the logical solution is to reduce the scaling factor between arrays. From the study of scaling factors already mentioned, it was found that the four scale factors greater than 1/2 (or less than 2) resulting in the most overlap between subarrays are: 2/3, 3/4, 3/5, and 4/5. In each case the proportion of coincident element positions shared

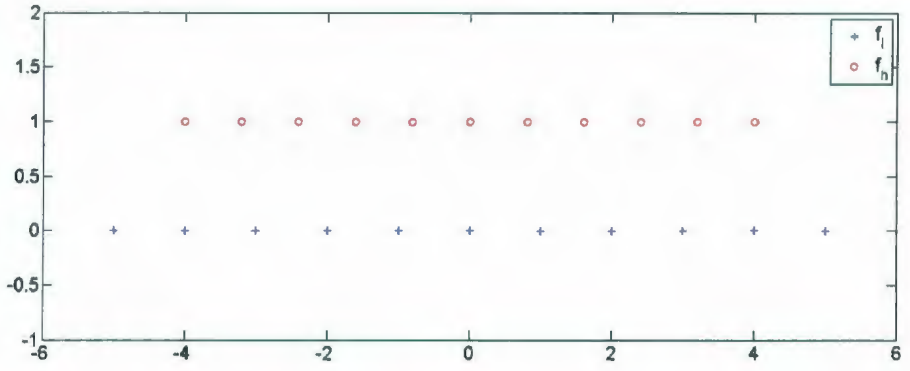

Figure 4.4: Relative array positions for two subarrays designed for frequencies f_l (in blue) and $f_h = 5/4 f_l$ (in red).

between subarrays asymptotically approaches the denominator of the scale factor: 1/3, 1/4, and 1/5, respectively. The benefit of sharing elements between subarrays is substantially less at these scaling factors, and so I have not been able to find any published examples of harmonically-nested arrays using these scale factors.

Take for example an 11-element subarray designed for f_l, and a subarray scaled by 4/5 designed for $f_h = f_l * 5/4$, as shown in Figure 4.4. The two subarrays only share three positions, requiring a total of 19 elements to implement this array designed to cover a relatively small range of frequencies. However, the entire center portion of the aperture is sampled much more densely than required by either subarray. Since the elements of the higher frequency f_h subarray are spaced closer than $\lambda_l/2$, it is no compromise to omit elements 2 through 10 of the lower frequency subarray entirely, acheiving adequate sampling at both frequencies with only 13 elements. The only remaining issue is that the array aperture at f_l is now sampled more densely in the center portion of the array than elsewhere.

To sample a desired continuous aperture function such as a Taylor or Dolph-Chebyshev distribution with unequally spaced sample points, trapezoidal integration

is used [54] throughout the discussion in Chapter 5. This ensures that signals from the central portion of the array are not too heavily weighted in the beamformer summation. Other design techniques discussed later such as MAS and MSD explicitly allow arbitrary array geometries.

The example of Figure 4.4 shows that expanding the array aperture by adding pairs of elements spaced to keep the overall aperture a constant multiple of λ will produce the optimum array in terms of most equal spatial resolution over the frequency range of the beamformer for a given number of array elements.

The following formulation for optimal array element spacing was independently derived, and then found to be essentially the same as given by Ward et al. [54] with a small adjustment for a symmetrical array centered on the origin (Ward et al. initially consider just the case of the half-array on the positive x-axis). While Ward et al. mention the optimality of the geometry, this is not the central point of that paper.

Assuming an element spacing of $\lambda/2$ and a discrete array on the x-axis centered on the origin, let

$$A_i = m\frac{\lambda_i}{2} \tag{4.14}$$

where λ_i is wavelength at the ith design frequency, A_i is the length of the active portion of the array at λ_i and m is an integer number of half-wavelengths characterizing the overall aperture size. At the upper design frequency f_h and shortest wavelength λ_u, there will need to be $n_u = m + 1$ elements spaced by $\lambda_u/2$.

Now consider frequencies just below the upper design frequency. At some lower frequency it will become true that adding a pair of elements spaced by $\lambda_i/2$ will

exactly increase the array size back to the multiple of wavelength given in Equation 4.14, so we can write another constraint on the elements

$$A_i = A_{i-1} + \lambda_i. \tag{4.15}$$

and from there we find

$$\begin{aligned} m\frac{\lambda_i}{2} &= m\frac{\lambda_{i-1}}{2} + \lambda_i \\ \lambda_i &= \frac{m}{m-2}\lambda_{i-1}. \end{aligned} \tag{4.16}$$

The expansion of Equation 4.15 can be repeated as many times as necessary to reach the desired lowest effective frequency and thus the desired bandwidth. After j repetitions the lowest effective wavelength of the array is

$$\lambda_l = \left(\frac{m}{m-2}\right)^j \lambda_u \tag{4.17}$$

and the total number of elements is

$$\begin{aligned} n &= n_u + 2j \\ n &= (m+1) + 2j. \end{aligned} \tag{4.18}$$

Define the scale factor $S = \frac{m}{m-2}$ and bandwidth ratio $\beta = \lambda_l/\lambda_u$ and rearranging Equation 4.17 we can state

$$\begin{aligned} \beta &= S^j \\ \beta &= \left(\frac{m}{m-2}\right)^j. \end{aligned} \tag{4.19}$$

The position of the ith element is given by

$$\begin{array}{ll} \pm i\frac{\lambda_u}{2} & 0 \leq i \leq m/2; \\ \pm\frac{\lambda_u}{2}(\frac{m}{2})(S^{i-m/2}) & m/2 < i \leq m/2 + j. \end{array} \tag{4.20}$$

Note that the size of the aperture in terms of wavelengths determines the maximum spatial resolution of the resulting broadband beamformer. If we define $P = m/2$ as the size of the aperture in wavelengths, then we can rewrite Equation 4.20 as

$$\begin{array}{ll} \pm i\frac{\lambda_u}{2} & 0 \leq i \leq P; \\ \pm\frac{\lambda_u}{2}(P)(\frac{P}{P-1}^{i-P}) & P < i \leq P + j \end{array} \tag{4.21}$$

and if we rewrite Equation 4.19 and combine with Equation 4.17 we find the required number of iterations to be

$$\begin{aligned} j &= \lceil \frac{\log \beta}{\log S} \rceil \\ j &= \lceil \frac{\log \frac{\lambda_l}{\lambda_u}}{\log \frac{P}{P-1}} \rceil \end{aligned} \tag{4.22}$$

and thus the total number of required elements becomes

$$n = (2P + 1) + 2\lceil \frac{\log \frac{\lambda_l}{\lambda_u}}{\log \frac{P}{P-1}} \rceil \tag{4.23}$$

which is equivalent to the original result [54] except for the difference between a single-sided array and a symmetrical array about the origin.

This is a system of two equations in four unknowns, and the four unknowns are the design parameters β, n, j, and m (or equivalently P). The design process is to decide which two parameters will be chosen by the designer, then choose values for those two parameters, and finally compute the other two parameters.

For example, to design a broadband beamformer with a mainlobe of approximately 12 degrees covering a decade in frequency we immediately know that $\beta = 10$. Analytical formulae exist to compute the beamwidth for various narrowband aperture functions, but it is easy to use BeamVisualizer to find that an 11-element Taylor beamformer with an aperture of 5λ has a mainlobe of approximately 12.5 degrees. So, choosing $P = 5$ implies $S = 5/4$, and we find from Equation 4.22 that $j = 11$ and from Equation 4.18 that $n = 33$.

As another example, it is shown in Section 5.1 that a five-element array with Dolph-Chebyshev weighting and -25 dB sidelobes has a mainlobe width of about 26 degrees. Since that beamformer assumes $\lambda/2$ spacing, five elements implies $m = 4$, $P = 2$, and $S = 2$. If we choose to expand the array in four steps (adding a total of 8 elements), $j = 4$ and by Equation 4.19 $\beta = 2^4 = 16$ and $n = 13$. This tells us that a broadband beamformer capable of forming beams with spatial resolution equivalent to the five-element narrowband beamformer can effectively cover a frequency ratio of 16:1 with $n = 13$ elements. Since $S = 2$ we can infer that this is equivalent to simple harmonic nesting as previously described.

General Harmonic Nesting

The final example in the previous section is a case of simple 2:1 harmoic nesting, designed using the equations for an optimal array spacing. This suggests there is a generalization that can include both harmonic nesting geometries as well as optimally spaced geometries.

To fully parameterize the array element placement rules from the previous section, we note that array elements may be placed at a spacing other than $\lambda/2$, and that subarrays at lower frequencies may add more than one pair of elements at a time.

If the element spacing at a given frequency is an arbitrary fraction of wavelength, then the equation for the desired aperture at any frequency becomes

$$A = m\delta\lambda \tag{4.24}$$

where A is the relative aperture size for wavelength λ, δ is the element spacing in fractions of a wavelength, and m is the spacing multiple.

At the highest frequency f_u the array still needs $n_u = m+1$ elements now spaced by $\delta\lambda_u$. Adding one element at each end of the array will increase the aperture size by $2\delta\lambda_i$ for some intermediate frequency f_i. However, an arbitrary number of elements could be added at each expansion step, which I will call the expansion increment, x. The total array size is

$$A_i = A_{i-1} + 2x\delta\lambda_i \tag{4.25}$$

and

$$\begin{aligned} m\delta\lambda_i &= m\delta\lambda_{i-1} + 2x\delta\lambda_i \\ \lambda_i &= \frac{m}{m-2x}\lambda_{i-1} \\ \frac{\lambda_i}{\lambda_{i-1}} &= \frac{m}{m-2x}. \end{aligned} \tag{4.26}$$

Now the scale factor is

$$\begin{aligned} S &= \frac{m}{m-2x} \\ S &= \frac{P}{P-x} \end{aligned} \tag{4.27}$$

and

$$\beta = \left(\frac{P}{P-x}\right)^j \tag{4.28}$$

and

$$j = \lceil \frac{\log \beta}{\log S} \rceil \tag{4.29}$$

and

$$n = (2P + 1) + 2xj. \tag{4.30}$$

Two new design parameters are added: δ and x, however δ is independent of the other parameters, so it can be freely chosen. It is well-known that for an unsteered linear array, spatial aliasing does not occur until the element spacing reaches λ [54]. Careful inspection of the directivity plots for classical narrowband beamformers without delay steering (that is, steered to broadside) shows that maximum directivity occurs not when the element spacing is $\lambda/2$, but at just less than λ. Therefore, if it is known that a beamformer will not be electronically steered off-axis it is advantageous to choose a spacing larger than $\lambda/2$, that is, $0.5 < \delta < 1$.

The other new parameter x can be thought of as a tuning parameter, allowing the designer to trade off between the subarray scaling ratio S and the overall beamformer bandwidth ratio β, for constant values of n. Large values of x result in larger values of S but smaller β. In other words, larger jumps between subarray design frequencies result in more frequency variation in beampatterns, but larger overall beamformer bandwidth. This will be illustrated in design examples in Section 5.2.

4.3.2 Modal Analysis Synthesis

As already explained, MAS [67] decomposes a beampattern into a set of elementary beampattern modes, which are orthogonal basis functions for the set of possible beampatterns. Each mode has a corresponding elementary aperture function. Any realizable beampattern is a linear combination of the elementary modes, and thus

its corresponding beamformer parameters can be found by a linear combination of the respective elementary aperture functions.

The MAS method allows the designer to compute the required gain for each array element at a given frequency to best approximate a desired pattern in a MMSE sense. By iterating this procedure over several frequencies a frequency-domain beamformer is designed. The method given by Abhayapala [67] is summarized below.

Any signal received by an array sensor must be a solution to the classical wave equation. Since the output of a beamformer is a linear combination of the sensor inputs, it too must be a solution of the wave equation. The modal analysis technique takes advantage of the fact that solutions to the wave equation can be decomposed into *modes* which are orthogonal functions of spatial coordinates. Using the modal decomposition of the output of a linear, continuous aperture beamformer, it is shown that the aperture weighting function $\rho_r(z;k)$ can be written as

$$\rho(z;k) = \sum_{n=0}^{\infty} A_n(k)(-i)^n 2k \frac{R_n(\infty,k)}{R_n(r,k)} j_n(kz) \tag{4.31}$$

where

$$A_n(k) = \frac{2n+1}{2} \int_0^{\pi} b_r(\theta;k) P_n(\cos\theta) \sin\theta d\theta \tag{4.32}$$

$$R_n(r,k) \triangleq re^{jkr} h_n^{(2)}(kr) \tag{4.33}$$

$$h_n^{(2)}(kr) = \sqrt{\frac{\pi}{2kr}} H^{(2)}_{n+\frac{1}{2}}(kr) \tag{4.34}$$

$b_r(\theta,k)$ is the beampattern, j_n is the spherical Bessel function of the first kind, P_n is the associated Legendre function, H_n is the half odd integer order Hankel function of the second kind, k is the wavenumber and r is the range from the array

at which the desired beampattern is to be realized. Note that this expression for the aperture weighting function is defined in terms of the desired beampattern. This is possible because of the Fourier transform relationship between a beampattern and the aperture weighting function. For the full derivation see Abhayapala [67].

Given a continuous aperture sensor, the final output of a frequency-domain beamformer (the Fourier transform of the time-series output) in the frequency-domain can be written as

$$Z(k) = \int_{-\infty}^{\infty} S(z;k)\rho_r(z;k)dz \tag{4.35}$$

where $S(z;k)$ is the Fourier transform of the received signal at a point z on the continuous sensor and $\rho_r(z;k)$ is the aperture weighting function.

Using trapezoidal integration [54] the final output of a continuous sensor given in Equation 4.35 can be approximated by a discrete set of array elements by

$$\tilde{Z}(k) = \sum_{q=-Q}^{Q} S(z_q;k)g_q\rho_r(z_q;k) \tag{4.36}$$

where z_q is a set of $2Q+1$ discrete sensors and g_q is a spatial weighting term to account for the possibly non-uniform sensor locations in the approximation of the integration. For trapezoidal integration

$$g_q = \begin{cases} \frac{1}{2}(z_{q+1} - z_{q-1}) & \text{if} |q| < Q \\ \frac{1}{2}(z_Q - z_{Q-1}) & \text{if} |q| = Q. \end{cases} \tag{4.37}$$

In the case of the continuous sensor or aperture it is natural to think of $\rho_r(z;k)$ primarily as a function of position along the sensor, however in the case of a discrete sensor it is helpful to think of $\rho_r(z_q;k)$ primarily as a function of frequency. The

total beamformer can then be seen as a collection of filter responses, one for each sensor location. The filter response for the qth individual array element is given by $g_q \rho_r(z_q; k)$.

It is helpful to rewrite Equation 4.31 as

$$\rho_r(z_q; k) = \sum_{n=0}^{\infty} A_n(k) G_n(r; k) F_n(z_q; k) \tag{4.38}$$

where

$$F_n(z_q; k) \triangleq 2(-i)^n j_n(kz) \tag{4.39}$$

$$G_n(r; k) \triangleq k \frac{R_n(\infty, k)}{R_n(r, k)}. \tag{4.40}$$

Since the desired beampattern $b(\theta, k)$ is produced solely by correct choice of $A_n(k)$, the $A_n(k)$ terms are referred to as the *beam shape filters*. Similarly all $G_n(r; k)$ are determined solely by the range r at which the desired beampattern should be realized so they are called the *radial focusing filters*. Since $F_n(z_q; k)$ only depends on the array geometry, specifically the sensor locations z_q, they are called the *elementary filters*. In an adaptive beamformer, these can be precomputed to reduce the computational requirements of each adaptive iteration.

To precisely represent the desired beampattern with a given aperture weighting function, an infinite number of modal terms are required in the summation in Equations 4.38. In practice, however, Abhayapala asserts that the first 16 modes (that is, $n = 15$) are sufficient to approximate most reasonable beampatterns [67].

To design a specific beamformer, first compute g_q and F_n according to Equation 4.37 and Equation 4.39. G_n can be calculated from Equation 4.40 and Equation 4.33, however it can also be simplified to

$$G_n(r;k) = \frac{2(-j)^{n+1}}{re^{jkr}h_n^{(2)}(kr)}. \tag{4.41}$$

Finally, calculate A_n from the desired beampattern according to Equation 4.32.

The number of uniformly spaced sensors in one side of the array is given by

$$Q = \lceil \frac{a_N}{\pi} \rceil, \tag{4.42}$$

where a_N is a constant determined by the number of modes used in the approximation of $\rho_r(z_q;k)$, and $\lceil \cdot \rceil$ is the ceiling function. For $n = 15$, $a_N = 20.54$. A table of constants is provided by Abhayapala [67] for modes up to 16.

The total number of elements is

$$L = Q + \lfloor \frac{\log(\frac{a_N k_u}{Q\pi k_l})}{\log(1+\frac{\pi}{a_N})} \rfloor, \tag{4.43}$$

where k_u and k_l are the upper and lower frequency limits, respectively, and $\lfloor \cdot \rfloor$ is the floor function. The element positions are given by

$$z_q = \begin{cases} \frac{q\pi}{k_u} & \text{for } |q| \leq Q \\ \frac{Q\pi}{k_u}(1+\frac{\pi}{a_N})^{|q|-Q} & \text{for } Q < |q| \leq L. \end{cases} \tag{4.44}$$

Note that in the calculation of the elementary filters F_n there is a division by zero. However, $\lim_{kz\to 0} F_n$ is finite. In a practical implementation it is necessary to compute the value of F_n at zero by substituting a sufficiently small value of kz.

The design example given by Abhayapala is discussed in Section 5.3.

4.3.3 Modal Subspace Decomposition

The Modal Subspace Decomposition (MSD) method [70] is designed to calculate the required FIR taps for a time-domain beamformer with MMSE relative to a desired beampattern. It presumes a beamformer based on a digitally sampled, discrete-time signal processing system. It is naturally suited to broadband array designs, which are often implemented with FIR filters at each array element. For frequency-domain implementations, the filter taps for each array element can be transformed into a discrete filter response.

In this method, the array geometry is defined by four coordinates for each array element: a three-dimensional position and a time-delay. This convention for specifying the array geometry is quite general and can handle irregular geometries, as well as sensors that move in time relative to the rest of the array.

If each tap of an FIR filter attached to an array sensor is considered a separate space-time sample point, then the entire beamformer can be seen as a large vector of gain values, or weights, for each space-time sample. The dimensionality of this space is the number of array elements multiplied by the number of taps in each FIR filter.

Given there are M space-time samples and the weight for each sample may be complex-valued, define the M-dimensional complex vector space $\mathcal{S}$ as the space of all finite energy weight vectors,

$$\mathcal{S} \triangleq \{\boldsymbol{w} : |\boldsymbol{w}| < \infty\}. \tag{4.45}$$

based on the inner product

$$\langle \boldsymbol{w}, \boldsymbol{y} \rangle_{\mathcal{S}} = \sum_{m=0}^{M-1} w_m y_m^*, \tag{4.46}$$

where $*$ denotes the complex conjugate, and associated norm

$$|\boldsymbol{w}|_{\mathcal{S}} = \sqrt{\langle \boldsymbol{w}, \boldsymbol{y} \rangle_{\mathcal{S}}}. \tag{4.47}$$

Each weighting vector $\boldsymbol{w} \in \mathcal{S}$ has a unique mapping to an achievable beampattern according to

$$W_{ach}(k, \phi) \triangleq \sum_{m=0}^{M-1} w_m e^{jk[ct_m + x_m \cos(\theta_m - \phi)]}, \tag{4.48}$$

so we define $\mathcal{W}$ as the space of achievable beampatterns, with a mapping to $\mathcal{S}$ defined by the invertible linear operator $A : \mathcal{S} \rightarrow \mathcal{W}$.

Given A^* exists [70, 75], the M eigenvectors of A^*A denoted $\boldsymbol{u}_n$ form a complete orthonormal basis for $\mathcal{S}$, and the M eigenfunctions of AA^* denoted $U_n(k, \phi)$ form a complete orthonormal basis for $\mathcal{W}$.

The desired beampattern is $W_{des}(k, \phi)$ and $\mathcal{F}$ is defined as the space of desired beampatterns with finite energy over the design ranges of k and ϕ,

$$\mathcal{F} \triangleq \{W_{des}(k, \phi) : |W_{des}|_{\mathcal{F}} < \infty\}, \tag{4.49}$$

based on the inner product

$$\langle W, Y \rangle_{\mathcal{F}} = \int_{k_1}^{k_2} \int_{-\pi}^{\pi} W(k, \phi) Y^*(k, \phi) k d\phi dk, \tag{4.50}$$

and associated norm

$$|W|_{\mathcal{F}} = \sqrt{\langle W, W \rangle_{\mathcal{F}}}. \tag{4.51}$$

Since $\mathcal{F}$ is an infinite dimensional, seperable, Hilbert space [70, 75] and $\mathcal{W}$ is a finite space, $\mathcal{W}$ is a subspace of $\mathcal{F}$. Given the desired beampattern $W_{des}(k, \phi) \in \mathcal{F}$, the projection of $W_{des}(k, \phi)$ onto the subspace $\mathcal{W}$ minimizes the mean square error (MSE) between $W_{des}(k, \phi)$ and $W_{ach}(k, \phi)$[75]. Having found the best achievable beampattern, the corresponding weight vector can be computed numerically.

The steps of the method are:

1. Calculate the $M \times M$ matrix $\boldsymbol{Z}$ according to

$$\boldsymbol{Z}_{m,m'} = 2\pi \int_{k_1}^{k_2} e^{jkc(t_{m'} - t_m)} J_0(k\|\boldsymbol{x}_m - \boldsymbol{x}_{m'}\|) k dk, \tag{4.52}$$

   where $\boldsymbol{x}_m$ is the position vector of the mth sensor, and t_m is the time delay of the mth sensor.

2. Calculate the eigenvectors $\boldsymbol{u}_n$ and eigenvalues λ_n that solve the matrix eigenvector equation

$$\boldsymbol{Z}\boldsymbol{u}_n = \lambda_n \boldsymbol{u}_n \text{ for } n = 0, \ldots, M-1, \tag{4.53}$$

   Order the real, non-negative eigenvalues to form a monotonically decreasing series $\lambda_0 \geq \lambda_1 \geq \ldots \geq \lambda_{M-1}$ and then calculate

$$U_n(k, \phi) = \frac{1}{\sqrt{\lambda_n}} \sum_{m=0}^{M-1} \boldsymbol{u}_{n,m} e^{jk[ct_m + x_m \cos(\theta_m - \phi)]}. \tag{4.54}$$

3. Calculate the weights of each array element by

$$\boldsymbol{w} = \sum_{n=0}^{M-1} \frac{\langle W_{des}, U_n \rangle_{\mathcal{F}}}{\sqrt{\lambda_n}} \boldsymbol{u}_n, \tag{4.55}$$

where

$$\langle W_{des}, U_n \rangle_{\mathcal{F}} = \int_{k_1}^{k_2} \int_{-\pi}^{\pi} W_{des}(k, \phi) U_n^*(k, \phi) k d\phi dk. \tag{4.56}$$

The design examples given by Williams et al. [70] involve designing beampatterns for uniform circular arrays with small numbers of elements over a 10:1, or decade, bandwidth. While this is interesting and shows the power of the technique, the designs appear to rely heavily on superdirectivity and the published beampattern plots use linear magnitude response rather than decibels, and so are hard to immediately compare with more familiar beampatterns. Since this thesis is focused on linear arrays I will not analyze the MSD authors' design examples further.

4.3.4 Stochastic Region Contraction

Global optimization is a difficult problem without specific information about the character of the function to be optimized. Problems may often have large numbers of variables and many, many local minima. Stochastic techniques such as simulated annealing are very general but often very expensive in terms of number of function evaluations. Stochastic Region Contraction (SRC) is intended to solve a restricted set of global optimization problems more efficiently than techniques like simulated annealing. Berger and Silverman [62] and Alvarado [76] applied the SRC method to designing broadband beamformers for speech applications.

There is other research cited in Section 1.2.7, which uses other global optimization

methods. The SRC method is included in this thesis because it played a role in the early development of this thesis, for both the computational efficiencies of the method as well as the application domain Berger and Silverman studied. It was later decided that the effort to implement an additional stochastic technique for comparison would be prohibitive.

The cost function that Berger and Silverman chose to minimize is the maximum value of the noise power in a forbidden zone, assumed to be where noise sources would be located, while holding beamformer output constant for sources at a target location directly in front of the array. The noise power for a source at each position in the forbidden zone is averaged across the design frequency band before finding the maximum value of the noise power. Berger and Silverman called their cost function the extended power spectral distribution (PSDX). This function is described in detail by Silverman in an earlier paper [77].

To successfully apply the SRC method, the cost function should meet the following conditions [62, 76]:

1. the function has a small number of large valleys, with perhaps a large number of small valleys superimposed on them;
2. the function has a strong global minimum;
3. the number of independent variables is relatively small (less than 100);
4. any variables which are quantized have a relatively large number of distinct possible values;
5. the desired uncertainty for a variable is small relative to the search range of that variable.

The SRC method operates by gradually reducing the search range of each independent variable. At each iteration candidate solutions are randomly chosen from the solution space. The cost function is evaluated for each candidate solution, and only solutions which are better than the mean of the previous iteration are kept.

Once a sufficient number of new candidates have been found that are potentially better solutions, the size of the solution space is updated. To update the solution space the best solutions are selected from the current set of candidate solutions. The number of solutions selected at this point is an internal parameter of the SRC algorithm.

The range of each independent variable is updated to only include the best solutions found so far, plus a small marginal zone. This usually results in a contraction of the solution space. It is possible for the region to occasionally expand if a good candidate solution is subsequently found in the marginal region. In no case is the solution space allowed to expand beyond the initial bounds.

The mean fitness of the best candidates is stored for use in the next iteration. Any existing candidate solutions that are better than the mean are automatically kept to the next iteration. This process is repeated until the stopping condition is met. The stopping condition can be either a specified value for the cost function, a specific volume of the solution space, or a fixed number of iterations. Formal presentations of the SRC algorithm can be found in [62] and [76]. Examples of designs using the SRC method are discussed in Sections 5.4 and 5.6.

4.4 Summary

This chapter described computation of time delays for beam steering, the classical narrowband beamformers, and several broadband design techniques. Particular attention was paid to the impact of array geometry on broadband performance. Both the fairly well-known harmonically nested approached to broadband array geometries, as well as the less well known optimal spacing were explained. The novel extension to the optimal spacing method was presented, which generalizes the method to include harmonically nested geometries. Finally, in general terms, the implementation of three broadband techniques was described. These methods are evaluated and compared in the design examples of Chapter 5.

Chapter 5

Design Examples and Discussion

In this chapter I will provide several design examples that illustrate both the principles of broadband beamformers designed for linear arrays, and also the use and benefit of BeamVisualizer to illustrate the design principles.

The first design examples will compare some of the classical narrowband synthesis techniques, comparing and contrasting their features both in the narrowband sense, as well as aspects of their broadband performance. I will then compare the design of a harmonically nested broadband beamformer with the optimally-spaced beamformer and discuss the implications for array geometry design.

Next, I will analyze the sample design problem presented by the author of the MAS technique, and compare its performance with a broadband design achieved using the optimally spaced array. Then I will introduce a design problem to compare all the design methods presented. This problem will reiterate the importance of array geometry and demonstrate the illustrative power of BeamVisualizer. The penultimate design example will address the issue of mainlobe widening with electronic beam steering and investigate the potential of several approaches to reduce this problem.

The final example will analyze the design given by the authors of the SRC method. This problem will show how visualization of beampatterns helps a designer to address the true underlying design problem instead of optimizing based on erroneous assumptions. While the SRC method may find the global optimum for the cost function given by the authors, I will show a design that is more suitable to the example problem, which also performs better according to their objective cost function.

Codes to reproduce the design examples are available from the author upon request.

5.1 Narrowband Beamformers

This design example will illustrate the use of BeamVisualizer to compare the performance of a simple classical narrowband design problem.

To compare the uniform, Taylor-weighted and Dolph-Chebychev-weighted narrowband beamformers, consider the problem of designing a beamformer with five elements, to operate in water (nominally $c = 1500\,\mathrm{m/s}$) at a design frequency of 750 Hz. Assume that this array may be electronically steered and the element spacing is fixed at $\lambda/2$, or 1 m.

Given that the geometry is fixed, the only task is to compute the element gains for each of the candidate aperture functions and compare the results.

The beampattern for a uniform-weighted beamformer using this geometry is shown in Figure 5.1. The display shows the beampattern from half to twice the design frequency (375 Hz to 1500 Hz). The polar plot is selected to be the design frequency, 750 Hz, and highlighted by the blue line in the main beampattern plot. As expected the sidelobes are at -13 dB, the white noise gain is 5 at all frequencies,

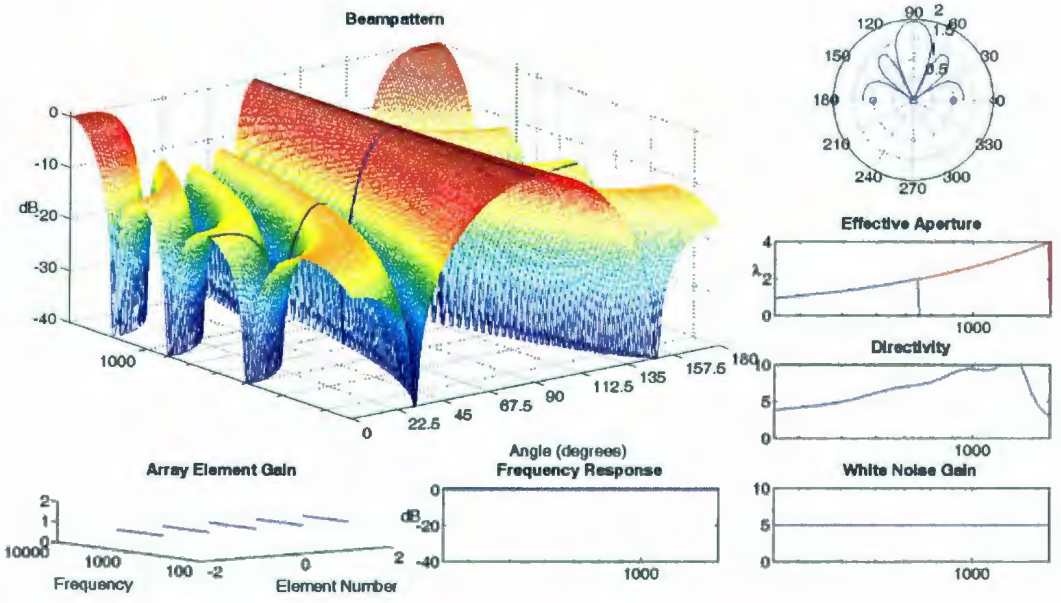

Figure 5.1: Beampattern of a five-element uniform linear array.

and the directivity peaks at just below 1500 Hz. Approaching 1500 Hz the element spacing is comparable to λ. At 750 Hz the mainlobe width is 20.9 degrees.

The beampattern for a Dolph-Chebychev beamformer using the same array geometry is shown in Figure 5.2. The Dolph-Chebychev weighting is calculated using a design specification of -25 dB sidelobes, and the sidelobes meet the specification, though the mainlobe width is wider at 25.2 degrees, and both the directivity and the white noise gain are lower than the uniform array.

If a Taylor aperture is designed for the same array geometry with sidelobe specification of -25 dB and $\bar{n} = 3$, the beampattern is shown in Figure 5.3. The mainlobe is 25.9 degrees and the directivity and white noise gain are slightly lower than the Dolph-Chebychev beamformer. Note that the sidelobes do not meet the -25 dB specification, though the mainlobe width is the same as the Dolph-Chebyshev beamformer. This is due to the way that the Taylor method adjusts the positions of the

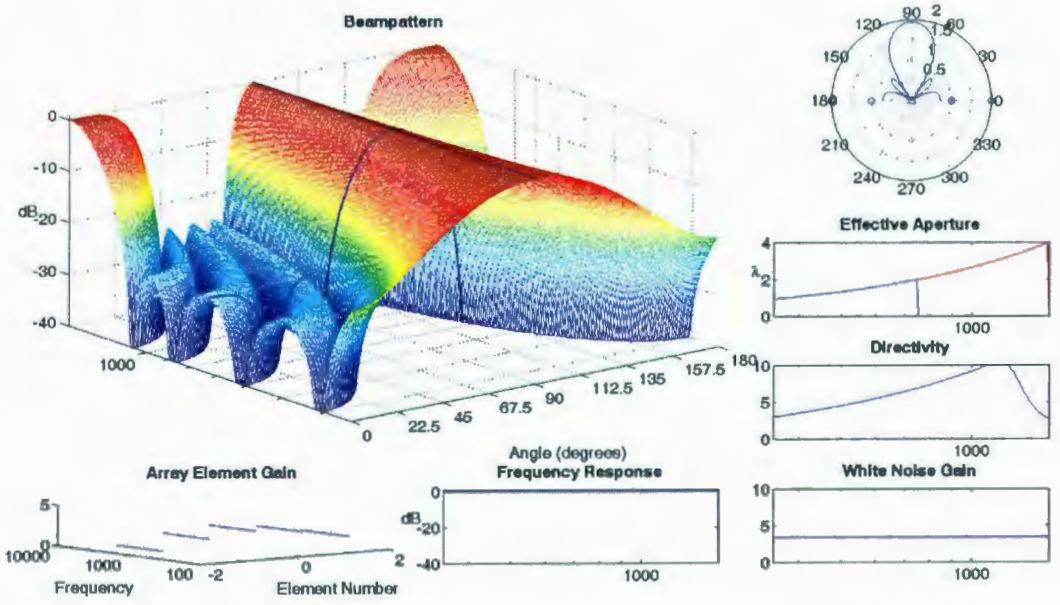

Figure 5.2: Beampattern of a five-element Dolph-Chebyshev beamformer.

first few sidelobes to meet the specification, while allowing the remaining sidelobes to decay with an approximate $\mathrm{sinc}(x)$ envelope.

Clearly, for small numbers of elements the Taylor weighting can in some cases exceed the sidelobe specification, with no compensating benefit of sidelobe decay further from the mainlobe. In this particular case the Dolph-Chebychev weighting would seem to be the best choice, unless -13 dB sidelobes were acceptable, in which case the uniform beamformer would give the narrowest mainlobe and best white noise gain.

5.2 Harmonic Nesting

This design example will demonstrate the use of the harmonic nesting equations from Section 4.3.1 to design the array geometry for a broadband beamformer.

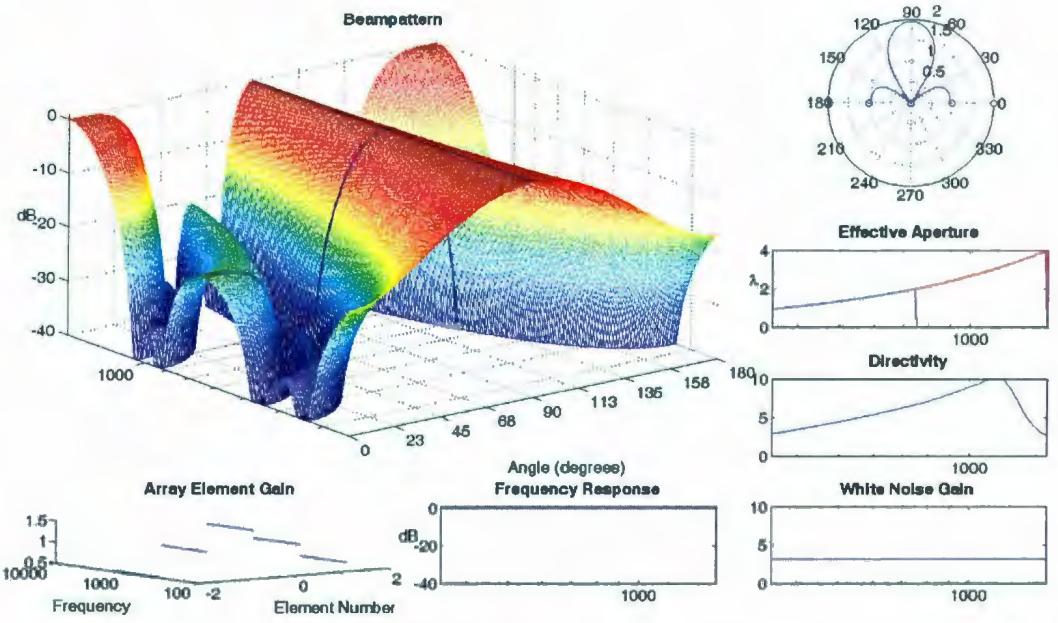

Figure 5.3: Beampattern of a five-element Taylor beamformer.

The problem is to design the geometry for an array that will cover a 4:1 frequency range with 81 elements. These numbers are chosen to be favorable to a traditional harmonically nested design using a 2:1 scaling factor and a basic subarray size of 20λ (i.e. $P = 20$ or $m = 40$), which requires 41 elements. With these constraints, the equivalent optimally-spaced geometry will be found and compared to the traditional harmonically nested geometry.

A harmonically nested array with base array of 41 elements will require 20 additional elements for each doubling of design frequency. This can be verified by rearranging Equation 4.27 and solving for x with $S = 2$ and $P = 20$, which gives a result of $x = 10$, meaning 10 elements are added to each end of the array with each frequency increment. Since the design requirement is a 4:1 frequency range, i.e. $\beta = 4$, this means two frequency increments are required desired ($j = 2$ according to

Equation 4.29 and $n = 81$ according to Equation 4.30).

Given the same number of elements, but wishing to achieve the smoothest possible beampattern, the designer should choose $x = 1$ to design an optimally-spaced geometry. From Equation 4.30 it is clear that $j = 40 - P$. At $P = 20$ we find that $\beta = 2.79$. Several values for P and β are shown in Table 5.1, computed by substituting $j = 40 - P$ into Equation 4.28. Since increasing the effective aperture at each frequency decreases the ratio between adjacent design frequencies it is logical to conclude that increasing P will decrease β. Conversely, to increase β while holding the number of array elements constant, the designer must decrease the array aperture P. The largest value of P for which $\beta > 4$ is $P = 17$, which gives $\beta = 4.03$.

P	β
20	2.79
19	3.11
18	3.52
17	4.03

Table 5.1: Some possible choices of aperture and corresponding bandwidth for an optimally spaced array of 81-elements.

Thus, assuming $\delta = 0.5$, it can be said that the most frequency invariant array possible with an operational range of 4:1 in frequency will have an aperture of approximately 17λ. A harmonically nested array designed to cover the same frequency range with the same number of elements will have an aperture of 20λ at three discrete frequencies, at the expense of smaller apertures in between those design frequencies.

In practice a Taylor weighting is often applied to this type of beamformer. To compare each geometry, the following beampatterns are all computed with Taylor apertures using $\bar{n} = 3$ and -25 dB sidelobes. The response of the nested array is

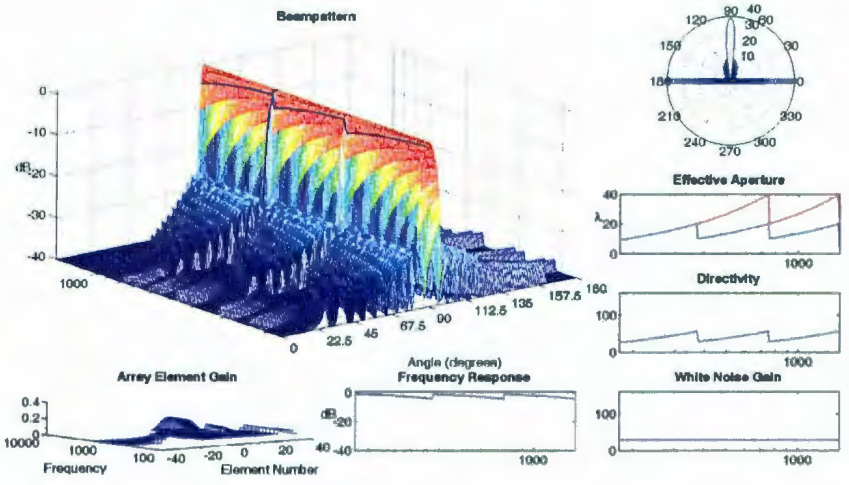

Figure 5.4: The beampattern of an 81-element harmonically nested beamformer with a 25 dB sidelobe Taylor aperture weighting.

shown in Figure 5.4 and the optimal array in Figure 5.6. Because the mainlobe is very narrow, Figures 5.5 and 5.7 show just the beampattern in a 60 degree sector around the broadside aiming direction. Note that the mainlobe for the nested array varies between 3.0 and 6.0 degrees, while the optimal array mainlobe is constant at 3.6 degrees over the design bandwidth of 375 to 1500 Hz. Both designs increase to nearly 7 degree beamwidth at half the lowest design frequency, 187 Hz.

The frequency response subplot in Figure 5.4 shows the response of the beamformer at 88.2 degrees – just 1.8 degrees off-axis. The beamformer response varies by up to nearly 5 dB. The variation in beampattern is mirrored by the large variation in effective aperture.

With simple harmonic nesting there seem to be relatively few design choices to be made for this problem. Interestingly, the general harmonic nesting formulas allow the designer far more freedom. As a further example, if the effective aperture is the

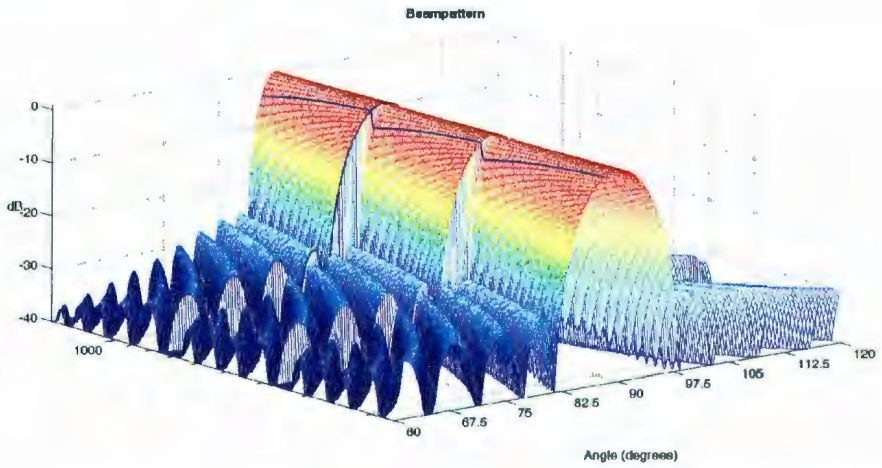

Figure 5.5: Closeup of the mainlobe of the harmonically nested beamformer.

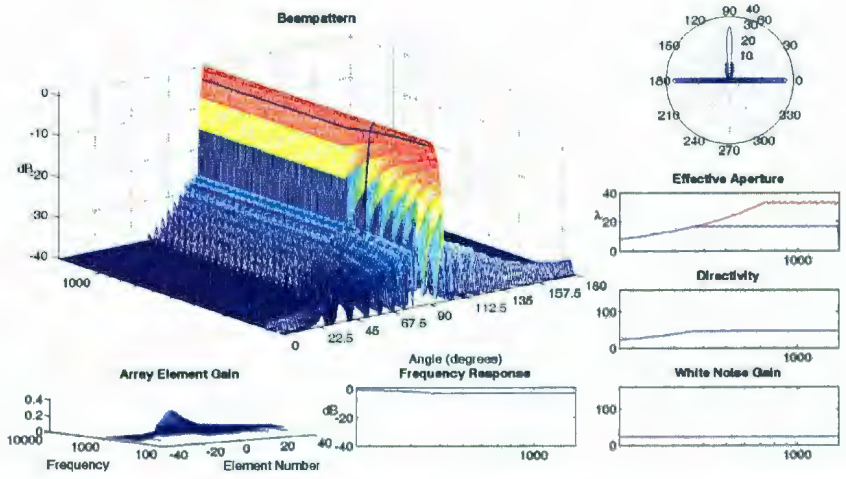

Figure 5.6: The beampattern of an 81-element optimally spaced beamformer with a 25 dB sidelobe Taylor aperture weighting.

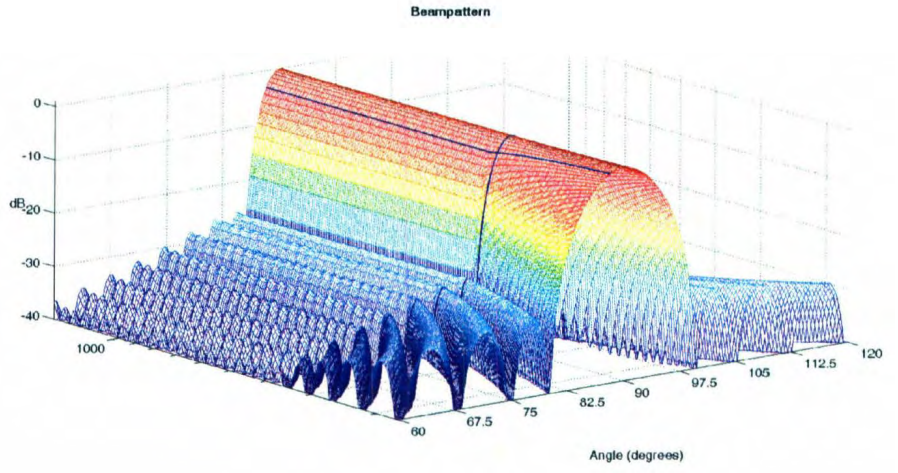

Figure 5.7: Closeup of the mainlobe of the optimally spaced beamformer.

most important criterion, then Table 5.2 shows the total number of array elements required to achieve $\beta = 4$.

P	n	β
17	81	4.03
18	85	4.17
19	91	4.08
20	95	3.99
20	97	4.20

Table 5.2: The number of elements required for an optimal beamformer to achieve $\beta = 4$ for various values of P.

Another approach is to consider values of x between 1 (optimal spacing) and 10 (simple 2:1 harmonic nesting). In Table 5.3 values of β are given for combinations of P and x while holding the total number of elements constant. From this table several reasonable alternatives to either the simple harmonic nested geometry and the optimal geometry are obvious. If maximum bandwidth is important, an aperture of

16λ expanding by step size $x = 6$ gives a mainlobe width that is always smaller than the simple harmonic nesting maximum of 6.0 degrees, but with nearly an additional octave of pattern control. If implementation details make it difficult to deal with 23 different subarrays of the optimal geometry, then an aperture of 19λ using only three scalings ($j = 3$) gives nearly identical bandwidth with a smaller mainlobe and less mainlobe variation, with only one additional subarray design frequency.

x	P	j	β	Low Freq. Cutoff	Beamwidth(degrees)
1	17	23	4.03	372	3.6
2	16	12	4.97	302	4.0 - 4.3
6	16	4	6.55	229	4.0 - 5.9
7	19	3	3.97	378	3.2 - 5.0
10	20	2	4.00	375	3.0 - 6.0

Table 5.3: The potential bandwidth of an 81-element broadband array geometry for various values of x and P.

Even if the designer chooses the simple harmonically nested geometry, the generalized harmonic nesting equations allow the designer to evaluate all reasonable possibilities and be confident in the ultimate choice. The general harmonic nesting equations are the tools to compare the range of possible geometries given the constraints, and BeamVisualizer allows the designer to investigate the performance of the various candidate geometries.

5.3 MAS Design Example

Abhayapala [67], uses the design of a beamformer with a linear array to demonstrate the MAS method. The beamformer is designed to operate in air ($c = 345\,\text{m/s}$) over a frequency range of 300 Hz to 3000 Hz, with the desired beampattern matching that of

a seven-element Dolph-Chebychev beamformer with a -25 dB sidelobe specification as in Figure 5.8. The beampattern resulting from the application of the MAS method is shown in Figure 5.9, using the first 16 modes to approximate the complete solution to the wave equation, that is, using $n = 15$. This somewhat matches the figure given by Abhayapala, however notice the sidelobes seem lower than the specification, at around -30 dB.

Although the author asserts that 16 modes are sufficient to achieve the desired beampattern, and the results confirm this, it is instructive to see what happens by using higher values of n to include more modes in the approximation of the modal decomposition. With $n = 21$, as shown in Figure 5.10 the resulting beampattern shows an increase in the uniformity of the beampattern over frequency, as well as a significant reduction in sidelobe level. This is a logical result, since the equations for choosing the array geometry are designed to produce a geometry that can realize any beampattern than can be approximated by the chosen number of modes. For 22 modes the technique requires a larger number of array elements: 67 instead of 49. Mathematically, increasing the number of modes used in an approximation, and physically, increasing the number of array elements and overall aperture size of an array, would both be expected to allow greater beampattern detail and precision.

A designer approaching this problem without using the MAS technique would first consider the array geometry. The optimally spaced array described in Section 4.3.1 presents a starting point. A seven-element Dolph-Chebychev beamformer will have an aperture of 3λ assuming $\lambda/2$ spacing. Therefore $P = 3$, $m = 6$, $S = 1.5$ and the bandwidth ratio is $\beta = 10$. From Equation 4.22 we find that $j = 6$ and from Equation 4.18, $n = 19$.

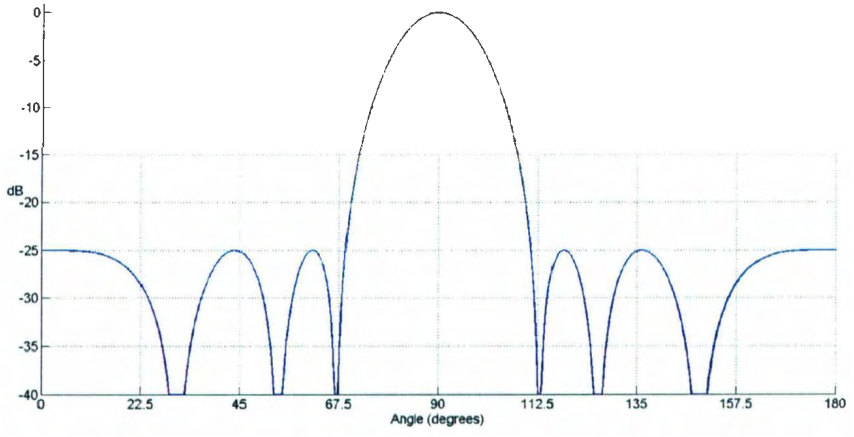

Figure 5.8: The beampattern of a seven-element beamformer with a -25 dB sidelobe Dolph-Chebychev aperture weighting.

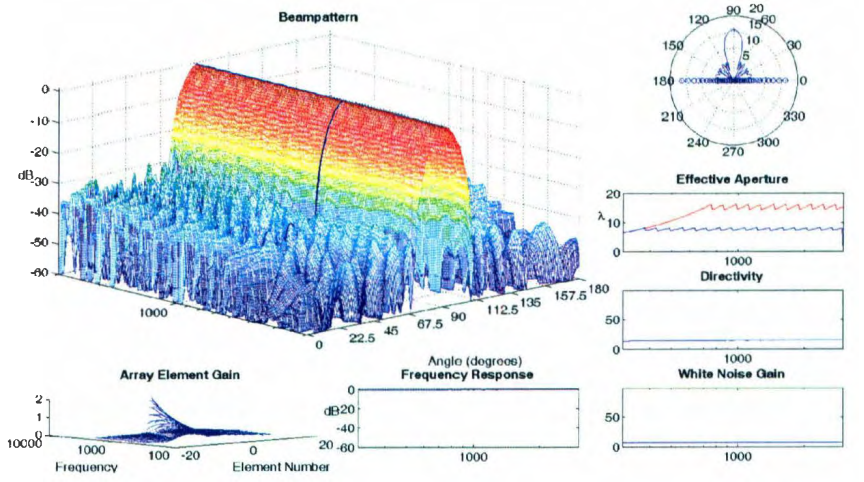

Figure 5.9: The beampattern designed by the MAS method using 16 modes.

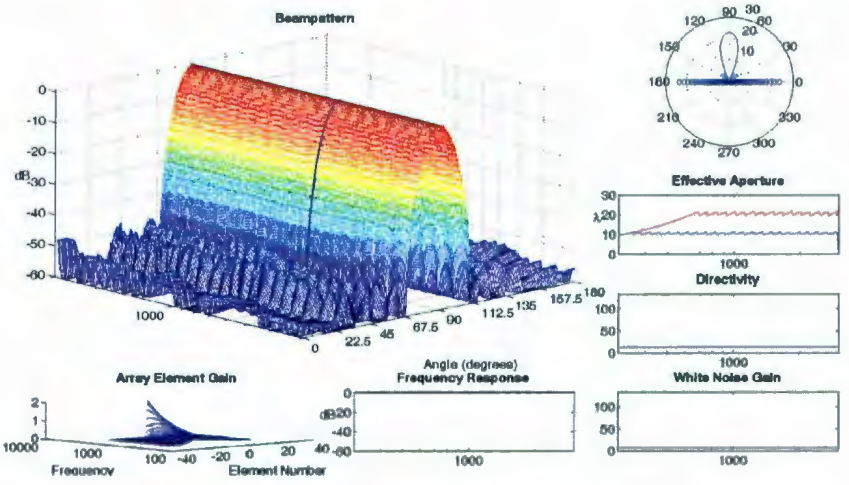

Figure 5.10: The beampattern designed by the MAS method using 22 modes.

Applying a Taylor weighting to this array geometry, with a -25 dB sidelobe specification results in the beampattern in Figure 5.11.

The sidelobe behavior is not as well controlled as in the MAS beamformer, however the beamformer requires less than half the elements required by the MAS design. It is trivial to increase the aperture to 3.5λ to match the mainlobe width and sidelobe level of the MAS design, while still only requiring 22 elements.

This does not prove that the MAS technique is incapable of a better design, but rather that the array geometry guidelines provided for the technique do not give insight into the maximum performance possible. Specifically, 16 modes are not required to suitably represent this particular desired beampattern in a broadband beamformer.

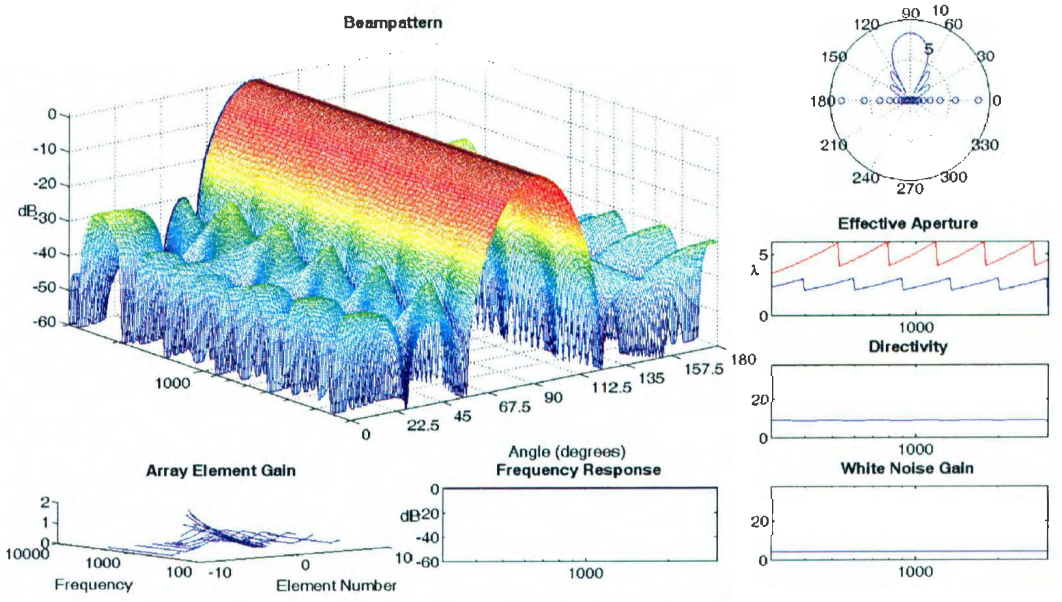

Figure 5.11: The beampattern of a 19-element array optimally spaced for a 3λ aperture over 300 Hz to 3000 Hz using a -25 dB Taylor aperture weighting.

Figure 5.12: The element spacing for the unequally-spaced array design problem.

5.4 8-Element Array with an Unusual Geometry

This example is based on the design of a commercial hydrophone array, intended for use in passive acoustic monitoring. The array is intended to detect vocalizations from large marine mammals, over the frequency range of 20 Hz to 750 Hz. The array geometry is predetermined, and the objective is to investigate the potential performance of this configuration using BeamVisualizer, and determine which broadband design method produces the best aperture weighting functions. The given element spacings, in meters, are 37.5,37.5,2,1,1,1,1,1, as shown in Figure 5.12. Expressed as distances from the origin, this is 0, 37.5, 75, 77, 78, 79, 80, and 81.

5.4.1 Analysis of Basic Geometry

The three different spacings used represent three different design frequencies. There are three elements spaced by 37.5 m, four elements spaced by 2 m, and five elements spaced by 1 m. Assuming a basic spacing of one-half wavelength and $c = 1500\,\text{m/s}$ (appromixately the speed of sound in water), this corresponds to three sub-arrays designed for 20 Hz, 375 Hz and 750 Hz. Note that the ratio of design frequencies is 18:1 and 2:1 between low to mid, and mid to high design frequencies. This suggests that there may be difficulty in the frequency range between the low and mid design frequencies.

Again assuming $\lambda/2$ spacing, the array aperture is 1λ at 20 Hz, 1.5λ at 375 Hz,

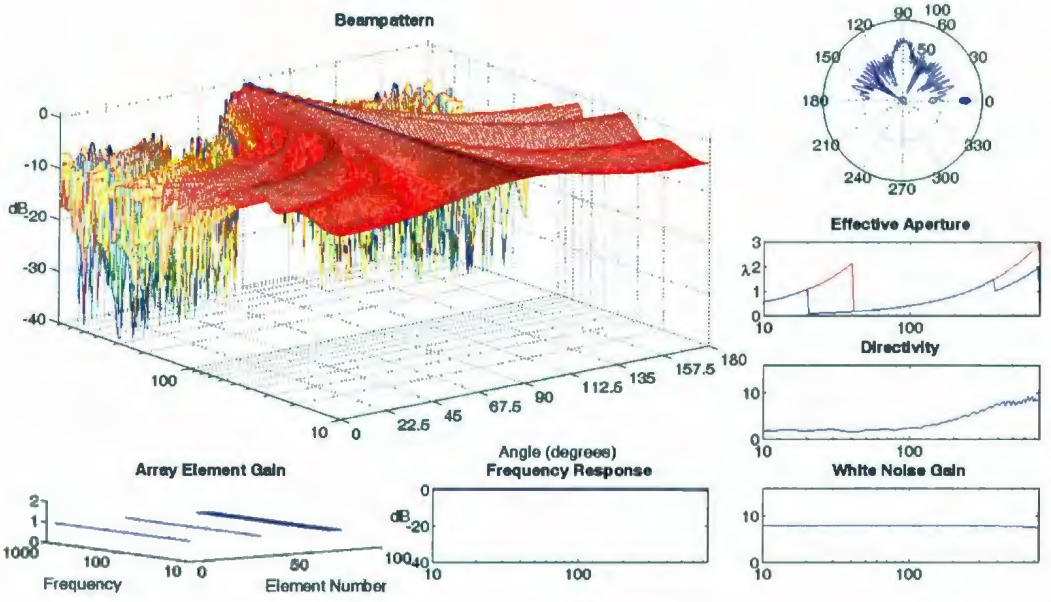

Figure 5.13: The output of a unity-gain summing of all eight elements of the array.

and 2λ at 750 Hz. Summing the output of the total array over 10 Hz to 750 Hz gives the beampattern shown in Figure 5.13. Considering the effective aperture of the array geometry it is not surprising that the directivity is low between 20 Hz and 200 Hz, although it would be expected that better directivity at 20 Hz is possible. When the 5 elements spaced close together are given equal weight in the beamformer summation they overwhelm the contribution of the wider-spaced elements, so the aperture is not regularly sampled and the directivity is low. Above about 200 Hz the beamformer is approaching the design frequency of the 2 m spaced elements, where the overall aperture is nominally 1.5λ.

The white noise gain is the best feature of a simple beamformer summing all eight elements. Since this is a uniform beamformer the white noise gain is maximum, equal to the number of elements in the array. We can see that a uniform beamformer using

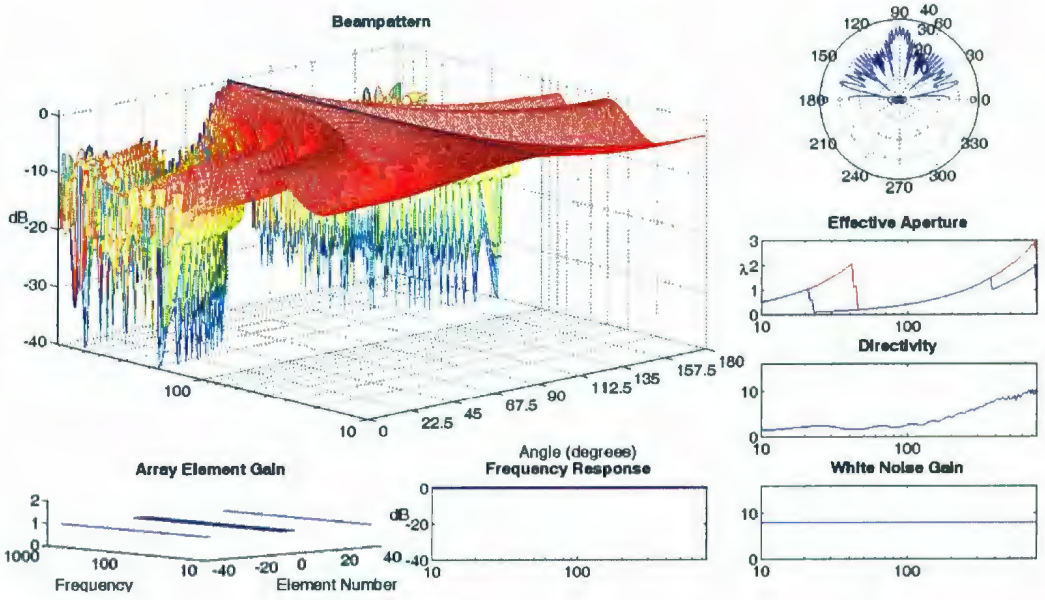

Figure 5.14: The output of a unity-gain summing of all eight elements of the array, with the closer spaced elements in the center of the array.

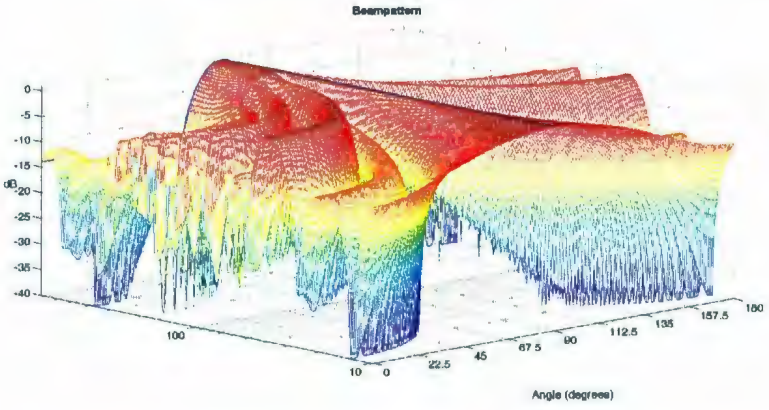

Figure 5.15: The output of only the frequency-specific subarrays, up to their design frequencies, respectively.

this array is primarily useful for its resistance to position errors and sensor self-noise. Below 200 Hz the beamformer directivity is only marginally better than an omnidirectional sensor.

The first thing that may occur to the designer is to rearrange the array geometry so that the elements spaced at 37.5 m are on either side of the center element of the five elements spaced by 1 m. This would cause the non-equal sampling of the aperture in the uniform beamformer to happen in the center of the aperture, similar to the way aperture weightings such as Taylor and Dolph-Chebychev weight the center of the aperture more. For simplicity the position of the 2 m spaced elements is unchanged relative to the five 1 m spaced elements. This is simulated and the result shown in Figure 5.14. The only effect of this is to slightly change the shape of the sidelobes in the region below 375 Hz. The directivity is also somewhat different, but not significantly higher. This configuration will not be further examined, and all remaining discussions refer to the geometry of Figure 5.12.

It is important to note, however, that this is the theoretical performance of the beamformer to an infinitely distant source (the simulation distance for the previous figures was set to 100000 m). When the simulation distance is set to 1000 m, the white noise gain and directivity both suffer in the middle of the frequency range. This is because the physical centers of the subarrays are not coincidental, therefore the direction of the maximum response axis differs slightly from the nominal steering direction over the frequency range, relative to a common reference. The computation of directivity and white noise gain can be adjusted for this by finding the actual maximum response axis before computing directivity and white noise gain. This adjustment is made without further comment throughout the remainder of this section. The lesson for the designer is that care must be taken when both designing

and analyzing arrays where the center of aperture changes with frequency.

To realize the potential directivity at the bottom end of the operational range of the array the designer must use each subarray separately. To turn subarrays on and off depending on frequency, each element must have a frequency-dependent gain. At each design frequency the gain for all elements should be zero except for the elements spaced for that design frequency. The total output of the beamformer will be proportional to the number of elements active at each design frequency. To achieve uniform output, the gain of each element is divided by the number of active elements at that design frequency. A linear transition between the gain settings for each subarray can be used in between the design frequencies. This effectively determines the frequency response of a filter for each array element.

The beampattern for this beamformer is shown in Figure 5.15. In this case fewer element arrays are active at any given frequency so the main lobe is wider. However, the directivity is clearly improved and there is a subjective improvement in the appearance of the beampattern.

5.4.2 Aperture Function Design

Using a weighted aperture with each subarray cannot be expected to increase directivity. However, it may further improve the beampattern, assuring that a larger proportion of the beamformer output originates from close to the desired direction. The following section presents the results of designing aperture functions for this array using a Taylor aperture, the MAS, MSD and SRC methods.

Figure 5.16 shows a Taylor window applied to each of the frequency ranges 6-20 Hz, 20-375 Hz, and 375-750 Hz. This has abrupt transitions in the beampattern between the subarrays, which results in a reduction in the beamformer directivity (see

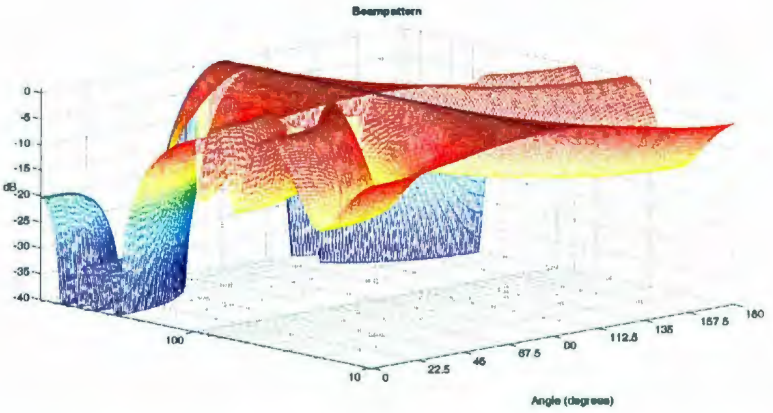

Figure 5.16: The beampattern of the array with a Taylor weighting applied to each subarray.

Figure 5.21). The subjective appearance of the beampattern can be further improved by transitioning from one subarray to the next, and this is shown in Figure 5.17. The transition is accomplished similarly to the transition used for the uniform beamformer just presented, by linearly interpolating the gain for each element at each frequency in between the main subarray design frequencies.

Using the MSD method, weightings were calculated for each of the subarrays for the frequency ranges 5 to 20 Hz, 100 to 375 Hz, and 376 to 750 Hz. The choice of frequencies is based on the observation that above the design frequency no choice of weightings is able to prevent the appearance of grating lobes, while experience with the MSD method has shown that matching the design beampattern without grating lobes is possible at frequencies a fraction of the design frequency as long as sufficient elements are available. This is another way of saying as the array aperature increases, pattern control is useful at lower frequencies.

Figure 5.18 shows the resulting beampattern. This beampattern is noticably

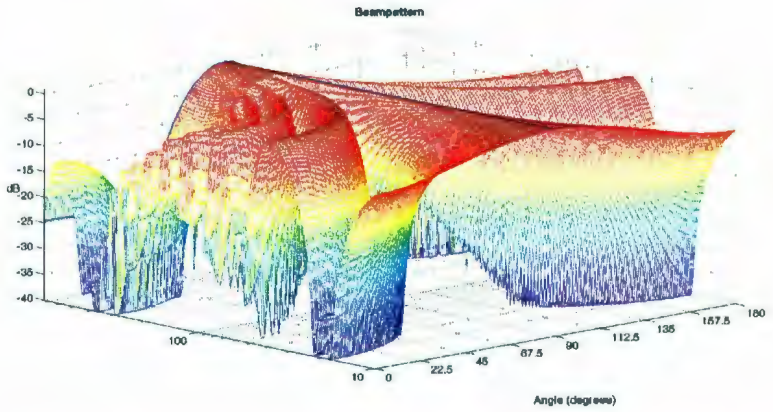

Figure 5.17: The beampattern of the array with Taylor weighting applied to each subarray, using a transition between adjacent frequency bands.

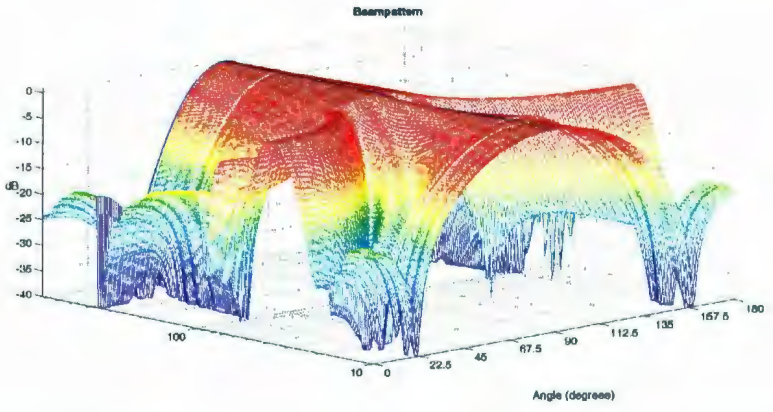

Figure 5.18: The beampattern achieved using the MSD design.

more appealing, although there is still a large region of poor directivity between approximately 50 Hz and 100 Hz. There are fewer sidelobes and the mainlobe is more consistent across the frequency range. The desired beampattern used for the MSD design of each frequency range is the equivalent Dolph-Chebyshev pattern at the design frequency of each band (20 Hz, 375 Hz, and 750 Hz).

This technique employs superdirectivity, so the white noise gain suffers as discussed in the next section. This technique requires several minutes of computation, and so the aperture function is pre-computed and stored in BeamVisualizer for rapid display and comparison between beamformers.

Using the MAS method, filters for each array element were designed, similarly to the approach used for the MSD method. Since the MAS method is not superdirective, it exerts relatively less control over the beampattern at frequencies below the design frequency. The weights were designed for 10 to 20 Hz, 100 to 375 Hz, and 400 to 750 Hz. The resulting MAS beamformer is shown in Figure 5.19. The MAS aperture function for this beamformer can be computed in a few seconds on a contemporary PC. This is efficient enough that it can be called dynamically within BeamVisualizer rather than pre-computed as with the MSD method.

Finally, a beamformer was designed using the SRC method to compare the stochastic with the analytical MAS and MSD methods. The SRC method was applied to choose the gains for each of the eight elements to achieve the lowest mean-square error between the realized beampattern and the target beampattern.

The target beampattern chosen for each subarray is the beampattern found using a Taylor aperture function on a narrowband beamformer of the same number of elements and same design frequency for the respective subarrays. The resulting beampattern is shown in Figure 5.20.

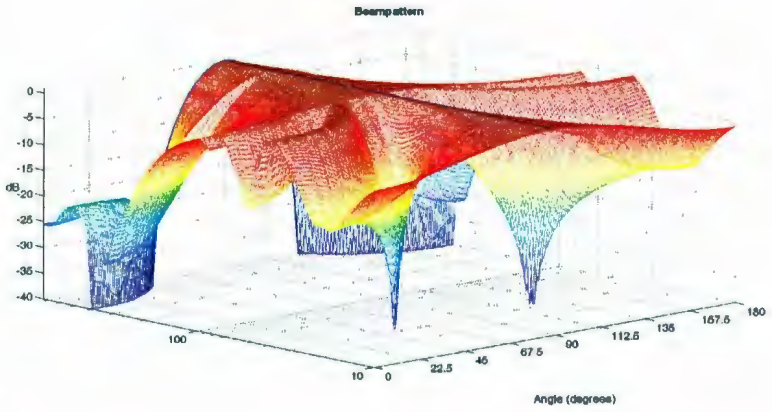

Figure 5.19: The beampattern achieved using the MAS design.

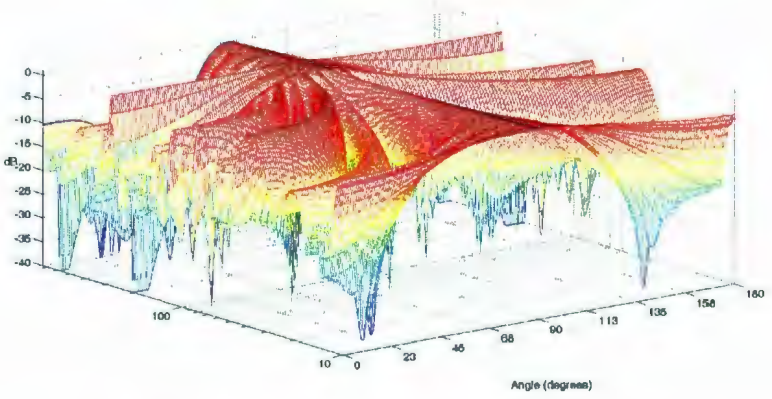

Figure 5.20: The beampattern achieved using the SRC design.

5.4.3 Directivity and White Noise Gain Comparisons

A comparison of the directivity and white noise gain of all the described beamformers for this array is shown in Figure 5.21. These plots are all computed at a simulation distance of 1000 m, and there are some artifacts of this simulation distance. For instance, the roll-off seen in the white noise gain for the uniform full array is due to the fact that at the upper end of the frequency band there is a significant phase difference between the same wavefront arriving at the closely spaced elements of the array and it arriving at the distant, 37.5 m spaced elements.

In general it is seen that a reduction in directivity is often mirrored by a reduction in white noise gain. Unsurprisingly, the uniformly-weighted beamformers display the best directivity and white noise gain performance. With a narrower mainlobe and larger sidelobes, the resulting beamformer may detect signals originating far from the desired array steering direction.

We can see that the MSD method is the only method that shows an appreciable increase in directivity throughout the mid-frequency region, even though both MAS and MSD produce beampatterns with noticably more uniform mainlobes within their design band. The increase in directivity comes from the use of superdirectivity, at the expense of white noise gain. The MSD beamformer has by far the worst white noise gain, making this beamformer especially susceptible to uncorrelated noise at each sensor (for example, flow noise in the case of an underwater hydrophone array). Other types of errors and imperfections that lead to uncorrelated noise include amplifier gain mis-matches, element position errors and sensor self-noise. In contrast, the only area that MAS shows an improvement over the MSD beamformer is in white noise gain.

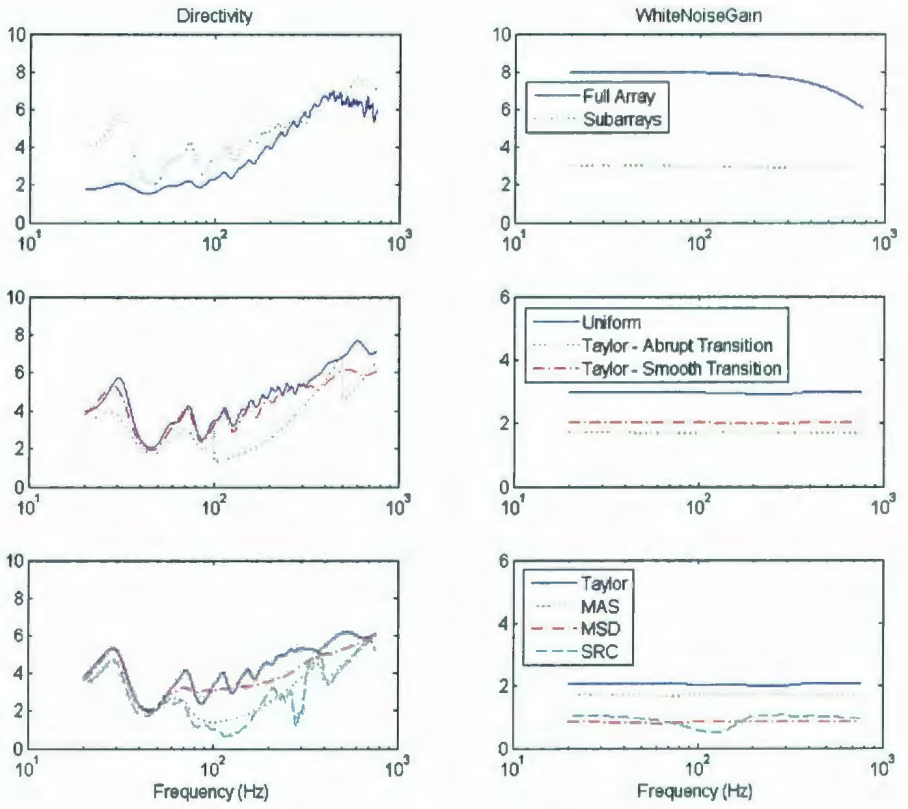

Figure 5.21: The directivity and white noise gain performance for uniformly-weighted full array beamformer, separate subarray beamformers, Taylor aperture weighted beamformer, as well as the MAS, MSD and SRC-derived beamformers.

While the directivity results for the SRC beamformer are somewhat comparable to the MAS and MSD methods, the beampattern is not as smooth. This is likely due to the stochastic design process. The array nearly loses all directivity at several frequencies where the other designs maintain pattern control. While this may be an artifact of the choice of SRC parameters, it shows that the optimality of the results is hard to guarantee. In addition, while the resulting beampattern shows higher directivity at some frequencies, this is at the expense of the beampattern deviating from the desired uniformity in frequency.

5.4.4 Discussion

Clearly this array geometry is undersampled in the frequency range of about 30 Hz to 300 Hz. If the array geometry can be precisely controlled and element gains carefully matched, it might be possible to compensate for this somewhat using superdirective aperture functions produced by the MSD method (or another superdirective technique not discussed in this thesis). However, for the described application of an underwater hydrophone array the drastic reduction in white noise gain is unacceptable. Therefore, for a static broadband design it is probably the simplest to use a Taylor aperture function transitioned between the design frequencies.

If the designer contemplates an adaptive beamformer, then methods such as MAS may hold more promise, since portions of the method can be pre-computed based only on the array geometry. Adaptive beamformers are outside the scope of this thesis.

In nearly all cases it seems that the computational overhead of the SRC and MSD methods are impractical for this design problem when equal or better results are obtained more efficiently with either classical narrowband techniques, or at most

the MAS method.

Several things are evident from the preceeding discussion: the array geometry plays a crucial role in determining the potential performance of a broadband beamformer, and a visualization tool like BeamVisualizer enables the designer to understand the value of different aperture functions and make rational design choices.

5.5 Constant Mainlobe Despite Beam Steering

This section analyses the effect of electronic steering on the mainlobe width for the 81-element harmonically nested beamformer considered in Section 5.2. For all of the beampatterns in this section the Taylor weighting coefficients are generated with $\bar{n} = 3$ and sidelobes of -25 dB, although with so many elements it is theoretically possible to achieve -40 dB or even -50 dB sidelobes at the expense of a few degrees of mainlobe width.

Figure 5.22 shows how the mainlobe widens when the array is electronically steered to 45 degrees off-axis (compare with Figure 5.4). The main lobe varies between 4.5 and 8.6 degrees, instead of 3.0 to 6.0 degrees when steered to broadside. The directivity of the beamformer ranges between 20 and 45 over its operational bandwidth, instead of 30 to 55 at broadside (white noise gain is unchanged). This beamformer is designed using the spatial weighting discussed in Section 4.3.2 so that at the lowest frequency every element in the array is used, not just those spaced at exactly $\lambda/2$.

The sidelobes are higher than might be expected, compared with Figure 5.23. Figure 5.23 shows the beampattern for the same array geometry computed using only the elements spaced closest to, but not less than $\lambda/2$ for each frequency range.

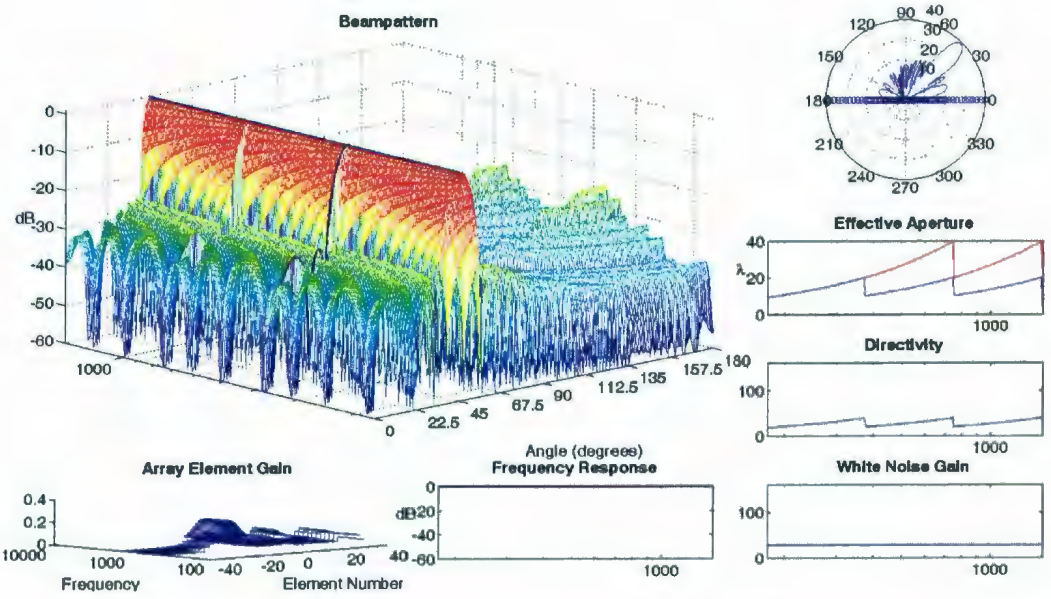

Figure 5.22: An 81-element harmonically nested array using all elements at or below $\lambda/2$ steered to 45 degrees off-axis.

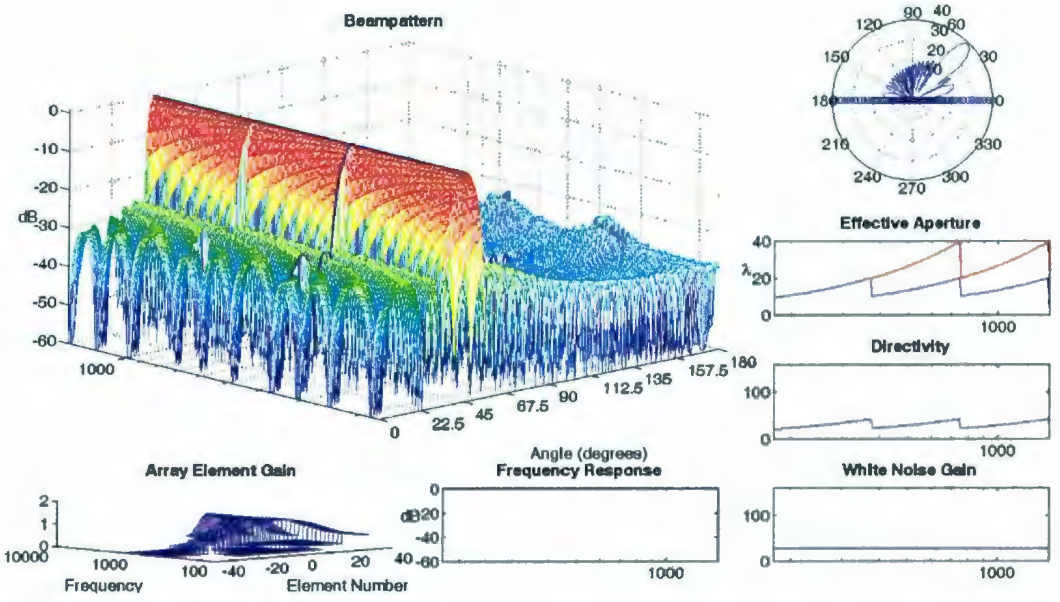

Figure 5.23: An 81-element harmonically nested array using only elements spaced by $\lambda/2$ steered to 45 degrees off-axis.

I do not have a good explanation for why the sidelobes are higher in the first figure. This may be a fundamental drawback of the use of unevenly spaced elements, but I cannot think of a good physical reason why this would be the case.

In either case the widening of the main lobe is undesirable and it begs the question: what causes this widening of the mainlobe and can the mainlobe width be maintained as the beam is electronically steered?

A geometrical argument can help to illustrate this problem caused by steering the array. A plane wave arriving from a distant source located broadside to the array "sees" the maximum length of the array. Reciprocally, the array presents its widest possible sampling aperture to sources at 90 degrees off-axis. Sources at other angles "see" a relatively smaller aperture - as if the array were shortened. The time delay

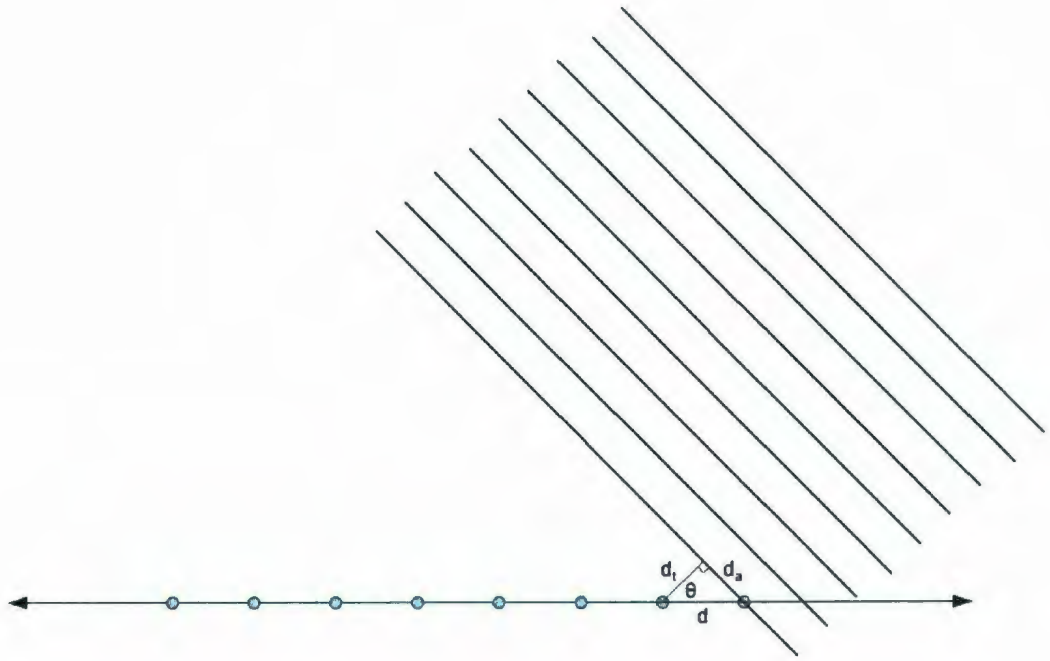

Figure 5.24: A plane wave arriving at a uniformly-space array.

of each element used to electronically steer the beam mainlobe can be thought of as projecting each array element's position onto a line parallel to the wavefront and passing through an array element chosen as reference, as in Figure 5.24.

The spacing between array elements is $d = \lambda/2$. The distance a given wavefront travels between array elements is $d_t = d\cos\theta$. After the time delays align the received wavefronts at each element, the apparent position of each element along the wavefront is $d_a = d\sin\theta$.

Inevitably, a smaller aperture means the array will be less able to discriminate

between farfield source direction, and the mainlobe widens. This effect is proportional at all frequencies. In the case of a uniformly-spaced array, there is no way to improve the effective aperture when electronically steering the beamformer, so the consequences of wider beams must simply be accepted. However, in the case of an array with multiple element spacings designed for broadband beamforming, there are often more elements at wider spacings available, but not in use at a given frequency.

I hypothesize that the use of more elements will allow the mainlobe width to be kept constant as the beamformer is electronically steered away from broadside.

Take the simple case of steering the main beam to 30 degrees from the array axis (60 degrees from broadside). The 750 Hz subarray projected onto the line perpendicular to the steering direction has a total length of $\cos(60) = 0.5$ relative to the physical length of that array segment. The apparent element spacing is similarly scaled by half. In filtering terms, the sample window is halved and the sample rate is doubled. The sample window reduction is the cause of the expected effect of mainlobe widening - equivalent to loss of frequency resolution in the filtering analogy. However, the doubling of sample rate indicates that this subarray may now be useful at a much higher frequency, and similarly a subarray designed for a lower frequency may be useful at this frequency.

Clearly, the spacing of the 375 Hz subarray projected onto the wavefront from a source 30 degrees off-axis will have the same apparent element spacing as the design spacing for the 750 Hz subarray. Similarly, the 375 Hz subarray has the same effective aperture as the 750 Hz subarray did at broadside. In fact, for any steering angle less than 90 degrees, there will be some frequency above the design frequency for which the elements projected onto the plane of the wavefront are apparently spaced by $\lambda/2$. I will call this frequency the apparent design frequency. By expressing the distances

in Figure 5.24 we can find the relationship between steering angle, design frequency and apparent design frequency, as follows

$$\sin\theta = \frac{\lambda_u}{\lambda_l} \tag{5.1a}$$

$$= \frac{f_l}{f_u} \tag{5.1b}$$

where θ is the steering angle, λ_l, f_l, λ_u, and f_u are the design wavelength, frequency, apparent wavelength and frequency, respectively.

To test the hypothesis I implemented this shift of the active frequency range for each subarray proportional to the steering angle, according to Equation 5.1. The effect of this is that at any frequency and steering angle, the portion of the array that is used is the widest part of the array where the element spacing projected onto the plane perpendicular to the steering direction is $\lambda/2$ or less. The result of this is shown in Figure 5.25.

Of course at the lowest portion of the frequency range there are no additional array elements that can be brought into the active portion of the array, so the mainlobe will widen at the bottom of the beampattern the same as without the steering compensation. In the mid- and upper-frequency areas the technique appears to work quite well - the mainlobe size and shape is now the same as when steered to broadside, varying between 3.0 and 6.0 degrees. However, spatial aliasing is clearly occurring. As the active range of each subarray is shifted higher, for any given frequency there comes a point at which the beampattern is not formed using the higher-frequency neighboring subarray (whose elements are spaced closer than $\lambda/2$ for the given frequency) but rather using the lower-frequency neighboring subarray whose elements are spaced too far apart.

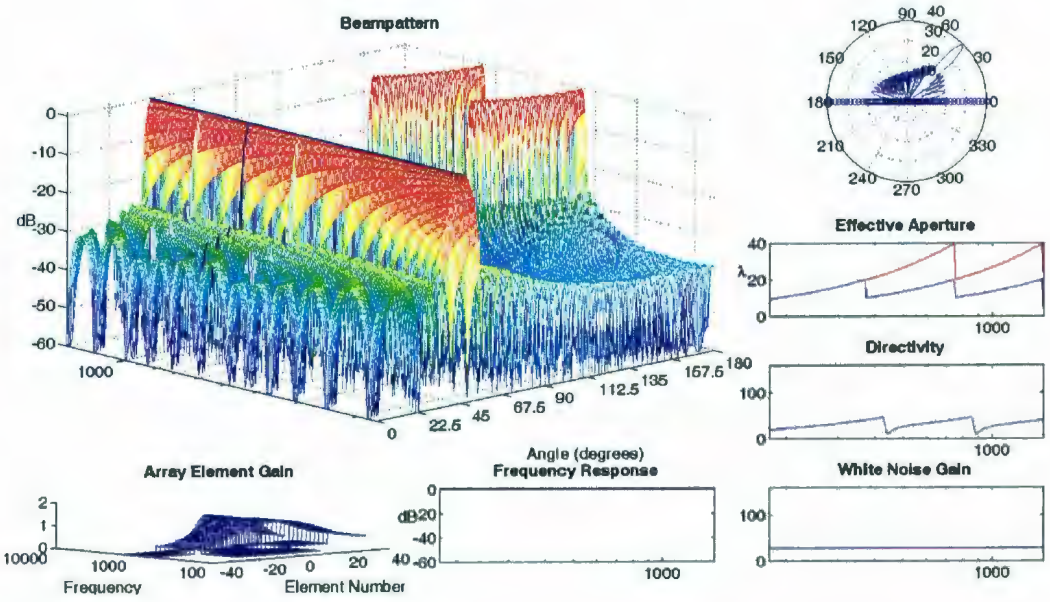

Figure 5.25: An 81-element harmonically nested array steered to 45 degrees off-axis with the frequency range of each subarray scaled by the steering angle.

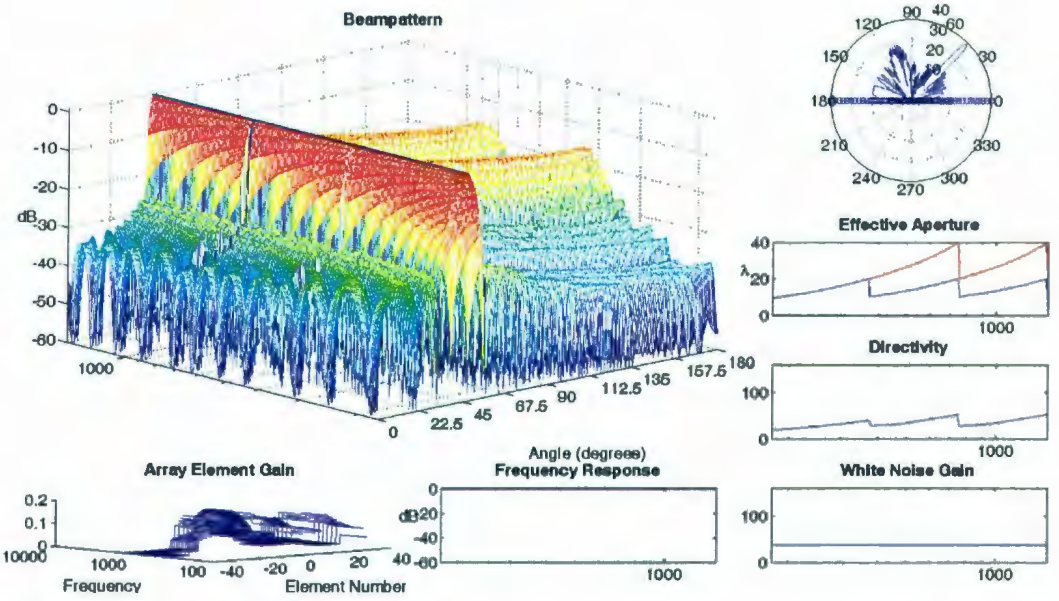

Figure 5.26: An 81-element harmonically nested array steered to 45 degrees off-axis, with the active portion of the array dynamically widened proportionally to steering angle.

There is another problem with this approach, and that is the shape of the mainlobe appears to move upwards in frequency as the steering angle is increased. So while the general shape of mainlobe widths stays constant, at any given frequency the mainlobe changes with steering angle, and may suddenly jump from wide to narrow as a larger subarray becomes active at that frequency. This is all quite obvious when the designer uses the steering angle slider in BeamVisualizer to adjust the beam through the steering range from broadside to endfire.

To address these issues I implemented a slightly different method of testing the hypothesis. Since Equation 5.1 implies a $\sin\theta$ relationship between the aperture size and steering angle, I rewrote the array generation function to dynamically select the current subarray plus some additional elements from the lower frequency subarrays

when possible. The number of additional elements added was chosen to maintain the apparent size of the aperture when projected onto the plane of the incoming wavefront. Then the Taylor weighting function was computed for this (slightly larger) subset of the total array. The results of this are shown in Figure 5.26.

This fully addresses one issue with shifting active frequency of each subarray. Now the mainlobe stays at a constant size at each frequency, until the array is steered far enough that even projecting the entire array on the plane perpendicular to the steering direction no longer gives an apparent aperture equal to the physical aperture at a given frequency. The steering angle at which this occurs naturally increases with frequency. In other words the mainlobe width can be held constant to greater steering angles at higher frequencies.

However, as steering angle is increased the use of more and more elements that are spaced further than $\lambda/2$ still affects the sidelobe level at higher frequencies. This makes sense since at higher frequencies there is an increasing proportion of elements in use which are only apparently spaced at below the Nyquist limit from the perspective of a plane wave from the steering direction. These elements are still in fact spaced further apart than the sampling theorem dictates.

One other interesting case is worth considering: the optimally spaced array for the same problem. With the harmonically nested array as additional elements are used at any particular frequency, the physical spacing is double the spacing of the original subarray for that frequency. This is true as each additional element is added until reaching the design frequency of the next subarray. Equation 5.1 shows that the first additional element is added as the beam is steered to 24.6 degrees. Only at 60 degrees off axis is the apparent spacing of the next lower subarray equal to the actual spacing of the neighboring higher subarray.

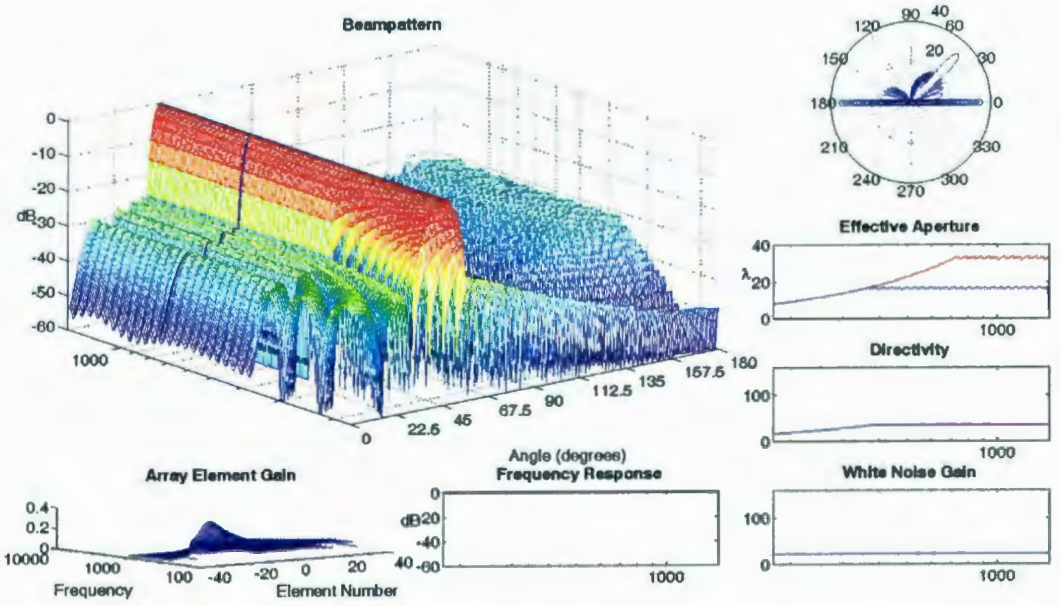

Figure 5.27: An 81-element optimally spaced array steered to 45 degrees off-axis.

Consider the way the optimally spaced array is extended in frequency. When the wavelength of a frequency below the design frequency is exactly λ longer than the the existing array, one more element is added at each end of the array, spaced at $\lambda/2$. This scaling of the array spacings in frequency is analogous to the scaling of the array elements as projected onto the plane perpendicular to the steering direction.

The next set of array elements is added to the active aperture when the array is steered to only 19.7 degrees. Additionally, when an additional element is added the apparent spacing for the new added element is exactly $\lambda/2$ and the actual element spacings are all less than that of the latest elements added to the active portion of the array. This suggests that the optimally spaced array may have better success with compensating the mainlobe width for steering (although clearly this will still violate the Nyquist rate).

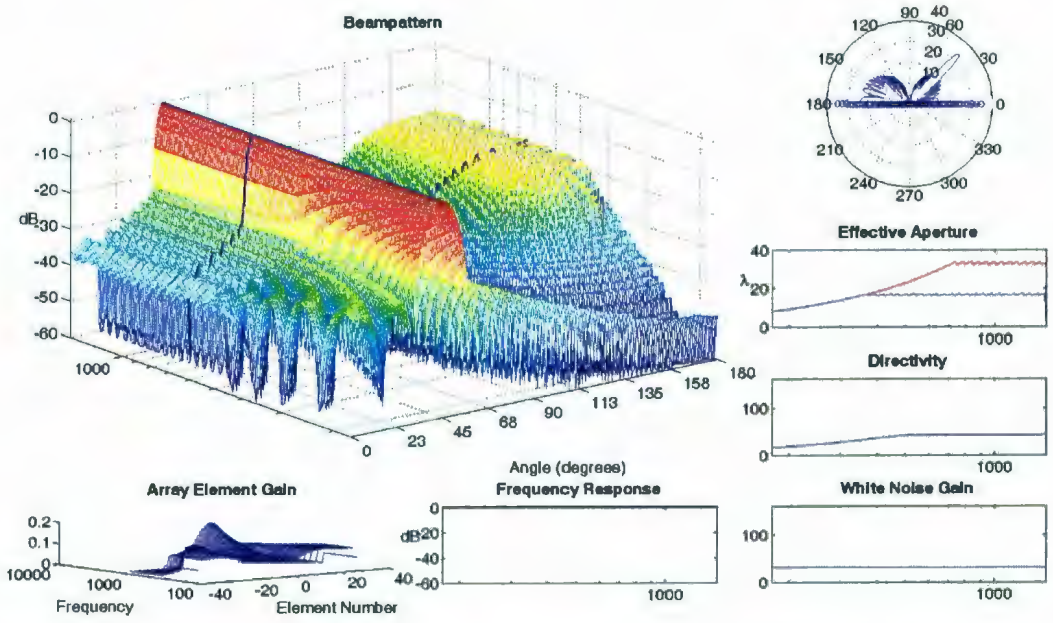

Figure 5.28: An 81-element optimally spaced array with steering compensation steered to 45 degrees off-axis.

The beampattern of an uncompensated optimal array steered to 45 degrees off-axis is shown in Figure 5.27. The mainlobe has widened to 5.2 degrees. Figure 5.28 shows the same beamformer with the active portion of the array determined by scaling the active portion at broadside by $1/\sin\theta$, where θ is the steering angle relative to broadside. Clearly this array does achieve the goal of keeping the mainlobe constant, at 4.0 degrees, the same as the array steered to broadside. As expected, the sidelobes have increased, partially due to aliasing from elements spaced further than the Nyquist limit.

Also worth noting are the directivity and white noise gain: both are nearly constant for the optimally spaced array, with a directivity of about 40 and white noise gain of about 22. The white noise gain of the harmonically nested array is constant at about 27, but the directivity fluctuates between 20 and 40 over the design bandwidth. The optimally-spaced array trades white noise gain for an improvement in directivity.

This shows that the subjective improvement in appearance for the optimally spaced array is supported by an objective improvement in one performance measure. It is up to the designer to decide whether directivity or white noise gain is more important for a given application.

5.6 SRC Design Example

The design example given by Berger and Silverman [62] is that of a microphone array intended for voice pickup, as in a conference room application. The desired source is located 1 m in front of the center of the array. A forbidden zone is located along the line parallel to the array axis, 1 m from the array, beginning 0.3 m on either side of

the desired source, and extending to 2 m from the desired source in either direction.

In the same paper [62] Berger and Silverman reported other experiments that had optimization variables for both array positions and gain. This gain value was a simple broadband gain, not a frequency-dependent filter. These experiments showed no consistent pattern in the gain values for the global optimums found for several simple problems, so the authors chose to fix all array element gains at unity for all subsequent experiments.

To verify my implementation of the SRC algorithm I first reproduced selected results for the problem outlined above [78]. Berger and Silverman implemented a closed form expression for the PSDX. I replicated the PSDX using the array simulation methods presented in this thesis. The array output due to a source in the unwanted region was calculated at many discrete frequencies and averaged. This was repeated for many sources throughout the unwanted region. From this a ratio was formed between the nominal output of the array from the target source and the maximum output from any unwanted source, which is the definition of the PSDX. I used the SRC method to select array element positions that minimized the PSDX.

The optimal array spacings I found using the simulated PSDX are in Table 5.4. The results published by Berger and Silverman are in Table 5.5. These optimizations are for 5, 7, and 9-element arrays that are oriented to have one element directly in front of the target source, and the remaining elements symmetrically arranged on either side of the center element. Because of the symmetry the number of optimization variables is 2,3, and 4, respectively.

Berger and Silverman did not report the spatial resolution they used to sample the unwanted region. A spatial resolution of 5 cm was found by trial and error to most closely approximate the Berger and Silverman results. Berger and Silverman's closed

form expression is based on an analytical solution to an integral with 500 Hz and 6000 Hz frequencies as integration boundaries. Experiments showed that a frequency resolution of 10 Hz is adequate to approximate the closed form PSDX.

BeamVisualizer is by default configured to produce the far field beampattern for sources in a full circle around the array center. This design problem is based on considering wanted and unwanted sources along a specific line in space, in the near field of the array. I had to modify BeamVisualizer slightly to produce the response of each candidate beamformer to sources along the line of both wanted and unwanted sources. In particular, the polar plots are modified to only display the angles from 26 degrees to 154 degrees, which is the range of angles covered by the forbidden zone, from the perspective of the array center.

The beampattern of the nine-element array is shown in Figure 5.29. The first thing to note is that the sidelobes reach levels significantly higher than the PSDX value of -12.2 dB relative to the peak mainlobe response. This is because the PSDX is an average over all frequencies for one source location. Another important thing to note is that the mainlobe narrows quite dramatically at the high end of the frequency range. In fact Figure 5.30 illustrates this very well by highlighting the polar pattern of the beamformer at the highest frequency, and the frequency response of the beampattern corresponding to a source location just 0.1 m left of the desired

	Spacings(m)	PSDX(dB)
5	0.076, 0.119	-8.12
7	0.149, 0.103, 0.058	-10.45
9	0.175, 0.147, 0.064, 0.059	-12.21

Table 5.4: Calculated array spacings and PSDX values for the SRC design problem.

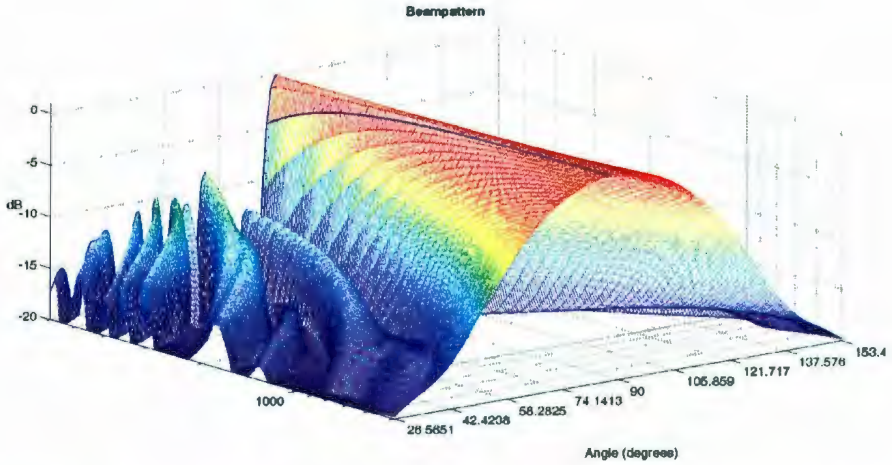

Figure 5.29: The beampattern of the optimal nine-element beamformer found by the SRC method for the SRC example design problem.

source. The frequency response at this location rolls off dramatically above a few kHz, illustrating one likely practical difficulty with this beamformer: if the head of the talker moves by only 10 cm in one direction or the other the frequency response of the beamformer will seriously attenuate most consonants.

Berger and Silverman did not produce the plots of PSDX versus position on the line. The PSDX as a function of position along the source line is shown in Figure 5.31. This provides another useful insight into the character of the beamformer which

	Spacings(m)	PSDX(dB)
5	0.076, 0.119	-8.15
7	0.150, 0.102, 0.058	-10.46
9	0.171, 0.144, 0.063, 0.059	-12.19

Table 5.5: Berger and Silverman array spacings and PSDX values for the SRC design problem[62].

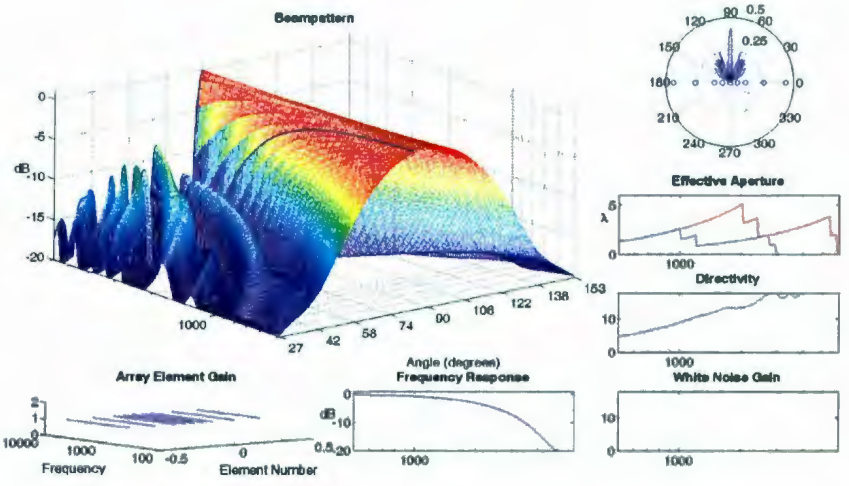

Figure 5.30: The beampattern of the SRC-optimized nine-element beamformer highlighting the frequency response for a source 0.1 m to the left of the target location.

produces the global optimum minimum value for the PSDX function. The peak value in the forbidden zone is highlighted, and this value occurs at the edge of the forbidden zone, and for most of the forbidden zone the PSDX value is far lower than -12.2 dB. This suggests that a better design may be possible. Looking at the main beampattern display we can see that the mainlobe is quite narrow at higher frequencies, so it is likely that the width of the mainlobe at lower frequencies is a significant factor in the PSDX value.

From the spacings in Table 5.5 we can see that the overall array length is 87.2 cm. Given $c = 340$ m/s, the wavelength of 500 Hz, the lowest frequency of interest, is 68 cm. Thus the maximum aperture is only marginally larger than λ, which explains why the mainlobe is broad at the bottom of the frequency range.

This is a case where the beamformer is never steered from broadside, which implies that the maximum directivity can be obtained when elements are spaced at

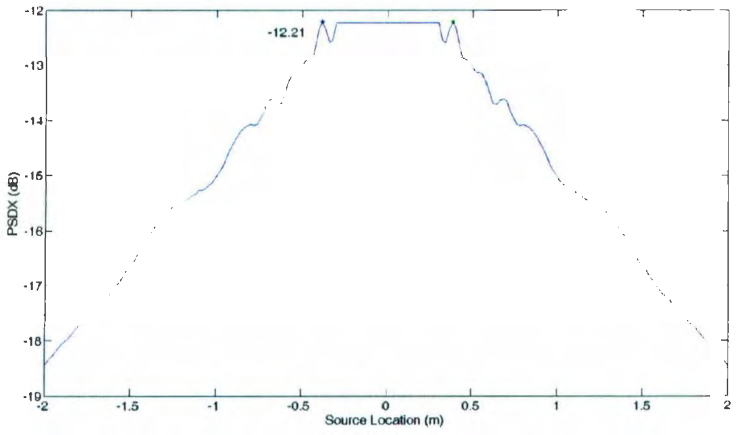

Figure 5.31: The PSDX of the optimum beamformer for the SRC design problem.

close to λ, as discussed in Section 2.5.2. This is confirmed by considering the Berger and Silverman SRC optimization results [62] for arrays sizes with odd numbers of elements up to 31 elements total. In all cases the center portion of the resulting array has several elements spaced by approximately 4 or 5 cm, which is just below the wavelength of the highest frequency of interest, 6 kHz.

With this information it is possible to apply the principles of the generalized harmonically nested beamformer to hypothesize an alternative array geometry. The center of the array is chosen to use three elements at 5.6 cm spacing, which is the wavelength at the highest design frequency. For a nine-element array, there can be three additional steps of adding pairs of elements to the array, meaning $j = 3$. The desired bandwidth ratio, β, is $6000/500 = 12$. According to Equation 4.19, the scale factor between design frequencies is 2.29. This leads to an array with positions 0, 5.6, 13.0, 29.7 and 68.0 cm, with symmetrical positions on the negative side of the origin. Note that the three elements in the center of the array have a spacing of 2λ

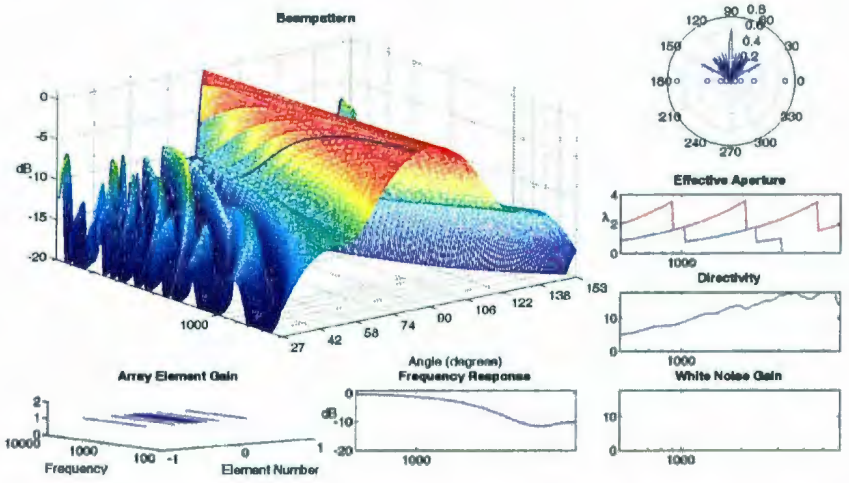

Figure 5.32: The beampattern of the nine-element beamformer for the SRC example design problem using the array geometry computed from the generalized harmonic nesting principles.

at 6 kHz, and the overall length of the array is 2λ at 500 Hz.

The beampattern of the array with this geometry is shown in Figure 5.32, and the PSDX plot is shown in Figure 5.33. Note that this geometry has a PSDX maximum value of -11.4 dB. While not exceeding the global optimum, this is a reasonably good PSDX value, and most significantly the frequency response of the beampattern to a source 10 cm from the target location is markedly better than the optimum array in Figure 5.30.

The truly powerful nature of the optimally-spaced geometry is only realized when the gains over the frequency band are varied to maintain the same effective aperture over the entire band. To demonstrate this, Figure 5.34 shows the same geometry as in Figure 5.32 but with Taylor weighting applied to the subset of the array that is less than 6λ from the center for any given frequency. The Taylor weightings are computed with $\bar{n} = 3$ and -16 dB sidelobes.

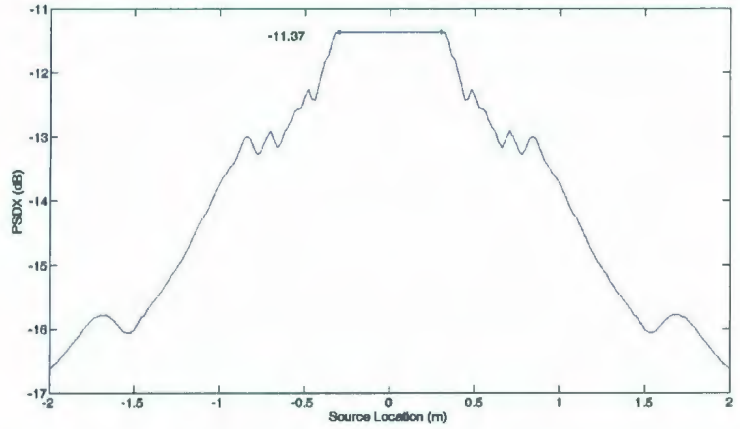

Figure 5.33: The PSDX plot for the beamformer of Figure 5.32.

Notice the frequency-dependent gains in the bottom left plot. Also, the frequency response of the beamformer to a source 10 cm left of the target is now between 0 dB and -4 dB over the entire bandwidth. The PSDX value for this configuration is -14.4 dB, and the PSDX plot is shown in Figure 5.35.

The choice of the value of -16 dB for the sidelobes was found by noticing that many of the PSDX plots showed PSDX values in the region of -16 dB. The choice of including a 6λ portion of the array in the Taylor aperture at any given frequency, was made by manually searching through various possibilities for the size of the Taylor aperture to find the lowest possible PSDX value.

The final question that comes to mind is whether or not the original array geometry found by the SRC method would exceed the performance of this new geometry with the benefit of similar frequency-dependent gains applied to the elements. The Taylor aperture weighting was applied to a 6λ portion of the aperture at each frequency. The choice of 6λ was determined by a manual search of all reasonable values.

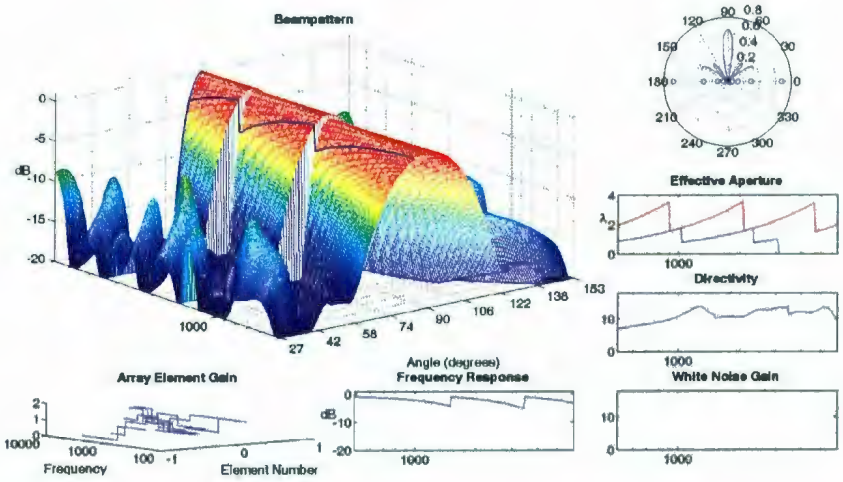

Figure 5.34: The beampattern of optimally-spaced beamformer designed for the SRC design example, with Taylor weightings applied to a 6λ portion of the array.

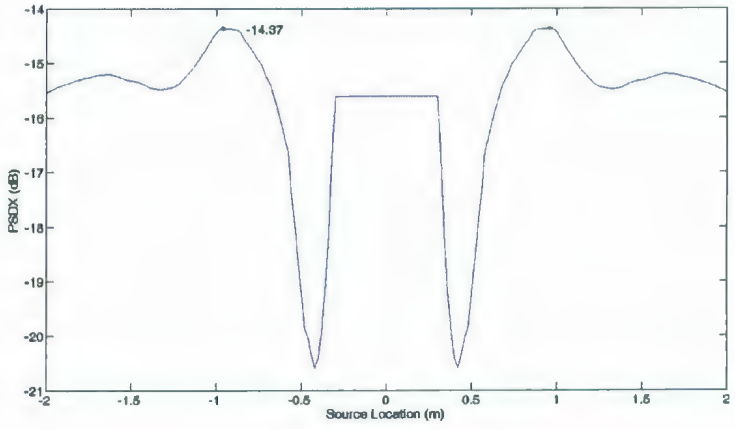

Figure 5.35: The PSDX plot for the beamformer of Figure 5.34.

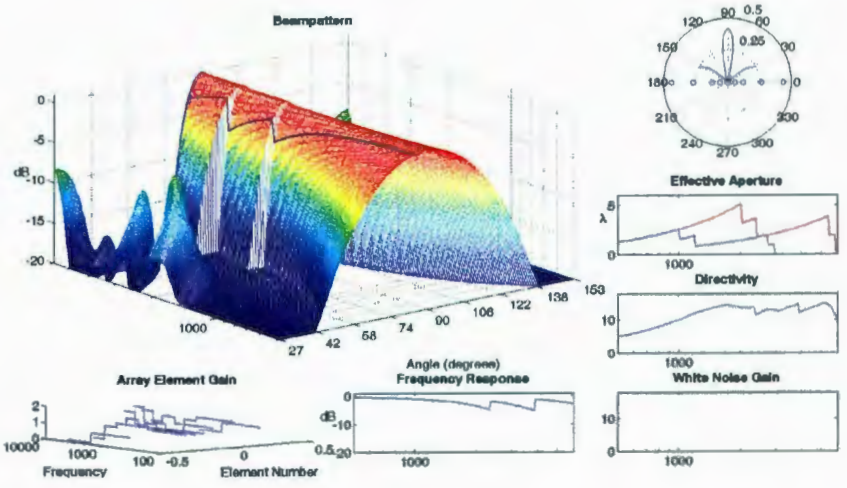

Figure 5.36: The beampattern of SRC-designed beamformer with Taylor weights applied to an aperture of 6λ across the operating bandwidth.

This beamformer achieves a maximum PSDX value of $-13.4\,\text{dB}$. The beampattern is shown in Figure 5.36, and the PSDX plot is shown in Figure 5.37.

Applying Taylor weighting to the SRC-designed beamformer improves the PSDX to $-13.4\,\text{dB}$, compared to $-12.2\,\text{dB}$ for the same geometry using the unity gains as Berger and Silverman did. Still, it does not match the performance of the geometry designed by using the principles of an optimally-spaced broadband beamformer, which achieves a minimum PSDX value of $-14.4\,\text{dB}$.

The key mistakes made by Berger and Silverman were assuming that the gain of each array element was not significant, and not investigating the beampattern of their stochastically-designed beamformer. The first glance at the beampattern revealed the dangerously narrow beampattern at high frequencies and suggested a frequency-dependent gain design to keep the active portion of the aperture more constant across the beamformer bandwidth. Familiarity with the broadband performance of

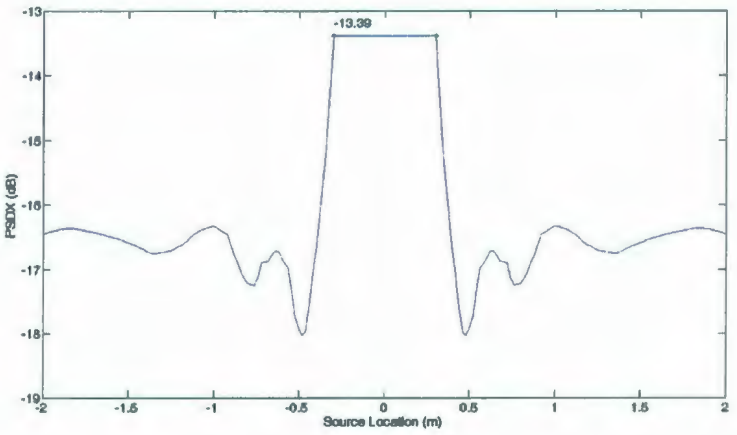

Figure 5.37: The PSDX plot for the beamformer of Figure 5.36.

linear arrays in general, and the principle of an optimally spaced broadband array, specifically led to a design which is not only more suited to the actual application of this design example, but also exceeds the performance of the SRC design on the objective measure of PSDX performance.

5.7 Summary

The narrowband design problems demonstrated the ways in which uniform, Dolph-Chebychev and Taylor apertures can be considered optimal. The uniform beamformer always produces the best white noise gain and narrowest mainlobe. The Dolph-Chebychev weighting will produce the narrowest mainlobe for a given sidelobe specification. The Taylor weighting will occasionally not meet the sidelobe specification, especially for small apertures and arrays with few elements, but it is often preferable since it allows the sidelobes to decay more as the beampattern moves

further from the mainlobe.

The harmonic nesting design example demonstrated the tradeoffs between the harmonically nested array geometry and the optimally spaced geometry. The most suitable of the two would likely be determined by application-specific details, but BeamVisualizer provides a designer with information to make an informed and rational selection.

The MAS design example provided a design for a broadband beamformer to match the beampattern of a seven-element beamformer with a Dolph-Chebychev weighting. The MAS method allows the designer a large amount of flexibility, but for this specific problem I showed that comparable performance can be achieved using an optimal spacing and judicious application of a frequency decomposition beamformer using far fewer elements.

The eight-element asymmetrical array demonstrated very clearly the importance of array geometry in broadband beamformer design. While this geometry severely restricted the possible performance of any beamformer, the application of the MSD method, with its controlled application of superdirectivity, offers some hope for enhanced performance if loss of white noise gain can be tolerated.

The beam steering design example shows that in some circumstances a designer can take advantage of the variety of element spacings in a broadband array to control the mainlobe width even when the beam is electronically steered well away from broadside, at the expense of increased sidelobe level. An optimally-spaced beamformer behaves better in this application than the harmonically-nested geometry.

Finally, the SRC design example shows that visualization of the beampattern of a broadband beamformer can highlight faulty assumptions in the design process and lead a designer to a better solution guided by fundamental principles rather

than blind optimization of a synthetic cost function. The generalized harmonic nesting equations give the designer the tools to quickly compare the range of possible geometries given the constraints, and BeamVisualizer allows the designer to quickly investigate the performance of the various candidate geometries.

Insights gleaned into broadband acoustic beamformer design are collected in a set of guidelines in Chapter 6 to assist the designer in successfully designing broadband beamformers.

Chapter 6

Conclusions

6.1 Summary of Thesis

In Chapter 1 the topic of beamforming in general, and broadband beamformer design specifically, is introduced. The motivation and approach for this thesis is given. In Chapter 2 background on beamformer theory, terminology and performance metrics is provided.

In Chapter 3 the simple equations that can be used to simulate arbitrary three-dimensional discrete aperture beamformers are described, and the BeamVisualizer MATLAB tool is presented. BeamVisualizer allows a designer to quickly inspect the broadband characteristics of a beamformer based on a linear array, and compare the results of various synthesis techniques using the same or similar input parameters. This tool is one of the main contributions of this thesis.

In Chapter 4 the main classical narrowband synthesis techniques are summarized, along with several more recent broadband design techniques. The discussion of array geometry and element spacing for broadband designs is another main contribution of the thesis.

In Chapter 5 several broadband design problems are given. Designs produced by several of the techniques previously discussed are compared using BeamVisualizer. This discussion shows some of the strengths and weaknesses of each technique but also demonstrates the usefulness of BeamVisualizer as a design tool, as well as the importance of the array geometry to a broadband beamformer design.

6.2 Discussion

In the harmonic nesting design problem it was shown that a more consistent frequency invariant beampattern is possible by using a non-uniform array geometry as indicated by Section 4.3.1. This approach involves tradeoffs that might not always make it superior to the traditional harmonically nested broadband beamformer, but BeamVisualizer allows the designer to compare the performance of each design for a specific application.

The optimally-spaced beamformer is clearly superior if the designer would like to maintain a constant mainlobe width as the array is electronically steered off-axis. This constant mainlobe design involves significant tradeoffs of sidelobe level, but is an interesting departure from the performance of harmonically nested beamformers.

The SRC design example shows that in at least this specific case no performance gain was achieved by simplifying a problem and applying a global optimization technique to a cost function for the design of a broadband beamformer. The authors of the SRC problem made some simplifying assumptions in designing their optimization approach that led to less than optimal conclusions. While the SRC method may very well have found the global optimum of the cost function under the chosen contraints,

visual evaluation of the resulting beampattern with BeamVisualizer provides a designer with some insight into the shortcomings of the result. A design that is both subjectively more suitable and objectively superior when evaluated with the original PSDX cost fuction is achieved using the immediate feedback of BeamVisualizer combined with the broadband geometry guidelines from Section 4.3.1

These examples show how the use of an analysis tool like BeamVisualizer and understanding of the underlying geometry helps the designer to recognize the significant tradeoffs and make reasonable design decisions.

6.3 Guidelines for Broadband Array Design

A good understanding of the effect of array geometry and the physical limits on broadband beamformer performance is a prerequisite for successful broadband beamformer design.

When embarking on a design the first issue is to determine the boundaries of the problem and narrow down a range of solutions. Applying the principles of Section 4.3.1 the designer will typically determine a required bandwidth, β, and either a maximum number of elements n, or else a required mainlobe width, which is related to the necessary aperture size P. From there the remaining parameters can be computed to determine the form and details of the array geometry.

Once the geometry is determined, a simple frequency decomposition beamformer using Taylor or Dolph-Chebychev aperture functions may be the simplest and most direct solution. However, in some cases the additional power of other techniques may be warranted.

When designing an array where superdirectivity is not tolerated, MAS is efficient

and optimal. This technique allows a large amount of flexibility in the design, including focusing the array to a specific distance instead of a simple far-field design. The MAS technique also allows some key algorithmic efficiencies that may be suited to an adaptive beamformer. The key is to remember that the algorithm computes the MMSE optimal approximation to the desired beampattern, not the optimal array design in terms of directivity or white noise gain.

If loss of sensitivity to errors can be tolerated (for instance, in the case of very precisely controlled element positions and gains) then MSD offers a method of synthesizing an array weighting that uses superdirectivity to closely approximate more aggresive beampatterns for a given number of elements and choice of element positions.

6.4 Future Work

The scope of this thesis is limited to broadband linear arrays, so there are many directions in which it can be expanded.

Despite the fact that this thesis produced a better design than that by the SRC method of Berger and Silverman, it is possible that the application of stochastic methods could produce even better results for the PSDX problem if the stochastic methods are applied with different constraints.

The technique of perturbations of array element spacings [37] uses non-linear minimax optimization on narrowband arrays with uniform element gains. The method finds element positions that nearly match the sidelobe performance of Dolph-Chebychev weighted aperture beamformers. It would be interesting to analyze the broadband performance of these beamformers to determine if the technique might

be useful for broadband design.

The complete generalization of the harmonic nesting geometry equations came after the bulk of software development on BeamVisualizer. The user interface does not support the direct dynamic generation of completely general harmonically nested geometries. It would be useful to implement this function in BeamVisualizer to allow more efficient comparisons between various broadband array geometries.

The BeamVisualizer software only visualizes the two-dimensional response of arrays, even though the underlying engine is fully capable of modelling the three-dimensional response of broadband arrays with arbitrary geometries. Future versions of the software could include balloon plots of three-dimensional array response at individual frequencies, as well as user interface features to allow the user to select an arbitrary plane for the standard two-dimensional plot of array response versus frequency.

Section 5.4 made use of comparisons of Directivity and White Noise Gain, which were fairly easily produced using BeamVisualizer, however they did require some modifications to the internals of the code along with some manual interaction with the UI to produce the data. It would be useful for BeamVisualizer to either provide UI functionality for such comparisons between beamformers, or else to be structured to better allow scripting so that comparison plots between different beamformers can be produced without the combination of manual interaction along with modifications to the code.

Section 5.5 showed that the effect of steering an array can be traded off against spatial aliasing by using elements spaced further apart than $\lambda/2$ to maintain the apparent aperture size. This implies that the mainlobe width is relative to the size of the array aperture projected onto the plane perpendicular to the steering direction.

However this is clearly not entirely true since beamformers do not asymptotically approach an isotropic sensor when steered to endfire, even though the projected aperture size goes to zero. It would seem that the beampattern of an endfire array may be fundamental in the same way as the sinc beampattern of a uniform linear array at broadside, and that the beampattern of a steered array gradually transitions between these two extremes.

It would be interesting to study if it is possible to decompose the beampattern of a steered linear array into orthogonal broadside and endfire components, determined solely by the array geometry. If the beampattern at any steering angle can be expressed as a linear combination of these two basis beampatterns, this may suggest an interesting method for evaluating planar and volumetric array geometries. Specifically, is it possible to project array elements onto two or more planes to determine some characteristic basis functions of the beampatterns possible with that geometry? Further, if that is possible, could such a decomposition be useful in designing two- and three-dimensional array geometries?

These are just a few of the potential areas for future work in the rich field of broadband beamformer design.

References

[1] "IEEE standard definitions of terms for antennas," *IEEE Std 145-1993*, March 1993.

[2] W. Kummer, "Basic array theory," *Proc. IEEE*, vol. 80, pp. 127 140, 1992.

[3] R. Hansen, "Array pattern control and synthesis," *Proc. IEEE*, vol. 80, pp. 141-151, 1992.

[4] B. V. Veen and K. Buckley, "Beamforming: a versatile approach to spatial filtering," *IEEE ASSP Mag.*, vol. 5, pp. 4–24, 1988.

[5] H. Krim and M. Viberg, "Two decades of array signal processing research: the parametric approach," *IEEE Signal Process. Mag.*, vol. 13, pp. 67 94, 1996.

[6] R. C. Hansen, *Microwave Scanning Antennas*, 2nd ed. Los Altos, CA: Peninsula Publishing Company, 1985.

[7] S. Silver, *Microwave Antenna Theory and Design.* London: IET, 1984.

[8] R. Chatterjee, *Antenna Theory and Practice*, 2nd ed. New Delhi: New Age, 1996.

[9] R. C. Hansen, *Phased Array Antennas*, 1st ed. New York: Wiley-Interscience, 1998.

[10] W. L. Stutzman, G. A. Thiele, and G. A, *Antenna Theory and Design.* J. Wiley, 1998.

[11] W.-D. Wirth, *Radar Techniques Using Array Antennas.* IET, 2001.

[12] R. S. Elliott, *Antenna Theory and Design.* John Wiley & Sons, 2003.

[13] L. Josefsson and P. Persson, *Conformal Array Antenna Theory and Design.* Wiley-IEEE, 2006.

[14] S. S. Haykin, J. H. Justice, N. Owsley, J. L. Yen, and A. C. Kak, *Array Signal Processing.* Prentice-Hall, 1985.

[15] W. S. Burdic, *Underwater Acoustic System Analysis.* Prentice Hall, 1991.

[16] S. U. Pillai and C. S. Burrus, *Array Signal Processing.* Springer-Verlag, 1989.

[17] S. S. Haykin, J. Litva, and T. J. Shepherd, *Radar Array Processing.* Springer-Verlag, 1993.

[18] D. H. Johnson, D. E. Dudgeon, and D. E, *Array Signal Processing: Concepts and Techniques.* P T R Prentice Hall, 1993.

[19] P. S. Naidu, *Sensor Array Signal Processing.* CRC Press, 2001.

[20] S. Stergiopoulos, *Advanced Signal Processing Handbook: Theory and Implementation for Radar.* CRC Press, 2000.

[21] C. Dolph, "A current distribution for broadside arrays which optimizes the relationship between beam width and side-lobe level," *Proc. IRE*, vol. 34, pp. 335 348, 1946.

[22] T. T. Taylor, "Design of line-source antennas for narrow beamwidth and low side lobes," *IEEE Trans. Antennas Propag.*, vol. 3, pp. 16–28, 1955.

[23] ——, "Design of circular apertures for narrow beamwidth and low sidelobes," *IEEE Trans. Antennas Propag.*, vol. 8, pp. 17–22, 1960.

[24] A. Villeneuve, "Taylor patterns for discrete arrays," *IEEE Trans. Antennas Propag.*, vol. 32, pp. 1089–1093, 1984.

[25] C. M. Lockhart and M. K. Miller, "Generalized shading formula from a given line shading," *J. Acoust. Soc. Amer.*, vol. 68, no. 4, pp. 1142–1148, Oct. 1980.

[26] J. Futterman and C. Lockhart, "Rapid determination of steered array shading coefficients by a method of aperture sample density correction," *IEEE Trans. Antennas Propag.*, vol. 30, pp. 565–570, 1982.

[27] D. Cheng and M. Ma, "A new mathematical approach for linear array analysis," *IEEE Trans. Antennas Propag.*, vol. 8, pp. 255–259, 1960.

[28] R. Wu, Y. Ma, and R. James, "Array pattern synthesis and robust beamforming for a complex sonar system," *IEE Proc. Radar, Sonar and Navigation*, vol. 144, no. 6, pp. 370–376, 1997.

[29] C. Olen and R. Compton, "A numerical pattern synthesis algorithm for arrays," *IEEE Trans. Antennas Propag.*, vol. 38, no. 10, pp. 1666–1676, 1990.

[30] L. Wu and A. Zielinski, "An iterative method for array pattern synthesis," *IEEE J. Ocean. Eng.*, vol. 18, no. 3, pp. 280–286, 1993.

[31] B. Ng, M. Er, and C. Kot, "A flexible array synthesis method using quadratic programming," *IEEE Trans. Antennas Propag.*, vol. 41, no. 11, pp. 1541 1550, 1993.

[32] H. S. C. Wang, "Amplitude shading of sonar transducer arrays," *J. Acoust. Soc. Amer.*, vol. 57, no. 5, pp. 1076 1084, 1975.

[33] R. Harrington, "Sidelobe reduction by nonuniform element spacing," *IEEE Trans. Antennas Propag.*, vol. 9, pp. 187 192, 1961.

[34] Y. Lo, "Sidelobe level in nonuniformly spaced antenna arrays," *IEEE Trans. Antennas Propag.*, vol. 11, pp. 511 512, 1963.

[35] A. Ishimaru, "Theory of unequally-spaced arrays," *IEEE Trans. Antennas Propag.*, vol. 10, pp. 691-702, 1962.

[36] H. Unz, "Linear arrays with arbitrarily distributed elements," *IEEE Trans. Antennas Propag.*, vol. 8, pp. 222 223, 1960.

[37] H. Schjaer-Jacobsen and K. Madsen, "Synthesis of nonuniformly spaced arrays using a general nonlinear minimax optimisation method," *IEEE Trans. Antennas Propag.*, vol. 24, no. 4, pp. 501-506, 1976.

[38] R. Hansen, "Fundamental limitations in antennas," *Proceedings of the IEEE*, vol. 69, no. 2, pp. 170-182, 1981.

[39] Y. Lo and S. Lee, "Optimization of directivity and signal-to-noise ratio of an arbitrary antenna array," *Proceedings of the IEEE*, vol. 54, no. 8, pp. 1033-1045, 1966.

[40] D. Scholnik and J. Coleman, "Superdirectivity and snr constraints in wideband array-pattern design," in *2001 - Radar's Odessey into Space*, Atlanta, GA, May 2001, pp. 181–186.

[41] R. P. Smith, "Constant beamwidth receiving arrays for broad band sonar systems," *Acustica*, vol. 23, pp. 21–26, 1970.

[42] E. L. Hixson and K. T. Au, "Wide-bandwidth constant-beamwidth acoustic array," *J. Acoust. Soc. Amer.*, vol. 48, p. 117, Jul. 1970.

[43] F. Pirz, "Design of a wideband, constant beamwidth, array microphone for use in the near-field," in *Proc. IEEE International Conf. on Acoust., Speech, and Signal Proc., ICASSP'79*, vol. 4, 1979, pp. 318–321.

[44] J. Lardies and J.-P. Guilhot, "An optimal broadband constant beamwidth end-fire line array," *Acoust. Lett.*, vol. 10, pp. 70–73, 1986.

[45] J. L. Flanagan, D. A. Berkley, G. W. Elko, J. E. West, and M. M. Sondhi, "Autodirective microphone systems," *Acustica*, vol. 73, pp. 58–71, 1991.

[46] S. Fischer and K. Kammeyer, "Broadband beamforming with adaptive postfiltering for speech acquisition in noisy environments," in *Proc. IEEE International Conf. Acoust., Speech, and Signal Proc. (ICASSP-97)*, vol. 1, 1997, pp. 359–362 vol.1.

[47] D. G. Tucker, "Some aspects of the design of strip arrays," *Acustica*, vol. 6, pp. 403–411, 1956.

[48] ——, "Arrays with constant beam-width over a wide frequency-range," *Nature*, vol. 180, pp. 496–497, 1957.

[49] J. Morris and E. Hands, "Constant-beamwidth arrays for wide frequency bands," *Acustica*, vol. 11, pp. 341 347, 1961.

[50] M. Goodwin and G. Elko, "Constant beamwidth beamforming," in *Proc. IEEE International Conf. Acoust., Speech, and Signal Proc. (ICASSP-93)*, vol. 1, 1993, pp. 169 172 vol.1.

[51] J. C. Morris, "Broad-band constant beam-width transducers," *J. of Sound Vib.*, vol. 1, p. 28, 1964.

[52] J. Jarzynski and W. J. Trott, "Array shading for a broadband constant directivity transducer," *J. Acoust. Soc. Amer.*, vol. 64, pp. 1266 1269, Nov. 1978.

[53] J. Doles and F. Benedict, "Broad-band array design using the asymptotic theory of unequally spaced arrays," *IEEE Trans. Antennas Propag.*, vol. 36, pp. 27 33, 1988.

[54] D. B. Ward, R. A. Kennedy, and R. C. Williamson, "Theory and design of broadband sensor arrays with frequency invariant farfield beam patterns," *J. Acoust. Soc. Amer.*, vol. 97, p. 10231034, Feb. 1995.

[55] M. van der Wal, S. Evert, and D. de Vries, "Design of logarithmically spaced constant-directivity transducer arrays," *J. Audio Eng. Soc.*, vol. 44, no. 6, pp. 497–507, Jun. 1996.

[56] S. S. Haykin and J. Kesler, "Relation between the radiation pattern of an array and the two-dimensional discrete fourier transform," *IEEE Trans. Antennas Propag.*, vol. 23, pp. 419 420, 1975.

[57] L. C. Godara, "Application of the Fast Fourier Transform to broadband beamforming," *J. Acoust. Soc. Amer.*, vol. 98, pp. 230–240, Jul. 1995.

[58] C. Liu and S. Sideman, "Digital frequency-domain implementation of optimum broadband arrays," *J. Acoust. Soc. Amer.*, vol. 98, no. 1, pp. 241–247, Jul. 1995.

[59] O. Bucci, G. D'Elia, G. Mazzarella, and G. Panariello, "Antenna pattern synthesis: A new general approach," *Proc. IEEE*, vol. 82, pp. 358–371, 1994.

[60] H. Lebret and S. Boyd, "Antenna array pattern synthesis via convex optimization," *IEEE Trans. Signal Process.*, vol. 45, no. 3, pp. 526–532, 1997.

[61] S. Blank and M. Hutt, "On the empirical optimization of antenna arrays," *IEEE Trans. Antennas Propag.*, vol. 47, no. 2, pp. 58–67, 2005.

[62] M. F. Berger and H. F. Silverman, "Microphone array optimization by stochastic region contraction," *IEEE Trans. Signal Process.*, vol. 39, pp. 2377–2386, 1991.

[63] A. Trucco, "Synthesizing wide-band sparse arrays by simulated annealing," in *OCEANS 2001. MTS/IEEE Conference and Exhibition*, vol. 2, 2001, pp. 989–994.

[64] A. Trucco and V. Murino, "Stochastic optimization of linear sparse arrays," *IEEE J. Ocean. Eng.*, vol. 24, pp. 291–299, 1999.

[65] A. Trucco and S. Repetto, "Frequency invariant beamforming in very short arrays," in *OCEANS'04. MTS/IEEE TECHNO-OCEAN '04*, vol. 2, 2004, pp. 635–640.

[66] A. Trucco, M. Crocco, and S. Repetto, "A stochastic approach to the synthesis of a robust frequency-invariant filter-and-sum beamformer," *IEEE Trans. Instrum. Meas.*, vol. 55, pp. 1407–1415, 2006.

[67] P. T. D. Abhayapala, "Modal analysis and synthesis of broadband nearfield beamforming arrays," Ph.D. dissertation, Australian National University, Dec. 1999. [Online]. Available: http://thesis.anu.edu.au/uploads/approved/adt-ANU20010905.121231/public/02whole.pdf

[68] T. D. Abhayapala, R. A. Kennedy, and R. C. Williamson, "Nearfield broadband array design using a radially invariant modal expansion," *J. Acoust. Soc. Amer.*, vol. 107, no. 1, pp. 392–403, 2000.

[69] L. C. Parra, "Steerable frequency-invariant beamforming for arbitrary arrays," *J. Acoust. Soc. Amer.*, vol. 119, pp. 3839–3847, 2006.

[70] M. I. Y. Williams, P. T. D. Abhayapala, and R. A. Kennedy, "Generalized broadband beamforming using a modal subspace decomposition," *EURASIP J. Adv. Signal Proc.*, vol. 2007, p. 199, 2007. [Online]. Available: http://users.rsise.anu.edu.au/thush/publications/beamforming.pdf

[71] H. Cox, R. Zeskind, and M. Owen, "Robust adaptive beamforming," *IEEE Trans. Acoust., Speech, Signal Process.*, vol. 35, pp. 1365– 1376, 1987.

[72] M. Brandstein and D. Ward, *Microphone Arrays.* Birkhuser, 2001.

[73] D. V. Rabinkin, R. J. Ranomeron, A. Dahl, J. French, J. L. Flanagan, and M. H. Bianchi, "A DSP implementation of source location using microphone arrays," *J. Acoust. Soc. Amer.*, vol. 99, pp. 2503–2529, Apr. 1996.

[74] P. Lynch, "The Dolph–Chebyshev window: A simple optimal filter," *Monthly Weather Review*, vol. 125, pp. 655 660, Apr. 1997.

[75] L. Debnath and P. Mikusinski, *Introduction to Hilbert Spaces with Applications*, 3rd ed. Academic Press, Sep. 2005.

[76] V. M. Alvarado, "Talker localization and optimal placement of microphones for a linear microphone array using stochastic region contraction," Ph.D. dissertation, Brown University, 1990.

[77] H. F. Silverman, "Some analysis of microphone arrays for speech data acquisition," *IEEE Trans. Acoust., Speech, Signal Process.*, vol. 35, no. 12, pp. 1699 1712, 1987.

[78] C. Whitt and C. Moloney, "Simulation of loudspeaker arrays," in *Proc. of IEEE NECEC 2001*, St. John's, NL, Canada, Nov. 2001.